The spatial regulation of astrocyte mitochondria by Miro1

Terri-Leigh Stephen

A thesis submitted to University College London

for the degree of Doctor of Philosophy

September 2015

Department of Neuroscience, Physiology and Pharmacology

I, Terri-Leigh Stephen, confirm that the work presented in this thesis is my own. Where information has been derived from other sources, I confirm that this has been indicated in the thesis.

Abstract

Mitochondria are energy generating organelles important for regulating the levels of Ca^{2+} inside cells. In terms of astrocytes, intracellular Ca^{2+} is crucial for many aspects of their signalling and for regulating their release of molecules that can profoundly modulate neuronal signalling. In addition, astrocytes take up potentially harmful molecules to prevent neuronal damage, a process that is energetically demanding. Therefore, it is expected that effective spatiotemporal provision of energy and Ca^{2+} buffering, by mitochondria, is important in astrocytes.

In this thesis, a mechanism is proposed for the spatial regulation of mitochondria within the processes of astrocytes involving the EF-hand Ca^{2+}-sensing motifs of the Mitochondrial Rho-GTPase protein, Miro1. Live-cell confocal microscopy of rat organotypic hippocampal slices, revealed that enhancing neuronal activity induces transient mitochondrial remodelling in astrocytes alongside a reduction in mitochondrial trafficking, mediated by elevations in intracellular Ca^{2+}. Stimulating neuronal activity also induces mitochondrial confinement within astrocytic processes close to synapses. Furthermore, the Ca^{2+}-sensing EF-hands of Miro1 are important for regulating mitochondrial trafficking in astrocytes and required for their confinement near synapses. Additionally, activity-dependent mitochondrial positioning, by Miro1, reciprocally regulates intracellular Ca^{2+} signalling within astrocytes. Disrupting the regulation of astrocyte intracellular Ca^{2+}, by Miro1, reduces the number of excitatory synapses, potentially though elevated gliotransmission. These results suggest that the spatial regulation of mitochondria in astrocytes is not only important for astrocyte communication and gliotransmission, but also for maintaining the function of surrounding neurons.

Acknowledgements

I would like to thank Josef Kittler for his constant support and supervision. I would also like to thank David Attwell for his valued advice. Thanks to all past and present members of the Kittler lab for constructive and sometimes unconstructive discussion- you made life in the lab rather enjoyable. Special thanks to Nathalie Higgs for teaching me a great deal- your support was invaluable (after all you made the adenovirus, without which most of this work would not have been possible). Thanks to Lorena for providing me with your molecular biology expertise and your knowledge regarding all things glia. Thanks also to Anusha for your friendship and constant support through the good and the sometimes-hard times (I will never forget our first neuroscience-day escapades).

I would also like to thank my friends, in particular Nat and Anna for always being there for relief from the lab. Thanks to Christine for your endless support even though the continent of Africa separates us. Also, special thanks to my greatest fans - my mum and dad.

Lastly, but most importantly, I am most grateful to David. I'm pretty sure I wouldn't have been able to do it without you and your comic relief. Your patience, emotional support and encouragement were always infallible.

I dedicate this thesis to my grandparents.

Contents

List of Figures and Tables

Abbreviations

CNS - central nervous system
AIS - axon initial segment
AP - action potential
ATP - adenosine tri-phosphate
PSD - postsynaptic density
VDCC - voltage-dependent calcium channels
SNARE - soluble N-ethylmaleimide-sensitive factor attachment protein receptor
NMDA - N-methyl-D-aspartate
AMPA - α-Amino-3-hydroxy-5-methyl-4-isoxazolepropionic acid
NMDAR - N-methyl-D-aspartate receptor
AMPA - α-Amino-3-hydroxy-5-methyl-4-isoxazolepropionic acid receptor
KAR - kinate receptor
VGLUT - vesicular glutamate transporter
mGluR - metabotropic glutamate receptor
SV - synaptic vesicle
LTP - long-term potentiation
LTD - long-term depression
IPSPs - inhibitory postsynaptic potentials
EPSPs - excitatory postsynaptic potentials
GABA - γ-Aminobutyric acid
GABAR - γ-Aminobutyric acid receptor
GPCR - G-protein coupled receptor
GlyR - glycine receptor
E/I - excitatory-inhibitory
AD - Alzheimer's disease
GLT-1 - glutamate transporter-1
GLAST - glial high-affinity glutamate transporter
EAATs - excitatory amino acid transporters

RGCs - retinal ganglion cells

ACM - astrocyte-conditioned media

TSPs - Thrombospondins

SPARC - secreted protein, acidic and rich in cysteine

Glypican - Gpc GLT1 - glutamate transporter 1

Sema3a - semaphorin 3a

MN - motor neuron

DRG - dorsal root ganglion

TrkA

TN - Tenascin

DG - dentate gyrus

SR - serine racemase

PKCα - protein kinase C-alpha

PICK1 - Protein Interacting with C-kinase

Acetyl CoA - acetyl coenzyme A

TCA - tricarboxylic acid

GTP - guanosine triphosphate

NAD - nicotinamide adenine dinucleotide

FADH - flavin adenine dinucleotide

ETC - electron transport chain

HD - Huntington's disease

PD - Parkinson's disease

ADP - adenosine diphosphate

ROS - reactive oxygen species

TTX - tetrodotoxin

GTP - Guanosine triphosphate

Miro - mitochondrial Rho-GTPase protein

EF - embryonic fibroblast

Trak - trafficking kinesin protein

ER - endoplasmic reticulum

OE - overexpression

Aβ -amyloid-β peptide

GSH - glutathione

MCU - mitochondrial calcium uniporter

mNCX - mitochondrial Na^+/Ca^{2+} exchanger

IP_3R - inositol 1,4,5-trisphosphate receptor

RyR - ryanodine receptors

FCCP - carbonyl cyanide p-trifluoromethoxy-phenyl-hydrazone

SERCA - sarcoplasmic/endoplasmic reticulum Ca^{2+}-ATPase pump

OMM - outer mitochondrial membrane

MAMs - mitochondria-associated ER membranes

iGluRs - ionotropic glutamate receptors

NCX - Na^+/Ca^{2+} exchanger

PCR - polymerase chain reaction

ETRs - endothelin receptors NO - nitric oxide

Trp - transient receptor potential

mIPSCs - mini inhibitory postsynaptic currents

nAChRs - nicotinic acetylcholine receptors

mAChRs - muscarinic acetylcholine receptors

KO - knock out

SOC - store operated Ca^{2+} channel

Drp1 - dynamin-related protein 1

Fs1 - fission 1 protein

Mfn - mitofusins

OPA1 - optic atrophy protein 1

NO - nitric oxide

iNOS - inducible nitric oxide synthase

PINK1 - phosphatase and tensin homologue deleted on chromosome 10-induced putative kinase 1

VDAC1 - voltage-dependent anion channel 1

TOM - translocase of OMM

LC3 - microtubule-associated protein light chain 3

HDAC6 - histone deacetylase 6

PARP-1 - poly ADP-ribose polymerase-1

mPTP - mitochondrial permeability transition pore

ONH - optic nerve head

HD - Huntington's disease

ALS - Amyotrophic lateral sclerosis

MND - motor neuron disease

FC - flurocitrate

FXS - fragile X syndrome

FMR1 - fragile X mental retardation 1 gene

FMRP - fragile X mental retardation protein

GFAP - glial fibrillary acidic protein

GECI - genetically encoded Ca^{2+} indicator

CaM - calmodulin

Publications arising directly from the work in this thesis

Stephen TL., Higgs N.F., Sheehan D.F., Al Awabdh S., Lopez-Domenech G., Arancibia-Carcamo I.L. and Kittler J.T. (2015) Miro1 Regulates Activity-Driven Positioning of Mitochondria Within Astrocytic Processes Apposed to Synapses to Regulate Intracellular Calcium Signalling. *J. Neuroscience* 35(48):15996-16011.

Stephen TL., Gupta-Agarwal S. and Kittler J.T. (2014) Mitochondrial dynamics in astrocytes. *Biochemical Society transactions* 42:1302-1310.

Chapter 1

Introduction

1.1 Neuronal Synaptic Transmission

Neurons are electrically excitable cells within the brain, first described over 100 years ago by Santiago Ramon Cajal, that transmit and process information (Finger, 2004). The point of information transfer between neurons is called the synapse (Figure 1.1), of which there are two types: chemical and electrical. Electrical synapses allow bidirectional transfer of information, where rapid passage of ions from the cytoplasm of one neuron to another occurs via small gap junctions of around 3.5 nm (Kandel et al., 2000). This transfer, however, does not allow signal gain, as the signal received by the postsynaptic neuron is the same or weaker than that of the source neuron. These synapses facilitate the fastest type of response, required for defensive responses, but they do not allow for signal modulation. Chemical synapses, however, are specialized for directional information transfer and are the main type of synapse in the central nervous system (CNS) (Eccles, 1964) *.

*All future reference to 'the synapse' in this thesis will allude to the chemical synapse.

1.2 Cytoarchitectural Organization of the Brain - Two classes of cells

A typical neuron is composed of a cell body (soma), dendrites and a single axon (Alberts, 2008). The axon emanates from the soma at the axon initial segment (AIS) or hillock) and can reach up to 1 meter in humans. The axon sends out signals to other neurons or muscles, thus forming the output end of the neuron. In most long neurons, signal propagation through the axon is enhanced by a myelin sheath (formed mainly of cholesterol), which prevents dissipation of the signal through insulation. Myelin is white in appearance and thus pertains to the white matter of the brain. Dendrites collectively referred to as the dendritic tree, form the input end of the neuron. The dendritic tree serves to maximize connections with neighbouring neurons (Figure 1.1).

The synapse is the point at which communication between neurons occurs. Typically, a synapse consists of a small protrusion from the axon (axonal bouton or terminal) and a projection of a dendrite (dendritic spine). Axons can also form synapses with the dendritic shaft, the soma of other neurons or other axons (axo-axonal synapses). The gap between the axonal bouton (presynaptic terminal) and the dendritic spine (postsynaptic terminal) is called the synaptic cleft. The distance separating the pre- and postsynaptic membranes is usually around 20-40 nm and it is here that small molecules called neurotransmitters traverse (Hormuzdi et al., 2004) (Figure 1.1).

However, this simple description makes light of the sheer complexity of the brain. Each neuron forms hundreds of connections with a multitude of other neurons, forming highly complex neuronal networks that coordinate signalling underlying every thought process, including our emotions.

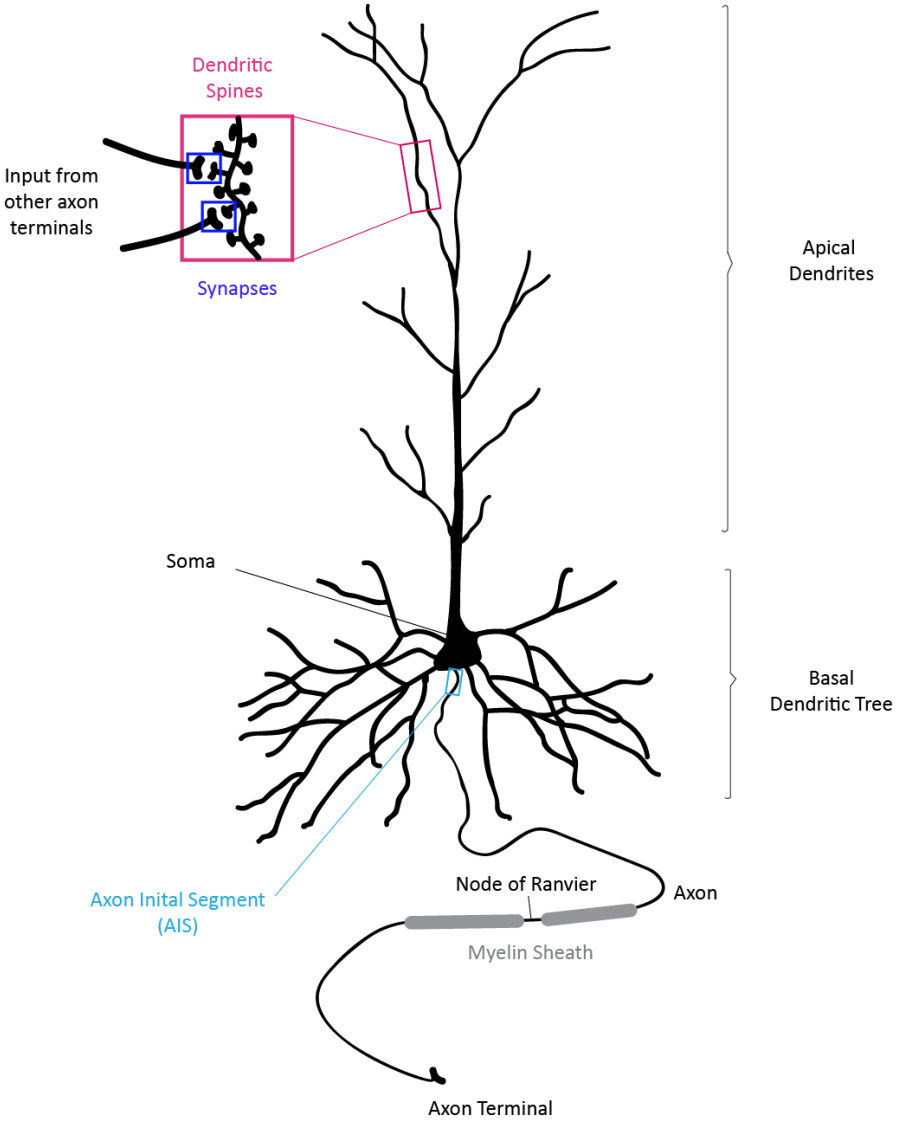

Figure 1.1 Neuronal morphology. A typical neuron composed of a cell body (soma), dendrites and a single axon. Axons contact dendritic protrusions called spines forming the synapse. Synapses are specialised subdomains that enable the communication between two neurons. These signals of communication propagate through the axon, insulated by myelin. Gaps in the myelin sheath are called nodes of Ranvier.

At the synapse, a third component influences the connections made by neurons. These cells are a type of glia known as astrocytes. Glial research first began when Virchow described a connective substance that formed a sort of 'glue', in which the neural cells appeared to be embedded (Virchow, 1858). They were later termed astrocytes by von Lenhossek in 1893, as they appeared to be star-shaped (von Lenhossék, 1893).

Astrocytes, also known as astroglia, are the most abundant cell-type in the brain (Azevedo et al., 2009) and they project out two types of processes; very fine perisynaptic processes that wrap themselves around most synapses, and vascular processes (end feet) that are much larger and closely appose blood vessels. Astrocytes can be classed into two groups: fibrous and protoplasmic. Fibrous astrocytes are found in white matter and have long thin, unbranched processes, whose end-feet ensheath gaps in the myelin sheath, surrounding axons, known as nodes of Ranvier (Sofroniew and Vinters, 2010). At nodes of Ranvier the axonal membrane is not insulated and it is here that signalling can occur. Protoplasmic astrocytes are instead found in grey matter and have branched processes that ensheath synapses, forming the tripartite synapse (Sofroniew and Vinters 2010) (Figure 1.2). This thesis will focus on the latter, protoplasmic type of astrocyte.

Protoplasmic astrocytes are the most numerous cell population in the rodent, primate and human cortex. However, human protoplasmic astrocytes are larger and more complex than their primate and rodent counterparts (Oberheim et al., 2009). The longest human protoplasmic processes were roughly 2.6 fold longer than the longest protoplasmic rodent processes (97 μm vs 37 μm, respectively). Human astrocytes also extend 10 times more processes than rodent astrocytes (37.5 vs 3.75 processes extending from the cell body) (Oberheim et al., 2009).

Other types of glia that exist include microglia, oligodendrocytes, Bergmann glia and radial glial cells.

1.2.1 Microglia

Microglia are the macrophages of the brain and their role is to remove debris and foreign material in the CNS. They contribute to the immune response by secreting cytokines and other signalling molecules in addition to the presence of antigens on their surface (Hanisch and Kettenmann, 2007, Facci et al., 2014).

1.2.2 Oligodendrocytes

Oligodendrocytes are a type of glia cell that produce myelin, which wraps around the axon, insulating it, to reduce signal leakage and increase the speed of propagation (Fields, 2008). Astrocytes can interact with oligodendrocytes to stimulate the production myelin (Ishibashi et al., 2006).

1.2.3 Bergmann Glia

Bergmann glia are a type of astrocyte in the cerebellum that play an important role during development (Lordkipanidze and Dunaevsky, 2005) and also influence the activity of neurons in the cerebellum (Purkinje cells) (Wang et al., 2012).

1.2.4 Radial Glia

Radial glial cells are bipolar-shaped cells that span the width of the cortex during development of the CNS. They form the primary progenitor cell pool and are capable of differentiating into neurons, astrocytes and oligodendrocytes (Kriegstein and Alvarez-Buylla, 2009). During development, neurons use radial glial cells as scaffolds, traveling along their fibres in order to reach their final destinations (Noctor et al., 2001).

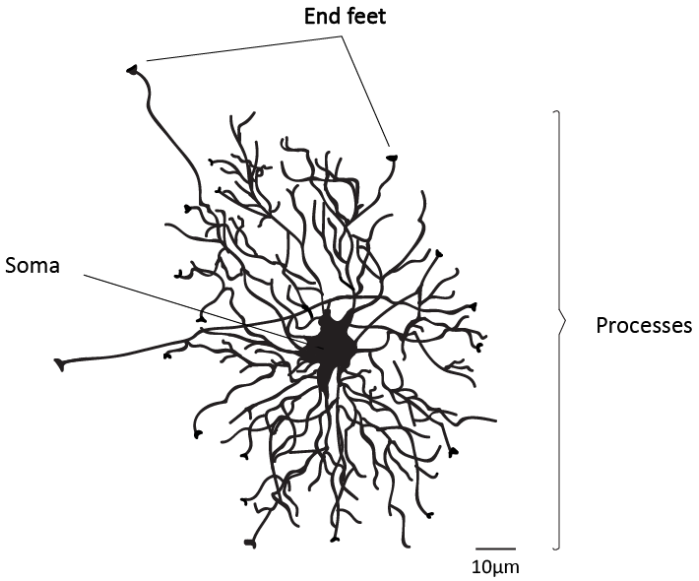

Figure 1.2 Astrocyte morphology. A typical protoplasmic astrocyte composed of a cell body (soma), many branched process and end feet. Their cell bodies are small and irregular from which numerous ramified extensions/processes protrude. Some processes terminate with bulbous end feet, which can contact synapses or blood vessels.

1.3 The electrical basis of signalling in the brain

Ion channels are found in all electrically excitable cells and are central to neuronal activity. They are membrane spanning, pore-forming protein complexes that exhibit selective permeability for specific ions (molecules that carry electrical charge). They allow certain ions to cross the cell membrane (lipid bilayer). These ions are specific to the composition of the channel. The most important ions that underlie neuronal signal conduction are sodium (Na^+), potassium (K^+), calcium (Ca^{2+}) and chloride (Cl^-) (Kew and Davies, 2010). An ion channel is only capable of conducting charge when it is in the open state. However, the ion channel may also exist in an inactivated or closed state. The difference between these two states is the propensity to return to the open state i.e. inactivated channels are more likely to return to the open conducting state.

Transmitter-gated ion channels are ligand activated ion channel. Upon binding of selective ligands, to their respective ion channels, their structure becomes altered to allow the flow of ions across the membrane. In contrast, voltage gated ion channels enter the open state when the transmembrane voltage potential surpasses a specific threshold. Ion channels can be further classified by their ion selectivity and membrane structure.

1.3.1 Excitatory neurotransmission and plasticity

In neurons, ion channels establish the resting membrane potential (the state at which neurons are quiescent) and also determine the propagation of signals in the brain through the firing of action potentials (APs). In its resting state a neuron is fairly negative (around -70 mV) in comparison to the extracellular environment (Eccles, 1964). Because the membrane is

polarised, an increase in the resting membrane potential is called hyperploarisation (e.g. from -70 mV to -75 mV), which decreases the ability of the cell to fire an AP (inhibitory). In contrast, a reduction in the resting membrane potential is called depolarisation (e.g. from -70 mV to -45 mV), which increases the ability of the cell to fire an AP (excitatory). At rest, Na^+/K^+-ATPases actively transport 2 K^+ molecules into the cell and 3 molecules of Na^+ out of the cell, at the energetic cost of 1 molecule of adenosine tri-phosphate (ATP). A neuron becomes depolarised when a presynaptic neuron releases a chemical transmitter that perturbs the resting membrane potential. This activates voltage-gated channels on the depolarised neuron that permit Na^+ influx. Consequently, an AP fires if depolarisation occurs above a specific threshold (-55 mV) and a cascade of positive ion entry ensues. Eventually K^+ flows out of the cell in order to restore the equilibrium gradient for K^+ and this restores the cell to its resting state. Depolarisation, therefore, is defined as the rapid increase in voltage across the membrane with a return to the resting state. APs are forward propagating depolarisation waves that spread from their point of origin at the AIS, along the axon, mediated by the flow of charged ions through voltage sensitive ion channels. They can also propagate backwards through the proximal dendritic tree (Eccles, 1964). Directionality of the AP is mediated by Na^+ channel inactivation. The speed of AP propagation along the axon is enhanced by myelin. The myelin sheath increases the speed of AP propagation by mediating saltatory conduction, where the signal hops/leaps from one node of Ranvier to the next (Figure 1.1).

Presynaptic terminals contain neurotransmitter-filled vesicles, which release their contents into the synaptic cleft upon arrival of an AP. The AP induces an influx of calcium (Ca^{2+}) ions through voltage-dependent, Ca^{2+}-sensitive ion channels (VDCCs) at the presynaptic terminal. These Ca^{2+} ions bind synaptotagmin and SNARE (soluble N-ethylmaleimide-sensitive factor attachment protein receptor) proteins located within the membranes of synaptic vesicles (SVs)

and this allows vesicle fusion with the plasma membrane and consequently, release of their contents into the synaptic cleft. These transmitters then diffuse across the synaptic cleft and bind to specialized receptors embedded in the postsynaptic membrane (Figure 1.3). Depending on the neurotransmitter, postsynaptic receptors determine the response triggered by the AP. To allow for further signal transduction, vesicular transporters (VGLUTs in the case of glutamatergic signalling) located on SVs replace the neurotransmitters released by exocytosis during signal propagation. Immediately apposed to these postsynaptic receptors is an elaborate interconnected network of proteins called the postsynaptic density (PSD). These proteins are important for anchoring, trafficking and modulating the activity of postsynaptic receptors.

The main excitatory neurotransmitter in the brain is glutamate (mono-sodium glutamate), which binds to postsynaptic glutamate-gated ionotroptic receptors: N-methyl-D-aspartate (NMDA), α-Amino-3-hydroxy-5-methyl-4-isoxazolepropionic acid (AMPA) and Kinate receptors (NMDAR, AMPAR and KAR). Binding of glutamate to AMPARs induces the influx of cations (Na^+, Ca^{2+} or K^+), dependent on the subunit organisation of the receptor (for example GluR2-containing AMPARs are Ca^{2+} impermeable). AMPAR opening induces depolarisation of the postsynaptic membrane and this promotes the opening of NMDARs, which are found together at the excitatory PSD (Scannevin and Huganir, 2000). NMDARs are ligand-gated, requiring the binding of glutamate and a co-agonist (glycine or D-serine) and voltage-gated, due to having a magnesium (Mg^{2+}) ion that blocks their opening until depolarisation removes it. In this way NMDARs are thought to be molecular coincidence detectors, reducing spontaneous activity and form association between neural events. NMDARs are highly permeable to Ca^{2+} (as well as being permeable to K^+ and Na^+) and are the primary site of postsynaptic Ca^{2+} influx (Bliss and Collingridge, 1993). Excess influx of

Ca^{2+} through NMDARs is thought to underlie neuronal excitotoxicity (cell death induced by excessive excitatory transmission). Glutamate can also bind metabotropic glutamate receptors (mGluRs), which instead induces a G-protein coupled intracellular signalling cascade that can affect ion channel conductance indirectly (Figure 1.3).

Modifications of AMPAR properties underlie the synaptic plasticity process of long-term potentiation and depression (LTP and LTD). LTD is the state of weakening of synaptic activity. LTP, on the other hand, is the process of persistent strengthening of synaptic activity and underlies learning and memory formation (Bliss and Collingridge, 1993, Matsuo et al., 2008). Initially a synapse is stimulated repeatedly and this results in an upregulatation of dendritic receptors followed by an upregulation of presynaptic neurotransmitter-containing vesicles. The initial connection is strengthened and maintained in this way.

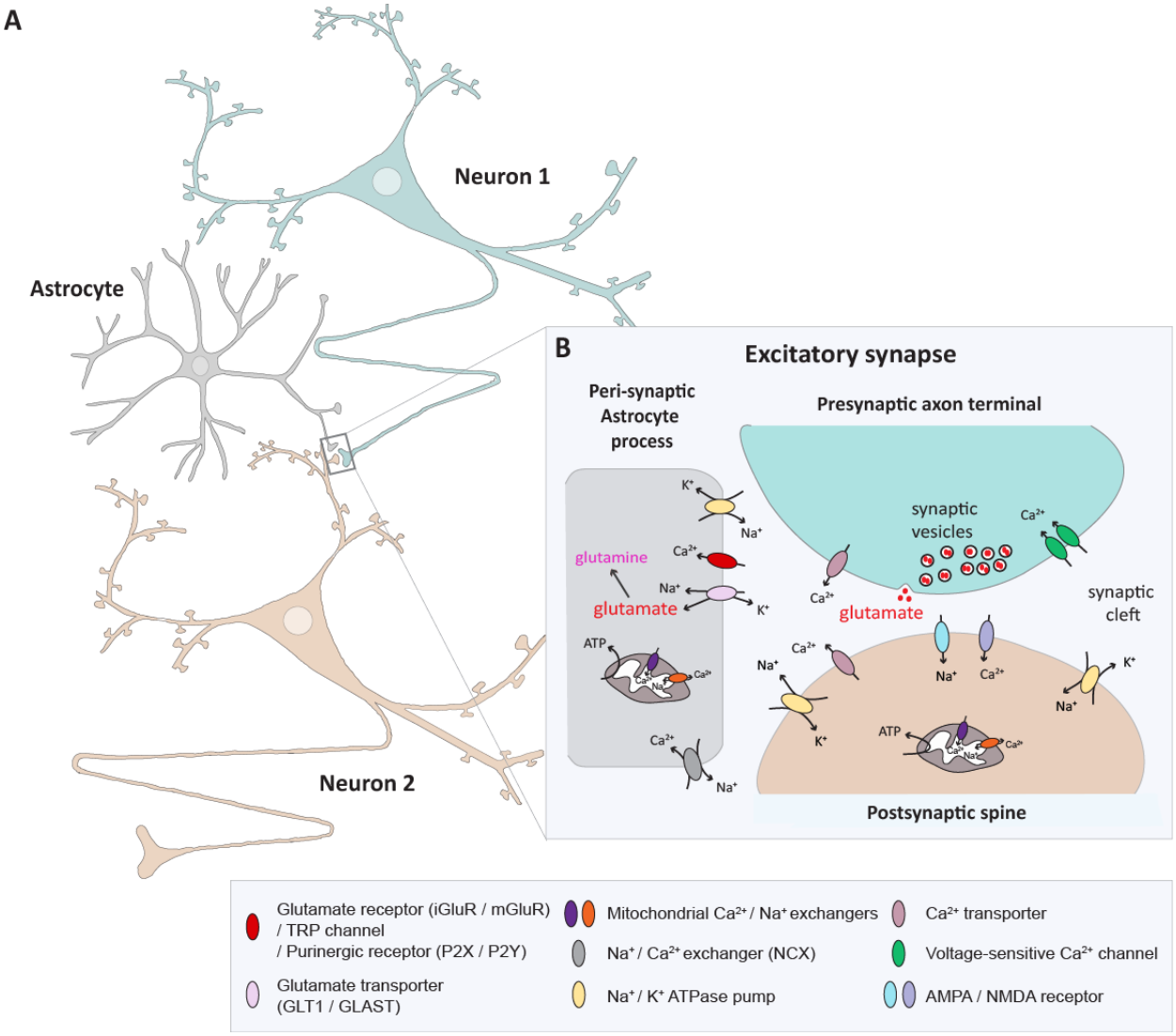

Figure 1.3 Structure of the excitatory synapse. **A**. Synapses are typically the point where the axon terminal of a neuron transmits signals to the spine of another neuron through the gap between them. This gap is called the synaptic cleft. Here, processes/end feet projected from nearby astrocytes can influence signal transmission. This is known as the tri-partite synapse. **B**. Inset shows the movement of important molecules at the synapse. Here, astrocyte processes/end feet can influence the concentration of these molecules. They can buffer glutamate and convert it to non-toxic glutamine. They can also buffer K^+, Na^+ and Ca^{2+}. This can influence the ability of neurons to fire action potentials. Glutamine can also be released from astrocytes and following being taken up by neurons it is broken down to produce substrates for energy production. The levels of astrocyte intracellular Ca^{2+} can also influence the release probability of gliotransmitters, which include glutamate, D-serine and ATP.

1.3.2 Excitatory/ Inhibitory balance

Whether a synapse is inhibitory or excitatory depends on which ion channels conduct the postsynaptic response as well as the postsynaptic receptor expression profile. Their receptor expression profile is determined by activity of the surrounding neuronal circuitry. Inhibitory signalling is a process that makes neurons less likely to generate an AP and arises from a more negative postsynaptic potential (inhibitory synaptic postsynaptic potentials (IPSPs)). The opposite are excitatory postsynaptic potentials (EPSPs) where a more positive current is generated. While glutamate acting on glutamate receptors is the main form of excitatory neurotransmission the primary transmitters involved in inhibitory signal transduction are GABA (γ-Aminobutyric acid) and glycine. GABA acts on GABA receptors (GABARs): $GABA_A$ and $GABA_B$. $GABA_A$Rs are permeable to Cl^- upon GABA binding, while $GABA_B$Rs are coupled to potassium channels via G-proteins (G-protein couple receptors (GPCRs)). Glycine acts on glycine receptors (GlyRs), which are also ionotropic and permeable to Cl^-.

Tight control must exist over the maintenance of excitatory-inhibitory (E/I) balance. Uncontrolled excitatory neurotransmission, for example, chronic NMDAR activation, can lead to excitotoxicity. Excitotoxicity eventually results in significant damage and ultimately cell death. Uncontrolled Ca^{2+} elevations in neurons have been implicated in ischaemic cell death during stroke (MacDonald et al., 2006). Excessive excitatory neurotransmission as well as defective inhibitory neurotransmission have been associated with epilepsy (McNamara et al., 2006). On the other hand, excessive inhibition or insufficient excitation may eventually lead to decreased brain function.

Interestingly, reactive astrocytes have been shown to release GABA in a mouse model of Alzheimer's disease (AD), reducing the spiking activity of granule cells in the dentate gyrus (Jo et al., 2014). Conversely, astrocytes can release glutamate, ATP and D-serine under certain conditions of neuronal stimulation. This suggests a direct role for astrocytes in maintaining the E/I balance that may go awry during pathology.

1.3.3 Role of astrocytes at the excitatory synapse

Astrocytes have a multitude of functions that include maintenance of the blood brain barrier (Abbott et al., 2006), nutrient support of neurons (Dienel and Cruz, 2004), promotion of oligodendrocyte myelinating activity (Ishibashi et al., 2006), modulation of vascular blood flow (Parri and Crunelli, 2003, Attwell et al., 2010), promoting repair of the brain in response to damage (Sofroniew, 2005) and transmitter uptake and release (Kimelberg and Nedergaard, 2010). This thesis will focus on the latter of these specialities.

1.3.3.1 Astrocyte excitability

A type of astrocyte excitability exists, based on changes in intracellular Ca^{2+} (Duffy and MacVicar, 1995). Astrocytes are connected by gap junctions and thus create an electrically coupled syncytium (Bennett et al., 2003). Consequently, changes in local astrocyte Ca^{2+} can propagate through their network, via these gap junctions and alter the function of distant astrocytes. This type of signalling is thought to occur on a slower timescale compared to neuronal signal transmission (19 μm/s for Ca^{2+} wave propagation versus 10-100 m/s for AP propapagtion) (Fiacco and McCarthy, 2006) but nevertheless exists as an important form of

long-range signal propagation. Astrocyte Ca^{2+} signalling or excitability can be evoked by neuronal synaptic activity (Schummers et al., 2008), which also increase the motility of their synapse-associated processes (Perez-Alvarez et al., 2014). Astrocyte Ca^{2+} signalling is termed a type of excitability because it can evoke the release of chemical modulators called gliotransmitters (glutamate, ATP, D-serine, GABA). In addition, because these transmitters play a crucial role in modulating synaptic transmission (Araque et al., 1998, Di Castro et al., 2011), plasticity (Haydon and Carmignoto, 2006) and LTP (Navarrete and Araque, 2011) the communicative link between neurons and astrocytes is said to be bidirectional.

1.3.3.2 Gliotransmission

Gliotransmission is the process by which astrocytes release vesicles packed with gliotransmitters via exocytosis. Astrocytes express proteins known to be involved in vesicle fusion including proteins of the SNARE complex (synaptobrevin-2, syntaxin), synaptotagmin, Munc18a and complexin-2, which are critical for gliotransmitter release (Parpura and Zorec, 2010). The transporters necessary for vesicle packaging of glutamate (VGLUT1 and VLGUT2) were expressed by isolated astrocytes (Zhang et al., 2004). Additionally, altering the SNARE complex, for example, resulted in the failure of astrocytes to release glutamate (Zhang et al., 2004). ATP released from astrocytes interacts directly with neurons, serving to regulate their own glutamatergic transmission and enhancing the levels of AMPARs (Theodosis et al., 2008). In addition, astrocyte released ATP can be converted to adenosine, which can act on G-protein-coupled adenosine receptors (A_1, A_{2A}, A_{2B} and A_3) to suppress synaptic transmission (Elmenhorst et al., 2007). A_1 receptors decrease cAMP levels and have been reported to decrease Ca^{2+} conductance. A_{2B} and A_3 receptors instead increase

phospholipase activity. Adenosine receptors have been shown to regulate the blood brain barrier and modulate blood flow through vasodilation (Newman, 2003). Reducing adenosine receptor activation has been linked to an increase in excitatory transmission (Pascual et al., 2005).

Moreover, astrocytes are actively involved in excitatory neurotransmission, as they remove excess glutamate from the synaptic cleft via glutamate transporters (glutamate transporter 1 (GLT1) and glutamate aspartate transporter (GLAST)), also known as excitatory amino acid transporters (EAATs 2 and 1, respectively). These transporters are important for maintaining physiological levels of extracellular glutamate (Figure 1.3B). Astrocytes also maintain homeostasis of various ions such as Na^+ K^+ Cl^- and H^+ (Simard and Nedergaard, 2004). For example, when the extracellular K^+ concentrations become high, astrocytes uptake K^+ and transfer it to adjacent astrocytes via gap junctions by a process called spatial buffering (Kofuji and Newman, 2004). Due to spatial buffering, astrocytes prevent toxic accumulation of extracellular K^+.

Therefore, via regulation of their intracellular Ca^{2+} levels, it is clear that astrocytes play an essential role in regulating information processing in the CNS. It is not clear, however, whether this bidirectional signalling, and the release of gliotransmitters, occurs exclusively under physiological conditions or reciprocally plays a role during pathophysiological conditions.

1.3.4 Astrocytes influence the formation and function of synapses

Astrocytes secrete many factors that have the potential to profoundly alter the structure and function of nearby neurons. Several important, studies elegantly revealed that culturing neurons in astrocyte-conditioned media (ACM) affected the number and function of synapses (Pfrieger and Barres, 1997, Nagler et al., 2001, Ullian et al., 2001) indicating that factors released specifically by astrocytes are responsible for these neuronal alterations. These molecules include Thrombospondins (TSPs1-4), the glycoprotein tenascin C, SPARC (secreted protein, acidic and rich in cysteine) and SPARC-like-1 (Hevin) (Kucukdereli et al., 2011).

Further studies investigated the influence of astrocyte-released factors on rat retinal ganglion cells (RGCs) in culture. Astrocyte-released cholesterol increased the number of RGC glutamatergic synapses (Mauch et al., 2001). Mauch and colleagues found that cholesterol applied to RGC cultures increases the frequency of spontaneous synaptic events by increasing the quantal content and release of SVs (Mauch et al., 2001). Cholesterol does this by binding to synaptophysin, an important molecule involved in the formation of SVs (Thiele et al., 2000). Similarly, a study by Christopherson and colleagues revealed that astrocyte-released TSPs (TSP-1 and TSP-2) increased the number of RGC synapses nearly 3-fold (Christopherson et al., 2005). Immunodepletion of TSPs from ACM decreased RGC synaptogenesis. The TSP-induced synaptogenesis was primarily observed in the developing brain (post-natal week 1) and downregulated in the mature adult brain (post-natal week 3) (Adams and Lawler, 2004). TSPs 3 and 4 were also expressed by astrocytes, where TSP-4 was primarily present in mature astrocytes (post-natal day 17) (Cahoy et al., 2008). This suggests a role for astrocyte-released TSPs in the adult CNS. More recently, the gabapentin

receptor alpha-2-delta-1 has been identified as the receptor responsible for the TSP-mediated excitatory synaptogenesis (Eroglu and Barres, 2010).

1.3.4.1 Glypicans

A study by Allen and colleagues identified Glypican 4 (Gpc4) and Glypican 6 (Gpc6), heparan sulphate proteoglycans, as astrocyte-secreted factors that increase synaptic AMPAR expression and strengthen their activity (Allen et al., 2012). Addition of purified Gpc4 to RGCs induced a 2.5-fold increase in surface GluR1-containg AMPARs. Gpc4 was sufficient to strengthen individual synapses, reflected in an increase in mEPSC frequency and amplitude, although very large amplitude events induced by astrocytes were absent. Gpc6 also increased surface GluR1 AMPARs. Reducing the levels of Gpc4 and Gpc6 in ACM, which was subsequently added to RGC cultures, was unable to increase the amplitude of RGC mEPSCs. In addition the clustering of surface GluR1 was reduced. However, it is important to note that synapse formation did occur, presumably due to the release of other astrocyte-specific synaptogenic molecules. Reducing the levels of Gpc4 or Gpc6, on their own, was not sufficient to reduce synaptic activity. From these results, they conclude that both Gpc4 and Gpc6 are necessary for enhancing postsynaptic activity in RGCs (Allen et al., 2012).

1.3.4.2 SPARC

SPARC on the other hand, negatively regulates synaptogenesis, which is important for preventing over-excitation in the CNS (Jones and Bouvier, 2014). Astrocyte-released SPARC influences the level of synaptic AMPARs. Neurons grown with SPARC KO astrocytes had

significantly more surface containing GluR1 and GluR2 synapses than neurons co-cultured with SPARC WT astrocytes. Jones and colleagues also found enhanced synaptic signalling and impaired LTP in hippocampal slices from SPARC KO mice (Jones et al., 2011). They show that SPARC regulates surface AMPARs through β3-integrin receptors, which have been shown to stabilise GluR2 subunits at synapses (Cingolani et al., 2008).

1.3.4.3 Semaphorin 3a

Molofsky and colleagues, identified semaphorin 3a (Sema3a) as an astrocyte-released molecule that has important consequences for synapse regulation, motor neuron (MN) AIS orientation, MN survival and normal patterning of a subtype of sensory neuron (TrkA) (Molofsky et al., 2014). The receptor for semaphorin, Nrp1, was more highly expressed by MNs and dorsal root ganglion (DRG) $TrkA^+$ sensory neurons, suggesting a specific neuronal subtype response induced by Sema3a. Additionally, Sema3a was shown to negatively regulate axon growth where it repelled axons (Molofsky et al., 2014). This research demonstrates that stable positional cues from developing astrocytes influences aspects of sensorimotor circuit formation and postnatal refinement of the neural network.

1.3.4.4 SPARC-like-1/Hevin

Kucukdereli and colleagues showed that SPARC-like-1 or Hevin increases synapses in RGCs *in vitro* and *in vivo* and is required for their maturation (Kucukdereli et al., 2011). Hevin is expressed primarily by astrocytes in the cortex of the developing CNS (peaking at post-natal day 15-25) (Risher et al., 2014). It is required for the connectivity of synapses in the thalamus

and cortex (Risher et al., 2014). In addition, Hevin interacts with Neuroligin-1 and Neurexin-1-alpha. Neuroligin-1 is important for regulating synaptic content and thus important for excitatory synaptic responses (Varoqueaux et al., 2006).

1.3.4.5 Tenascins

Tenascins are a family of extracellular matrix glycoproteins. Tenascin-C (TN-C) is expressed by astrocytes in the developing nervous system and has been shown to be important for their proliferation and differentiation (Wiese et al., 2012). Evers and colleagues observed impaired plasticity in the hippocampus of 1-month-old TN-C KO mice. Indeed, LTP induction was shown to be significantly reduced and LTD abolished at CA1-Schaffer collateral synapses, whereas, LTP in the dentate gyrus (DG) and CA3 were described as normal in TN-C KO mice (Evers et al., 2002). The study also draws a link between TN-C deficiency and impaired L-type Ca^{2+} channel-dependent synaptic plasticity in the CA1, mediated by proteoglycans/integrins.

1.3.4.6 Other mediators

Tumour necrosis factor alpha is also linked to both glutamate release and the insertion of AMPARs into nearby neurons (Beattie et al., 2002, Santello et al., 2011). In addition, chemokines released from astrocytes have a strong regulatory effect on the activity of NMDARs (Gao and Ji, 2010). Astrocytes also express ephrin-A3, which interacts with EphA4 (expressed by dendritic spines) to decrease levels of GLT-1 and GLAST (Carmona et al., 2009). EphB receptors and ephrin-B ligands are also expressed by astrocytes, ephrin-B3 being

the most active during LTP (Zhuang et al., 2010). Ephrin-B3 enhances D-serine release by regulating serine racemase (SR), the enzyme responsible for the conversion of L-serine to D-serine and an SR-interacting protein, protein kinase C-alpha (PKCα). Specifically, ephrin-B3 downregulates PKCα, increasing the interaction between SR and Protein Interacting with C-kinase (PICK1), resulting in D-serine release (Zhuang et al., 2010). Zhuang and colleagues identified that both EphB3 and EphA4 receptors were necessary for astrocyte D-serine release, by measuring D-serine levels in Eph-B3 and EphA4 KO cultured astrocytes. Therefore, while ephrin-A signalling regulates levels of GLT-1 and GLAST, ephrin-B signalling regulates D-serine release for activation of postsynaptic NMDA receptors and thus is important for LTP.

Taking into account the above studies, it is abundantly clear that astrocytes release molecules that can profoundly influence many aspects of synapse formation and function. The question, however, remains as to what exactly controls the release of these synaptogenic molecules from astrocytes.

1.4 Metabolic Specialization of Neurons and Glia

Most energy in the brain comes from the metabolism of blood glucose either by glycolysis, through the Krebs/tricarboxylic acid (TCA) cycle or oxidative phosphorylation. Glycolysis is the first stage of energy production where glucose is oxidised, in the cytosol, to pyruvate via a series of enzymatic reactions, with a net gain of two molecules of ATP. This process does not involve oxygen and so is termed anaerobic. When oxygen is available pyruvate is decarboxylated to acetyl coenzyme A (Acetyl CoA) and transported inside the matrix of

mitochondria. There, Acetyl CoA enters the Krebs/TCA cycle were it is completely oxidised into two molecules of CO_2, one molecule of guanosine triphosphate (GTP) is produced and three NAD^+ (oxidised nicotinamide adenine dinucleotide) and one FADH (flavin adenine dinucleotide) are reduced to three molecules of NADH and one $FADH_2$. These molecules are energy-rich in that they carry electrons that are necessary for the electron transport chain (ETC) of oxidative phosphorylation- the major source of ATP in aerobic organisms (Alberts, 2008). The process of oxidative phosphorylation means that, through mitochondria, cells can produce a significant amount of energy in the form of ATP in the presence of oxygen, which is supplied by the circulatory system.

Neurons are thought to rely more on oxidative phosphorylation and astrocytes are thought to be more glycolytic, however the latter is still debated in the field where significant oxidative metabolism has been observed in astrocytes (Wyss et al., 2009). Certainly, tight metabolic coupling must exist, at glutamatergic synapses, between neurons and nearby perisynaptic astrocyte processes (Chatton et al., 2003).

The large ion movements that underlie synaptic signalling upon AP induction (mainly Ca^{2+}, Na^+ and K^+) impose a large localised energetic demand on neuronal function. In fact, 50 % of brain energy is used to restore these ionic gradients. Other processes relying on an abundant ATP supply include filling SVs and LTP.

In terms of astrocytes, glutamate represents a significant metabolic cost. Following GLT-1 or GLAST-dependent uptake, glutamate is converted to non-toxic glutamine and this process requires energy in the form of ATP. Glutamine can be released from astrocytes to supply neurons with a source of glutamate, which they cannot synthesise themselves. Along with the

uptake of glutamate GLT-1 and GLAST couple the inward movement of one molecule of glutamate to three Na^+ ions and one hydrogen (H^+) ion and the outward movement of one K^+ ion. This gives rise to a significant accumulation of Na^+ in the processes of astrocytes (Rose and Ransom, 1996, Bergles and Jahr, 1997). This rise in Na^+ activates the astrocytic Na^+/K^+-ATPase (Magistretti and Pellerin, 1999) (Figure 1.3B). This represents a further energy demanding process that generates a diffusion gradient for glucose within the astrocyte network, directly coupled to synaptic activity. However, evidence suggests that oxidative activity exists in astrocytes (Hertz et al., 2007, Lovatt et al., 2007). Using nuclear magnetic resonance spectroscopy, it was estimated that astrocytes account for ~ 25 % of total brain oxidative metabolism (Serres et al., 2008). Indeed ultrastrucutal analysis revealed that fine astrocytic processes ensheathing synapses contain a substantial quantity of mitochondria (Grosche et al., 1999, Lovatt et al., 2007, Oberheim et al., 2009). Alongside this, astrocyte glutamate transporters were shown to physically interact with mitochondria (Rose et al., 2009, Genda et al., 2011, Bauer et al., 2012). Therefore, if mitochondria are able to position themselves in the vicinity of glutamate transporters in order to provide energy for glutamate uptake and metabolism what are the mechanisms involved in mitochondrial spatial regulation?

1.4.1 The mechanisms of energy supply by mitochondria

The brain consumes a disproportionate percentage of the body's energy supply (making up only 2% of the body's weight, it consumes 20% of the body's resting energy i.e. 10 times more relative to its weight) in order to maintain proper signal propagation (Mink et al., 1981). Because energy cannot freely diffuse throughout the extensive neural network, tight

regulatory mechanisms must exist to ensure adequate energy delivery on a rapid timescale. At the synapse, where communication between neurons occurs, energy supply is particularly important.

In neurons, energy supply is tightly coupled to demand by mitochondria. Mitochondria are membrane bound organelles (Figure 1.4A) that came to be found in most eukaryotic cells through an ancient bacterial symbiotic relationship (Henze and Martin, 2003). In addition to supplying cellular energy in the form of ATP, mitochondria are involved in cellular differentiation, growth and cell death (McBride et al., 2006). Mitochondrial dysfunction has been implicated in several neurological disorders such as Autism (Oliveira et al., 2005) and Schizophrenia (Kolomeets and Uranova, 2010) as well as neurodegenerative diseases such as AD (Pereira et al., 1998; Wang et al., 2008), Huntington's disease (HD) (Mangiarini et al., 1996, Lin et al., 2001) and Parkinson's disease (PD) (Exner et al., 2012). The number and morphology of mitochondria can vary extensively between cells, tissue and organisms. For example, red blood cells have no mitochondria, while liver cells can contain more than 2000 (Alberts et al., 2002). Structurally, mitochondria are composed of an outer and inner membrane, juxtaposing the intermembrane space, cristae and matrix (Figure 1.4A).

The molecular machinery for energy production, the ETC, is located within the cristae of mitochondria and is comprised of five protein complexes (Figure 1.4). The process of ATP generation begins with the transfer of electrons from electron donors: NADH (complex I) or $FADH_2$ (complex II) to electron acceptors: NADH-ubiquinone reductase or succinate-ubiquinone reductase, respectively. Electrons are then passed along a chain of carriers (ubiquinone, cytochrome C oxidoreductase (complex III), cytochrome C and cytochrome C oxidase (complex IV)) before being donated to oxygen (O_2) to make water. The energy of the

movement of electrons through complex I, III and IV is used to move H^+ ions out of the matrix into the intermembrane space. This movement of H^+ ions creates an electrochemical gradient across the mitochondrial membrane termed proton motive force. The movement of ions back into the matrix is used to power ATP synthase, which creates ATP from the phosphorylation of ADP (adenosine di-phosphate), termed oxidative phosphorylation or chemiosmosis (Alberts, 2008) (Figure 1.4B). The outcome of this is that mitochondria generally have a negative membrane potential relative to the cytoplasm (between -150 and -180 mV) termed delta psi ($\Delta\Psi$). Although vital for metabolism, oxidative phosphorylation produces reactive oxygen species (ROS) that lead to the production of free radicals. These damage cells, contributing to aging and disease. Therefore, the maintenance of mitochondria is of particular importance to overall cell health and survival.

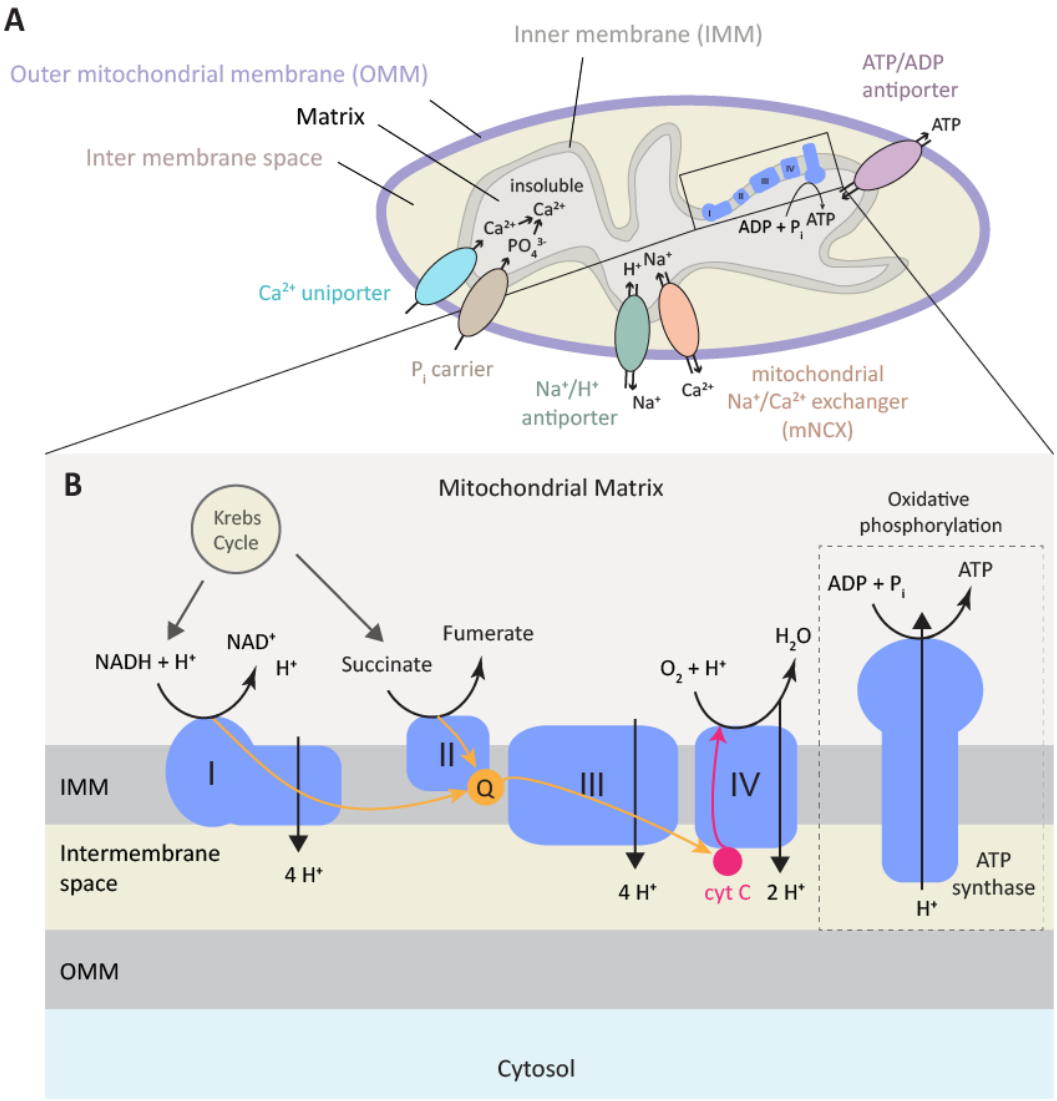

Figure 1.4 Structure of the mitochondrion and the mitochondrial respiratory chain. **A**. Mitochondria are composed of an outer mitochondrial membrane (OMM) and an inner membrane (IMM). Between these two membranes is the inter membrane space. Within the inner membrane is the mitochondrial matrix. Mitochondria can also buffer calcium (Ca^{2+}) and sodium (Na^{+}) via the mitochondrial Ca^{2+} uniporter (MCU) and the mitochondrial Na^{+}/Ca^{2+} exchanger (mNCX) and the Na^{+}/H^{+} antiporter, respectively. ATP is released from mitochondria via the ATP/ADP antiporter. **B**. ATP is produced in the mitochondrial matrix by the electron transport chain, which enables oxidative phosphorylation.

1.4.2 Mitochondria in neurons and astrocytes

Mitochondria are non-uniformly distributed in neurons and localise at sites of elevated demand for energy production or Ca^{2+} buffering, such as synapses (Chang et al., 2006), active growth cones (Morris and Hollenbeck, 1993) and nodes of Ranvier (Fabricius et al., 1993). Synaptic activity itself acts as a cue for mitochondria to position themselves at post-synaptic sites where they can provide ATP and buffer Ca^{2+} directly (Macaskill et al., 2009). Mitochondria are required to be mobilized in order to transport damaged mitochondria back to the soma for degradation and to replenish the useable pool of mitochondria throughout the axons and dendrites (Miller and Sheetz, 2006, Frederick and Shaw, 2007).

In addition, there is evidence to suggest that mitochondria, in particular their positioning, is important for the regulation of neuronal morphology and synapse formation in E18-19 rat cultures (Li et al., 2004). Li and colleagues find that dendritic mitochondria localise to spines upon stimulation of neuronal activity (Li et al., 2004). They subsequently depleted dendritic mitochondria by overexpressing the dominant negative form of the dynamin-related protein 1 (Drp1) or the optic atrophy 1 protein (OPA1) in E18-19 hippocampal neuron cultures (Li et al., 2004). Decreasing mitochondrial density in cultured neurons (at 13 DIV) decreased the density of spines and synapses, while the reverse was true for increasing the density of mitochondria in the dendrites (overexpressing the WT form of Drp1) (Li et al., 2004). Although it is well established that Drp1 plays an important role in controlling mitochondrial fission, it also maintains normal ER morphology and distribution as well as vesicle endocytosis (Pitts K.R, 1999, Li et al., 2013). These results indicate that mitochondrial density and positioning within dendrites is directly correlated with the formation and functionality of excitatory synapses.

Mitochondria are present in the processes of astrocytes that ensheath synapses (Grosche et al., 1999, Lovatt et al., 2007, Oberheim et al., 2009) and are reportedly mobile within their processes (~ 600 nm in diameter) (Ito et al., 2009, Lavialle et al., 2011, Jackson et al., 2014). Jackson and colleagues reported that astrocyte mitochondrial trafficking was bidirectional in organotypic hippocampal slices, with 44 % and 56 % moving in the retrograde (towards the soma) and anterograde (away from the soma) direction, respectively (Jackson et al., 2014). Instead, in neurons 61 % and 39 % where moving in the retrograde and anterograde direction, respectively. Interestingly, they found that astrocyte mitochondria moved significantly slower and covered shorter distances than in dendrites. This suggests that different mechanisms regulate mitochondrial trafficking in neurons and astrocytes.

Jackson and colleagues report that mitochondrial trafficking within astrocyte processes, in organotypic hippocampal slices, seems to be regulated by both microtubule and actin cytoskeletons (Jackson et al. 2014). They show that pharmacological disruption of microtubule (with vinblastine) or actin (with cytochalasin D) assembly significantly decreased the fraction of moving mitochondria. However, Kremneva and colleagues, report that microtubules are the main regulators of mitochondrial trafficking in cultured astrocytes (Kremneva et al., 2013). They report that mitochondria align more with microtubules than actin filaments under basal conditions. They show that pharmacological disruption of microtubules (with nacodazole) disrupts basal mitochondrial motility while depolymerisation of actin filaments (with Latrunculin B) does not disrupt basal mobility. However, disrupting actin filaments did block Ca^{2+}-dependent mitochondrial stopping. From this they conclude that mitochondria couple to microtubules when intracellular Ca^{2+} is low and are highly motile. When elevations in intracellular Ca^{2+} occur, mitochondrial motility is reduced and they become anchored to actin filaments due to Ca^{2+}-dependent interactions. In addition, they

suggest that the motility of astrocytic mitochondria is inversely related to intracellular Ca^{2+} and mitochondrial mobility requires intact microtubules. An inability of mitochondria to translocate to high Ca^{2+} microdomains, wherein they become immobilized and take up excessive Ca^{2+}, is likely to result in cell death through excitotoxicity and give rise to neurological disorders (MacAskill and Kittler, 2010, Rintoul and Reynolds, 2010, Larsen et al., 2011). It is not currently known whether this is the case in astrocytes.

Astrocyte mitochondria have been shown to localise at sites of glutamate uptake in astrocytes (Chaudhry et al., 1995, Bezzi et al., 2004). Genda and colleagues reported, using mass spectrometry, that immunoaffinity purified GLT-1 from rat cortices interacts with mitochondrial proteins (Genda et al., 2011). They also show that mitochondria co-localise with GLT-1 in astrocytes in slices and *in vivo*. Furthermore, mitochondria were less likely to appose GLT-1 when neuronal activity was blocked with the Na^{+} channel blocker tetrodotoxin (TTX) in astrocyte processes in slices (Jackson et al., 2014). Alongside this, TTX and TFB-TBOA (astrocyte specific glutamate transporter blocker) increased mitochondrial mobility in astrocytes. They infer from this that neuronal activity regulates mitochondrial trafficking via glutamate transporter activation in astrocyte processes. This suggests that astrocyte mitochondria may be able to respond to the demands of astrocyte signalling and position themselves at sites of energy consumption or Ca^{2+} buffering.

Apart from the above, very little is known about the specific mechanisms that control the spatial regulation of mitochondria in astrocytes. Their positioning could be important for regulating intracellular Ca^{2+}, which underlies Ca^{2+}-dependent processes such as gliotransmission. Downstream, Ca^{2+}-dependent gliotransmission can have important consequences for neuronal function. Thus, elucidating the mechanisms that control

mitochondrial trafficking and positioning within astrocyte processes appears to be necessary to further our understanding of astrocyte biology.

1.4.3 The Mitochondrial Rho-GTPase protein (Miro)

In neurons, an important regulator of mitochondrial trafficking and positioning is the outer-mitochondrial membrane Rho-GTPase protein, Miro. Miro consists of two cytoplasmic GTPase domains and two EF (embryonic fibroblast)-hand Ca^{2+}-binding motifs (Figure 1.5A). There are two mammalian isoforms of Miro, Miro1 and Miro2, which share 60 % homology (Fransson et al., 2006). The first evidence that Miro played a role in mitochondrial trafficking came from a study in *Drosophila* where knocking out the protein disrupted the transport of mitochondria into neuronal axons (Guo et al., 2005). Further experimentation has revealed that Miro couples mitochondria to microtubules via Kinesin or Dynein motors in neurons (Macaskill et al., 2009b, Wang and Schwarz, 2009). Binding of Miro to Kinesin or Dynein motors is mediated by trafficking kinesin proteins (Trak1 or Trak2) (Figure 1.5B). Trak1 mediates Kinesin binding and, therefore, anterograde mitochondrial transport, while Trak2 mediates Dynein binding and, therefore, retrograde mitochondrial transport (Schwarz, 2013). Long-range mitochondrial transport is mediated by the microtubule cytoskeleton (Morris and Hollenbeck, 1995, Schwarz, 2013), while short-range trafficking is regulated by actin filaments (Ligon and Steward, 2000, Hollenbeck and Saxton, 2005).

Mechanistically, when Ca^{2+} binds the EF-hand domains of Miro1, a conformational change (of either Miro1 itself or the motors) results in uncoupling of mitochondria from the microtubule network. This results in mitochondrial docking at sites of high Ca^{2+}, such as the synapse, in order to maintain ionic homeostasis (Macaskill et al., 2009b) (Figure 1.5B). Wang

and Schwarz proposed that Ca^{2+} elevations in neurons lead to a change in the conformation of the kinesin motor KIF5 (also known as kinesin-1), which results in it binding directly Miro1 thus preventing the binding of Miro1 to the microtubule network (Wang and Schwarz, 2009) (Figure 1.5B2). They show this using co-immunoprecipitation experiments where elevating free Ca^{2+} does not disrupt Miro-kinesin heavy chain binding. Functionally, they show that disrupting the EF-hand-dependent regulation of mitochondrial trafficking diminishes neuronal resistance to excitotoxicity. Another study by MacAskill and colleagues showed, using a GST-pulldown assay, that binding of KIF5C to Miro1 is inhibited when Ca^{2+} concentrations are elevated in an EF-hand dependent manner (Figure 1.5B1). They also show that indirect binding of KIF5 to mitochondria is inhibited when intracellular Ca^{2+} concentrations are elevated with glutamate (100 μM for 10 minutes with 1 μM glycine) (Macaskill et al., 2009b).

The GTPase domains of Miro1 may also be involved in transducing cellular signalling cascades into alterations in mitochondrial transport (MacAskill et al., 2009a). For example the recruitment of Trak2 to neuronal mitochondria is dependent on the activity of the first GTPase domain of Miro1 (GDP-bound Miro1 recruits Trak2, allowing mitochondrial coupling to the microtubule network) (MacAskill et al., 2009a). However, far less has been established regarding the GTPase domains of Miro1.

In addition to being implicated in mitochondrial trafficking, Miro proteins have other important functions, for example the profusion proteins mitofusins (Mfn1/Mfn2) were shown to interact with both Miro1 and Miro2 (Misko et al., 2010) and this suggests that Miro proteins play a role in regulating mitochondrial morphology. Indeed, Miro1 increases

mitochondrial fusion at resting levels of intracellular Ca^{2+}, whilst it increases fragmentation when intracellular Ca^{2+} levels increase in a Drp1-dependent manner (Saotome et al., 2008). In *Drosophila*, overexpression (OE) of phospho-resistant dMiro in the brain was found to be toxic and caused age-dependent loss of dopaminergic neurons, the cell type selectively affected in PD (Liu et al., 2012, Tsai et al., 2014). As well as this, knockdown of Miro in *Drosophila* neurons results in a reduction in mitochondria and induces tau-mediated neurodegeneration by increasing tau phosphorylation at Ser262 (Iijima-Ando et al., 2012). This implicates defects in Miro-mediated mitochondrial regulation in the pathogenesis of AD. In addition, knocking out Miro1 is lethal prior to birth (prenatally) and specific neuronal knock out (KO) of Miro1 reduces the number of mitochondria from cortico-spinal tract axons (Nguyen et al., 2014). Furthermore, mice with neuronal loss of Miro1 exhibit symptoms of motor neuron disease (MND). Nguyen and colleagues conclude that defects in neuronal mitochondrial motility and distribution are sufficient to cause neurological disease (Nguyen et al., 2014).

In conclusion, whilst Miro1 is an important regulator of mitochondrial trafficking in neurons, next to nothing is known regarding Miro proteins in astrocytes. At the RNA level, Miro1 (*Rhot1*) is present in astrocytes at higher levels than in neurons (fragments per kilobase of exon per million fragments mapped) (Cahoy et al., 2008). Whether it is expressed at the protein level and how it functions to regulate astrocyte mitochondria is not known.

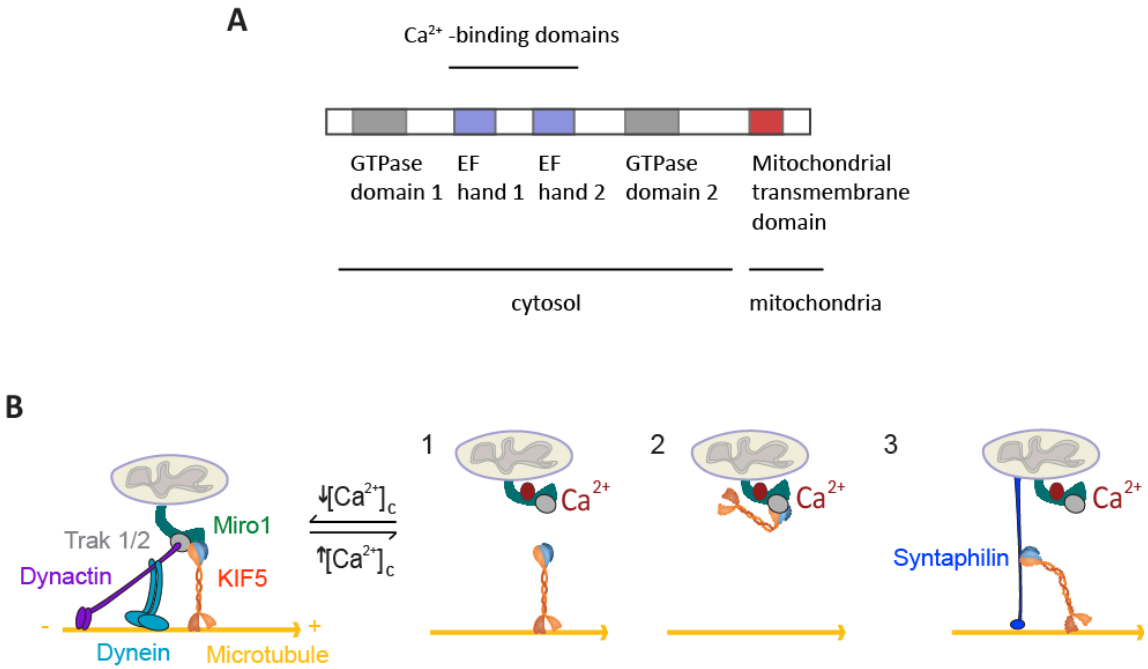

Figure 1.5 The structure of the mitochondrial Rho-GTPase protein Miro1. **A**. Miro1 contains two Ca^{2+}-binding domains flanked by two GTPase domains and a mitochondrial-binding domain. **B**. Miro1 enables mitochondria binding to the microtubule network via adaptor proteins Trak1/2 and KIF5 for anterograde transport (away from the some) and dyein, via dynactin for retrograde transport (towards the soma). When Ca^{2+} binds Miro1 via its EF-hand domains, it causes mitochondria to detach from the microtubule transport network. Three models have been proposed for how this uncoupling occurs. 1- Upon Ca^{2+} binding Miro1, Trak1/2 remains bound to Miro1 and this complex uncouples from the KIF5-microtubule complex. 2- Upon Ca^{2+} binding Miro1, KIF5 remains bound to Miro1 and Trak1/2 in a complex that uncouples from the microtubule network. 3- Upon Ca^{2+} binding Miro1, KIF5 and the mitochondrial-Trak1/2 complex binds syntaphilin, which acts like an anchor.

1.5 Astrocyte Ca^{2+} signalling

Ca^{2+} signalling in astrocytes is essential for their function as well as for the function of neurons. Astrocyte Ca^{2+} fluctuations underlie the release of gliotransmitters, which profoundly affect aspects of neuronal synaptic transmission (Panatier et al., 2011, Navarrete et al., 2013), including LTP and LTD (Pascual et al., 2005, Chen et al., 2013a), thus impacting on the mechanisms of learning and memory. Astrocyte Ca^{2+} signalling also has important consequences for the regulation of blood flow in the CNS (termed functional hyperemia) (Filosa et al., 2004, Mulligan and MacVicar, 2004, He et al., 2012, Otsu et al., 2015). In addition, astrocyte Ca^{2+} signalling can impact on the regulation of sleep, where impairing SNARE-dependent gliotransmission impairs aspects of sleep induction (Halassa et al., 2009). This mechanism was proposed to involve ATP release from astrocytes, which regulates the levels of adenosine (Halassa et al., 2009). Adenosine levels are elevated during periods of wakefulness and are reduced during sleep (Huang et al., 2011). Elevations in astrocyte Ca^{2+} have also been implicated in the regulation of breathing. They have been shown to respond to physiological decreases in pH with elevations in intracellular Ca^{2+} and subsequently release ATP. ATP induced increases in breathing through the activation of neurons of the retrotrapezoid nucleus (region of the brainstem responsible for regulating breathing) (Gourine et al., 2010).

Astrocyte Ca^{2+} signalling can take many forms. Srinivasan and colleagues separated astrocyte Ca^{2+} fluctuations into somatic responses and process responses that consisted of waves (propagating fluctuations within an area of 14.8 ± 1.4 μm^2) and microdomain responses (spatially confined fluctuations within an area of 0.7 ± 0.01 μm^2) (Srinivasan et al., 2015).

They revealed that significantly more Ca^{2+} fluctuations occur in the processes of astrocytes rather than the soma, in hippocampal slices and in the cortex, *in vivo*. Process microdomain responses were defined as non-propagating fluctuations that occurred within an area of ~ 0.7 μm^2. Their somatic responses occurred within a region of ~ 80 μm^2 and Ca^{2+} waves (confined to the processes) were defined as expanding and contracting fluctuations that spread within an area of ~ 15 μm^2 (Srinivasan et al., 2015). The speed of the Ca^{2+} wave propagation in human acute slice cortical astrocytes was 43.4 μm/sec and was unaffected by TTX (Oberheim et al., 2009). On the other hand, in mouse acute slice astrocyte cortices these Ca^{2+} waves propagated at a slower speed of 8.6 μm/s (Oberheim et al., 2009). These Ca^{2+} waves are considered a form of intercellular astrocyte communication (Dani et al., 1992) and have been observed to efficiently modulate synaptic activity (Pasti et al., 1997, Araque et al., 1999).

1.5.1 Mitochondrial Ca^{2+} buffering in astrocytes

Mitochondria actively uptake Ca^{2+} via the mitochondrial Ca^{2+} uniporter (MCU), powered by a negative membrane potential and release Ca^{2+} to the cytosol via the mitochondrial Na^+/Ca^{2+} exchanger (mNCX) (Grosche et al., 1999, Kintner et al., 2007, Palty et al., 2010, Drago et al., 2011, Parnis et al., 2013). Release of Ca^{2+} from the ER internal stores, via activation of both inositol 1,4,5-trisphosphate receptors (IP_3Rs) and ryanodine receptors (RyRs) (Hua et al., 2004), contributes to an increase in cytosolic Ca^{2+} in astrocytes. Synaptic activity can also evoke feedback cytosolic Ca^{2+} transients in astrocytes, which have the potential to alter the release probability of gliotransmitters (Perea and Araque, 2005, Serrano et al., 2006, Di Castro et al., 2011, Navarrete et al., 2013). These Ca^{2+} transients can propagate in a wave like manner, expanding from its point of origin through the astrocyte

network, via gap junctions. Mitochondria have been implicated in the propagation of these Ca^{2+} waves in cultured astrocytes (Simpson and Russell, 1998) and the up-regulation of mitochondrial function in *Xenopus oocytes* increased the velocity of these Ca^{2+} waves (Jouaville et al., 1995). Increases in intracellular Ca^{2+} precedes an increase in mitochondrial Ca^{2+} that can persist for ~ 30 minutes in cultured astrocytes. This suggests that mitochondrial Ca^{2+} uptake plays an essential role in the clearance of physiological intracellular Ca^{2+} loads (Boitier et al., 1999).

Interestingly, altering mitochondrial Ca^{2+} buffering alters the release probability of glutamate from cultured astrocytes. Reyes and Parpura decreased mitochondrial Ca^{2+} handling with the mitochondrial un-coupler carbonyl cyanide p-trifluoromethoxy-phenyl-hydrazone (FCCP, 1 μM), which depolarises the mitochondria by disrupting the H^+ gradient of the inner membrane and found that this increased glutamate release from astrocytes. Increasing mitochondrial Ca^{2+} accumulation with CGP37157 (an mNCX blocker, which blocks mitochondrial Ca^{2+} efflux) resulted in increased glutamate release by astrocytes (Reyes and Parpura, 2008). These data suggest that intracellular Ca^{2+} levels are directly correlated with glutamate release and more importantly altering the Ca^{2+} buffering capacity of mitochondria can affect this phenomenon (Reyes and Parpura, 2008). Taken together, this reveals that the ability of mitochondria to buffer Ca^{2+} in astrocytes is important in terms of both astrocyte functionality and neuronal signalling. Ca^{2+}-dependent gliotransmission has been shown to have important consequences for synaptic transmission and plasticity (Navarrete et al., 2013, Perez-Alvarez et al., 2014, Volterra et al., 2014). Moreover, in a model of AD, astrocytes show elevated resting Ca^{2+}, increased Ca^{2+} transients and enhanced intracellular Ca^{2+} waves (Kuchibhotla et al., 2009), all of which, may contribute to elevated gliotransmitter release.

In addition, Simpson and Russel showed that mitochondria in cultured astrocytes are found in close association with sarcoplasmic/endoplasmic reticulum Ca^{2+}-ATPase (SERCA)-expressing ER sites (Simpson and Russel, 1998). This close association infers that mitochondria are important for the propagation of Ca^{2+} released from nearby ER IP_3Rs/RyRs. Csordas and colleagues showed, using drug-inducible fluorescent inter-organelle (Pericam-tagged) linkers (FKBP-FRB heterodimerization system) in a basophilic leukaemia RBL-2H3 cell line, that increasing the distance between the outer-mitochondrial membrane (OMM) and the ER to ~ 15 nm enhanced the efficiency of Ca^{2+} transfer from the ER to the mitochondria. In contrast, reducing the mitochondria–ER gap to 5 nm blocked the accommodation of IP_3Rs (shown to protrude ~ 10 nm from the ER membrane) and thus prevents efficient ER-mitochondria Ca^{2+} transfer (Csordas et al., 2010). Moreover, structural and functional analysis has revealed zones of close contact between mitochondria and the ER called mitochondria-associated ER membranes (MAMs) (Giorgi et al., 2009). MAMs enable highly efficient lipid exchange and transmission of Ca^{2+} from ER to mitochondria (Hayashi-Nishino et al., 2009, Scharwey et al., 2013). In addition, the close association of mitochondria and the ER occurs during apoptosis, where MAPL induces an interorganellar platform between the ER and mitochondria by SUMO (Small Ubiquitin-like Modifier 1)-ylating Drp1, stabilizing its oligomeric form (Prudent et al., 2015). This is required to drive the disassembly of OPA1 oligomers, which leads to remodelling of the mitochondrial cristae and cytochrome c release (Prudent et al., 2015). However, discerning the components of ER–mitochondria contact sites and the regulation of Ca^{2+} and lipid exchange at the MAMs within astrocytes remains to be resolved.

1.5.2 Potential routes for elevating astrocyte Ca^{2+}

Many potential routes exist for elevating astrocyte intracellular Ca^{2+} and factors that determine which route is involved include age or stage of development and brain region (Verkhratsky et al., 2012, Rusakov et al., 2014). The most established route is via synaptic glutamate activation of group I mGluRs, in particular mGluR5, which trigger G-protein-coupled receptor cascades via Ca^{2+} release from internal stores (Cai et al., 2000, Carmignoto, 2000, D'Ascenzo et al., 2007, Fellin et al., 2007, Rusakov et al., 2014). Activation of these mGluRs induces the release of gliotransmitters (D'Ascenzo et al., 2007, Fellin, 2009).

1.5.2.1 Release from internal stores

Release of Ca^{2+} from the ER internal stores, via activation of both RyR and IP_3Rs, contributes to an increase in intracellular Ca^{2+} in astrocytes (Hua et al., 2004). Interestingly, Boitier and colleagues showed using cultured astrocytes, that ER-induced intracellular Ca^{2+} was followed by an increase in mitochondrial Ca^{2+} (Boitier et al., 1999). Genetically removing IP_3R2 (knock out (KO) mouse) seemed to abolish Ca^{2+} transients in astrocytes. In these mice no neuronal deficits were observed and this lead to the premature conclusion that astrocyte Ca^{2+} signalling was not involved in maintaining neuronal function (Agulhon et al., 2010). However, Srinivasan and colleagues found that IP_3R2 KO mice do exhibit Ca^{2+} transients both in the soma (although these were dramatically reduced) and processes (Srinivasan et al., 2015). They determined that somatic Ca^{2+} responses mainly result from internal store release,

while Ca^{2+} responses in the processes occur as a result of entry from the extracellular environment and are not dependent on internal store release of Ca^{2+} (*in vitro* and *in vivo*). IP_3R2 KO mice also exhibited frequent *in vivo* cortical astrocyte Ca^{2+} fluctuations (in the soma and processes) in response to a 3 second air puff to the space (startle response). They reveal an early and late stage of Ca^{2+} fluctuations. The early stage appeared to be dependent on alpha1-adrenergic receptors, while the late stage was neither dependent on alpha1-adrenergic receptors or IP_3R2 receptors (Srinivasan et al., 2015).

1.5.2.2 Store-operated Ca^{2+} channels (SOCs)

Ca^{2+} entry from the extracellular space can occur via store-operated Ca^{2+} channels (SOCs) (these include TrpC1 channels) when the internal ER Ca^{2+} stores are depleted in astrocytes. This also triggers significant mitochondrial Ca^{2+} transients (Lo et al., 2002, Golovina, 2005, Singaravelu et al., 2006, Malarkey et al., 2008), which implies that mitochondria may be in close association with the astrocytic plasma membrane. In addition, compromising mitochondrial Ca^{2+} buffering, through mNCX silencing, reduced SOC entry. These results reveal the importance of mitochondrial Ca^{2+} handling, and in particular mNCX activity, for proper regulation of intracellular Ca^{2+} through SOC-dependent Ca^{2+} entry in astrocytes (Parnis et al., 2013).

1.5.2.3 Ionotropic glutamate receptors (iGluRs)

Ionotropic glutamate receptors (iGluRs- NMDA and AMPA receptors) represent another route for astrocyte Ca^{2+} entry. However, it is important to note that separating the

contributions of neuronal and astrocyte NMDARs is difficult. Initially, immunocytochemical analysis of adult rat cortical astrocytes showed that some distal processes, and only rarely cell bodies, express the NMDAR subunits NR1 and NR2A/B (Conti et al., 1996). NR1, NR2B and NRC subunits were also detected in mouse cortices by polymerase chain reaction (PCR), which amplifies DNA from specifically targeted genes, if they are present (Schipke et al., 2001). Glutamate and NMDA induced Ca^{2+} transients in cultured cortical rat astrocytes (Zhang, 2003, Palygin et al., 2010) and NMDA evoked Ca^{2+} transients in cortical slice astrocytes (astrocyte responses were measured by whole-cell patch clamp) (Schipke et al., 2001, Lalo et al., 2006). It has also been confirmed that human astrocytes (foetal and adult) express all known NMDAR subunits (NR1, NR2A-D, NR3A-B) and that these receptors are functional, inducing Ca^{2+} influx upon stimulation (Lee et al., 2010). More recently, a transcriptome screen (RNAseq) revealed that NR2C was the most highly expressed NMDAR subunit in astrocytes (Zhang et al., 2014). In addition, astrocytic NMDARs are not blocked by magnesium (Mg^{2+}) as greatly as neuronal NMDARs (Lalo et al., 2006). Interestingly, transient global forebrain ischemia was shown to result in the expression of functional (NR2B containing) NMDARs in the CA1 and subicular regions of the hippocampus (Krebs et al., 2003). Moreover, glutamate was shown to illicit Ca^{2+} entry via these astrocyte NMDARs. However, while the presence of functional astrocytic NMDARs in rodents and humans is apparent in the cortex, the existence of NMDARs in hippocampal astrocytes, under physiological conditions, is still debated. TTX-resistant NMDA-induced Ca^{2+} responses were reported in astrocytes in hippocampal slices of young rats (< 12 days) (Porter and McCarthy, 1995) but not in mature rats (Shelton and McCarthy, 1999). These results suggest that age and preparation could influence whether or not hippocampal astrocytic NMDARs are concluded to be present and functional. AMAPA receptors have also been shown to play a role in

mediating Ca^{2+} entry (Araque et al 2001). This suggests that astrocytes may utilise ionotropic glutamate receptors, thus providing a greater arsenal for glutamate buffering at the synapse by astrocytes.

1.5.2.4 Endothelin receptors (ERTs)

Ca^{2+} influx has also been proposed to occur via G_q protein-coupled endothelin receptors (ETRs) (Srinivasan et al., 2015). Edothelin binds to ETRs and induces astrocyte Ca^{2+} influx. Purinergic receptors are also capable of eliciting astrocyte Ca^{2+} influx. Studies of astrocytes in culture (Neary et al., 2003) and in brain slices (Porter and McCarthy, 1996) revealed robust Ca^{2+} responses to ATP and to more selective agonists of specific purinergic receptors. Astrocytes were found to express P2Y1, P2Y2, P2X1-4, P2X6 and P2X7 purinergic receptors (Fields and Burnstock, 2006; Hashioka et al., 2014) and ATP signalling was shown to regulate Ca^{2+}-dependent glutamate release via astrocyte P2Y metabotropic G-protein-coupled receptors (Guthrie et al., 1999). Additionally, P2X7 ionotropic receptor activation is capable of mediating the release of glutamate from astrocytes, which is dependent on increases in intracellular Ca^{2+} (Duan et al., 2003). Interestingly, P2Y receptor antagonists have been proposed as potential neuroprotective agents in the hippocampus, cortex and cerebellum following neuronal death associated with neurodegenerative diseases such as Alzherimer's, Parkinson's, Huntington's disease as well as Amyotrophic lateral sclerosis (Volonte et al., 2003). In addition, activation of purinergic signalling in astrocytes via P2Y4 receptors, which can be induced by instances of trauma, stimulates the release of thrombospondin-1, an extracellular matrix molecule that induces synapse formation during development and might have a role in CNS repair and remodelling after injury (Tran and Neary, 2006).

1.5.2.5 Alpha1-adrenergic receptors

Alpha1-adrenergic receptors have also been shown to play a role in regulating intracellular Ca^{2+} signals in astrocytes. Locus coeruleus released norepinephrine (induced by whisker stimulation or air-puff startle response) gave rise to long-range Ca^{2+} signals through activation of astrocytic alpha1-adrenergic receptors *in vivo* (Ding et al., 2013). Locomotion also induced astrocyte Ca^{2+} signals that were blocked by Terazosin (a selective alpha1-adrenergic receptors antagonist) (Paukert et al., 2014). Norepinephrine acting on alpha1-adrenergic receptors induces G_q-protein coupled increases in intracellular astrocyte Ca^{2+}.

1.5.2.6 Transient receptor potential A1 (TrpA1) channels

Shigetomi and colleagues showed that transient receptor potential A1 (TrpA1) channels induce Ca^{2+} responses in membrane microdomains in astrocytes (using the membrane tethered genetically encoded Ca^{2+} indicator (GECI) Lck-GCaMP3) (Shigetomi et al., 2013). They used the specific TrpA1 antagonist HC030031 to block these microdomain Ca^{2+} responses in astrocyte in slices. These TrpA1-mediated transients appear important for maintaining signalling at the inhibitory synapse (where HC030031 reduced CA1 pyramidal neuron mini inhibitory postsynaptic currents (mIPSCs)). Ca^{2+} signalling in astrocytes was also shown to affect the levels of extracellular GABA and therefore inhibitory signalling. The study finds that TrpA1-mediated Ca^{2+} transients regulate GAT-3-dependent astrocyte GABA influx, which impacts on interneuron mIPSCs.

1.5.2.7 Nicotinic acetylcholine receptors (nAChRs)

Nicotine influences memory by inducing synaptic transmission at acetylcholinergic synapses (Kenney and Gould, 2008). Astrocytes express nicotinic acetylcholine receptors (nAChRs) (Gahring et al., 2004, Hernandez-Morales and Garcia-Colunga, 2009) and nicotine binding to astrocyte nAChRs increases intracellular Ca^{2+} concentrations (Sharma and Vijayaraghavan, 2001) and stimulates the release of D-serine (Lopez-Hidalgo et al., 2012). D-serine binding postsynaptic NMDARs allows the ion flux necessary for inducing LTP (Lopez-Hidalgo et al., 2012). Interestingly, in AD, patients treated with nicotine exhibited improved cognitive function (Rangani et al., 2012). Similarly, activation of muscarinic acetylcholine receptors (mAChR) also increases intracellular Ca^{2+} concentrations (Shelton and McCarthy, 1999).

1.5.2.8 Glutamate transporter-mediated entry

Glutamate, released during synaptic activity, can be taken up by the astrocyte glutamate transporters (GLT-1) along with Na^+. The plasma membrane Na^+/Ca^{2+} exchanger (NCX) extrudes Na^+ and brings Ca^{2+} into the cell (Goldman et al., 1994, Rojas et al., 2008, Reyes et al., 2012, Jackson et al., 2014). During low levels of activity the NCX extrudes Ca^{2+} in exchange for Na^+ (Goldman et al 1994). Jackson and colleagues report that blocking the reverse mode of the NCX (blocking Ca^{2+} entry) increases mitochondrial trafficking in astrocytes. From this, they hypothesise that neuronal activity regulates glutamate transporter induced Ca^{2+} entry (via the NCX), which arrests mitochondria at sites of glutamate uptake.

Due to the many potential routes that have been implicated in mediating the influx of astrocyte Ca^{2+}, it can be concluded that astrocytes are highly variable in the channels and receptors they express (Verkhratsky et al., 2012, Rusakov et al., 2014). It may be that astrocytes are plastic in the components they exhibit, altering which receptors or channels are present on their membrane in response to their surrounding environment. It may be that this is regulated by neuronal-secreted factors. Thus, narrowing down the mechanisms involved in elevating astrocyte Ca^{2+} and the downstream impact on mitochondrial trafficking requires further clarification. The interplay between mitochondrial trafficking and intracellular Ca^{2+}, in response to astrocyte activation, may be important for regulating their proximity to glutamate release sites i.e. synapses.

1.6 Mitochondrial quality control - Fission, Fusion and Mitophagy

Mitochondria are dynamic organelles that constantly undergo fission and fusion events, which profoundly alter their morphology. These events ensure sufficient exchange of genetic material and proteins amongst the mitochondrial network, which is essential for proper mitochondrial function (Chang et al., 2006). Fission is the process of elongated mitochondria breaking into smaller more rounded mitochondria involving Drp1 and the fission 1 protein (Fis1). Fusion is instead the formation of elongated mitochondria from smaller mitochondria and involves the mitofusins (Mfn1 and Mfn2) as well as OPA1 (Chang and Reynold 2006; Leisa et al 2009).

1.6.1 Fission and fusion

Under basal conditions, astrocyte mitochondria undergo fission and fusion events (50 % of events were fusion and 50 % fission) in acute cortical slices (Motori et al., 2013). Pharmacologically elevating intracellular Ca^{2+} in astrocytes resulted in remodelling or rounding of mitochondrial (Tan et al., 2011). Although the functional relevance of altering mitochondrial morphology is not clear, it may affect their ability to buffer Ca^{2+} and release ATP. Longer mitochondria, perhaps, might allow a greater area for ATP production and Ca^{2+} buffering, while it may be easier for shorter, more rounded mitochondria to position themselves in spatially restricted regions of the cell (i.e. very fine astrocyte processes or near synapses in neurons) (Chang and Reynolds, 2006).

Interestingly, cellular injury alters the balance between mitochondrial fission and fusion events in astrocytes. Cortical injury and treatment with pro-inflammatory stimuli in acute slices induced rapid mitochondrial fission, along with an increase in Drp1 activity (Mortori et al., 2013). The induced inflammatory insult induces the production of nitric oxide (NO), which activates Drp1 and induces mitochondrial fission in astrocytes. ATP production was compromised in fragmented astrocyte mitochondria and the generation of ROS was elevated, affecting cell survival (Mortori et al., 2013). NO, itself, can alter gene transcription, mitochondrial respiration and induce cell death by apoptosis, directly. Interestingly, inducible nitric oxide synthase (iNOS), which catalyses the production of NO from L-arginine, was elevated in astrocytes (significantly more than in neurons) from AD patient tissue (Heneka et al., 2001) and mouse models of AD (Heneka et al., 2005). These results reveal the importance of identifying the mechanisms that regulate mitochondrial morphology in astrocytes as well as how it is dysregulated during disease.

1.6.2 Mitophagy

Mitophagy is the process by which damaged mitochondria are degraded. Upon mitochondrial damage or stress, various proteins are recruited to their surface, which targets them for lysosomal degradation. Lysosomes are vesicles that contain hydrolytic enzymes that are capable of degrading virtually every type of biomolecule, thus it acts as the cell's waste disposal system. The main pathway for mitochondrial degradation involves activation of phosphatase and tensin homologue deleted on chromosome 10-induced putative kinase 1 (PINK1) and the E3 ubiquitin ligase, parkin. Upon mitochondrial damage, PINK1 accumulates on the OMM, recruits parkin from the cytosol and activates it by phosphorylation. Activated parkin then ubiquitinates various substrates on the OMM. These include VDAC1 (voltage-dependent anion channel 1), Drp1, Mfns, TOM (translocase of OMM)-20 and Tom-40 (Cai et al., 2012). Ubiquitination is the process of accumulation of the protein ubiquitin (a small regulatory protein). This physically alters the structure of the protein being ubiquitinated and signals for it to be degraded by the lysosome.

Once ubiquitinated by active parkin, mitochondria are subsequently recognized by ubiquitin-binding autophagic components, e.g. LC3 (microtubule-associated protein light chain 3), HDAC6 (histone deacetylase 6) and p62 sequestosome, that promote the formation of autophagosomes and induce mitochondrial clearance by fusion with lysosomes. Loss-of-function PINK1/parkin mutations have been associated with forms of early-onset PD (Exner et al., 2012).

1.6.3 The role of Miro in mitophagy

Miro has also recently been shown to be involved in the cascade that regulates mitophagy (Wang et al., 2011, Tsai et al., 2014). It has been identified as a substrate for Parkin mediated-ubiquitination (Birsa et al., 2014) and PINK1-mediated phosphorylation (Wang et al., 2013 leading to its degradation thus preventing trafficking of damaged mitochondria and allowing for their clearance (Wang et al., 2011, Liu et al., 2012, Birsa et al., 2013). These findings suggest a possible link between Miro-mediated transport pathways and PD-associated disruption of mitochondrial turnover.

1.6.4 Mitophagy in astrocytes

Interestingly, parkin dysfunction has been shown to impair mitochondrial function in astrocytes and contribute to the pathogenesis of PD (Ledesma et al., 2002). Glial cells cultured from parkin-null mice exhibited increased expression of pro-apoptotic proteins and reduction in heat-shock protein 70, which is protective. Together this contributes to decreased neuroprotection by astrocytes (Solano et al., 2008). Moreover, Ledesma et al. 2002 have shown that astrocytes express lower levels of parkin, which has been suggested to exhibit differences in subcellular distribution compared to neurons. These data warrant further investigation into the importance of astrocyte specific differences in parkin expression and localisation, the cellular response to a lack of parkin, and the subsequent effect on PD pathogenesis.

Regulation of the autophagy (programmed cell death) machinery is crucial for mitochondrial clearance and affects mitochondria function in astrocytes (Motori et al. 2013). For example,

knocking out the gene encoding Atg7 (essential for autophagosome production and lipidation of LC3-B), in astrocytes, resulted in highly hyperfused mitochondria, ROS production and ultimately cell death (Motori et al. 2013). Importantly, Motori and colleagues highlight that a failure to maintain the functional architecture of mitochondria affects astrocyte survival (Motori et al. 2013). With amyloid-β peptide treatment (a model of AD) astrocyte Ca^{2+} overload occurred along with excessive ROS production. This was observed to induce mitochondrial depolarisation through activation of the DNA repairing enzyme poly ADP-ribose polymerase-1 (PARP-1) and opening mitochondrial permeability transition pore (mPTP) (Angelova and Abramov, 2014).

A recent discovery by Davis and colleagues revealed that RGC axons shed mitochondria at the optic nerve head (ONH) that are internalized and degraded by adjacent astrocytes. They show that axonal mitochondria accumulate in large protrusions that are subsequently pinched off to form membrane-enclosed evulsions that are engulfed by astrocytes. Axonal mitochondria were confirmed within adjacent astrocytes, exhibiting phagocytic activity (high expression of the phagocytic marker Mac2) (Davis et al., 2014). This process was termed transcellular mitophagy and is predicted to be a widespread phenomenon, occurring elsewhere in the CNS (Davis et al. 2014).

Taken together these data suggest that the pathway of mitophagy exists in astrocytes, but it remains to be determined how similar or dissimilar this mechanism is to neurons. Many questions exist regarding the components involved in the putative astrocyte mitophagy pathway and also how it may be regulated.

1.7 Implicating astrocyte mitochondria in disease

It has been mentioned previously in this thesis that astrocytes provide both structural and energetic support for neurons. However, relatively little attention has been given to establishing the link between maintaining mitochondrial function in astrocytes and neuronal dysfunction. Some evidence does exist that directly implicates astrocyte mitochondrial dysfunction in neurological disorders (Table 1.1).

1.7.1 Alzheimer's disease (AD)

Alzheimer's disease (AD) is a chronic, progressive neurodegenerative disease where amyloid plaques, neurofibrillary tangles and tauopathies result in synapse and neuron loss (Abramov et al., 2004). Interestingly, a model of AD (beta-amyloid peptide treatment) causes loss of the mitochondrial resting membrane potential, inducing free radical production and oxidative stress specifically in astrocytes and not in neurons (Abramov et al., 2004). This impaired the ability of the astrocytes to maintain neuronal integrity and ultimately resulted in neuronal damage. It is particularly important to note that any mitochondrial phenotype in this model of AD precedes any neuronal phenotype. Interestingly, the astrocyte mitochondrial response to β-Amyloid was supressed by antioxidants (TEMPO).

Another interesting study conducted by Angelova and Abramov 2014, revealed that in a model of AD (amyloid-β peptide, Aβ), Ca^{2+} signalling was elevated in astrocytes but not in neurons. This was due to the high levels of membrane cholesterol expression in astrocytes. Aβ significantly reduced the levels of glutathione (GSH) in neurons and astrocytes, an effect that was dependent on Ca^{2+} entry from external sources. Altering membrane cholesterol

regulation modified the astrocyte response to Aβ (elevated Ca^{2+} signalling, ROS production and mitochondrial depolarisation), which lead to improved neuroprotection (Angelova and Abramov, 2014, Narayan et al., 2014). This indicates that astrocyte intracellular Ca^{2+} regulates mitochondrial function and that both are disrupted in disease.

1.7.2 Huntington's disease (HD)

Huntington's disease (HD) manifests in preferential striatal neurodegeneration associated with mitochondrial dysfunction (Shin et al., 2005). In a model of HD (expression of mutant Huntington, mHtt), astrocyte mitochondrial dynamics were severely disrupted. mHtt impaired mitochondrial Ca^{2+} buffering and altered their membrane permeability, which can be particularly damaging (Oliveira, 2010). Mice expressing mHtt specifically in astrocytes show weight loss, have motor function deficits, and premature mortality compared to WT or control transgenic mice (Bradford et al., 2009). Brains from HD patients and from mouse models of HD show accumulation of mHtt in striatal astrocytes (Bradford et al., 2009). mHtt also decreased GLT-1 and GLAST expression, which are critical for the uptake and subsequent detoxification of glutamate (Oliveira, 2010). The compromised ability of astrocytes to buffer glutamate, at the synapse, decreased the threshold for excitotoxic neurodegeneration (Oliveira, 2010). These results indicate a potential new therapeutic target for HD.

1.7.3 Parkinson's disease (PD)

Parkinson's disease (PD) is a progressive neurodegenerative disorder, caused by the death of dopaminergic neurons in the Subtantia nigra. It manifests in resting tremors with impairments in movement. Similarly, expression of proteins containing PD-related gene mutations (for

example, human protein deglycase DJ-1 mutations) in cultured astrocytes impairs mitochondrial dynamics. This compromises their neuroprotective ability and thus renders neurons more sensitive to toxic insults (Larsen et al., 2011, Schmidt et al., 2011, Lev et al., 2013).

1.7.4 Amyotrophic lateral sxlerosis (ALS)

Amyotrophic lateral sclerosis (ALS) or motor neuron disease (MND) is characterised by degeneration of motor neurons in the spinal cord, brain stem and motor cortex. It results in progressive muscle weakness, atrophy and spasticity (Wong et al., 1995). In mutant SOD-1 astrocytes, a model of ALS/MND, mitochondria displayed severely impaired oxygen consumption and respiratory control, increased ROS production and disrupted membrane potential. This deceased the ability of the astrocytes to sustain motor neuron survival. However, mitochondrial-targeted antioxidants prevented this neuronal death (Wong et al., 1995, Cassina et al., 2008).

1.7.5 Epilepsy

In addition, specific disruption of astrocyte mitochondrial function has dramatic consequences for aspects of neuronal function and in some cases survival. Treatment with flurocitrate (FC) induced specific disruptions in astrocyte mitochondrial function and resulted in focal, followed by global epileptiform activity (epilepsy) with some animals exhibiting convulsive seizures (Volobouéva et al., 2007). This resulted in neuronal damage and eventual death. In addition to this, abnormal synapse development, function and elimination were observed along with an imbalance in the E/I balance.

1.7.6 Other diseases and disorders

Other diseases such as Down's syndrome, Fragile X, and Rett Syndrome all exhibit astrocyte defects, impacting on neuronal development and/or function, but their impact on astrocyte mitochondrial function remains unclear. Fragile X syndrome (FXS) is the most common form of inherited mental impairment, and typically results from the transcriptional silencing of the FMR1 (fragile X mental retardation 1) gene and loss of the protein, FMRP (fragile X mental retardation protein) (Bhakar et al., 2012). FXS symptoms include neurodevelopmental delay, anxiety, hyperactivity, motor abnormalities, autistic-like behaviour and epilepsy. FMRP was thought to be expressed only in neurons, however, it was more recently shown to have specific roles in astrocytes (Pacey and Doering, 2007), where it is expressed at might higher levels (Cahoy et al., 2008). In FXS, astrocytes contribute to abnormal dendrite and synapse development in Fmr1 (loss of which induces Fragile X) deficient mice (Jacobs and Doering, 2010).

These data highlight the need to elucidate the mechanisms that regulate mitochondrial function in astrocytes. Mitochondrial trafficking may be actin or microtubule dependent (Jackson et al., 2014) but the exact motor proteins are unknown. The regulation of mitophagy in astrocytes is another important mechanism that remains to be addressed.

Astrocytopathy /pathology	Manifestation/cause	Consequence for astrocyte mitochondria	Impact on neural function /development	References
Huntington's Disease	Preferential striatal neurodegeneration associated with mitochondrial dysfunction. *Huntingtin* gene (Htt) mutation.	Mutant *Huntingtin* (mHtt) impaired mitochondrial Ca^{2+} buffering and altered permeability transition (mPT). mHtt also decreased expression of GLT-1 and GLAST	mHtt compromises neuroprotective role of astrocytes by impairing synaptic glutamate clearance (decreasing the threshold for excitotoxic neurodegeneration). Astrocyte mitochondrial impairment may disrupt protective astrocyte-neuron lactate trafficking or result in increased production of damaging ROS	Oliveira 2010 Shin *et al.*, 2005 Bradford *et al.*, 2009
Alzheimer's Disease (AD)	Amyloid plaques, neurofibrillary tangles and tauopathies resulting in synapse and neuron loss.	β-amyloid (model of AD) causes loss of mitochondrial potential (Δψm) inducing free radical production and oxidative stress in astrocytes but not in neurons	Impairs the abilty of astrocytes to maintain neuronal integrity and results, eventually, in neuronal damage	Abramov *et al.*, 2004 Song *et al.*, 2014
Amyotrophic lateral sclerosis (ALS) / Motor Neuron Disease (MND)	Degeneration of motor neurons of the spinal cord, brain stem and motor cortex. Results in weakness, atrophy and spasticity	Mitochondria in mutant SOD1 (G93A- model of ALS) astrocytes display severely impaired oxygen consumption and resipiratory control, increased superoxide production and Δψm	Mitochondrial dysfunction results in decreased ability to sustain motor neuron survival. Can be prevented by mitochondrial-targeted antioxidants	Wong *et al.*, 1995 Cassina *et al.*, 2008
Parkinson's Disease (PD)	Progressive, neurodegenerative disorder caused by death of subtantia nigra, dopaminergic neurons. Resting tremours present with impaired movement	DJ-1 gene knock-down (model of PD) in astrocytes co-cultured with WT neurons showed decreased mitochondrial mobility. DJ-1 KD appeared to enhance the damaging effects of rotenone in astrocytes	DJ-1 KO and KD in astrocytes impaired their neuroprotective ability, rendering neurons more sensitive to toxic insults	Lev *et al.*, 2013 Larsen *et al.*, 2011
Epilepsy	Seizures characterised by a-synchronous brain activiy	Selective, focal disruption of astrocyte mitochondria (using fluorocitrate (FC)) induced, focal followed by generalized epileptiform discharges, with some animals exhibiting convulsive seizures	FC-induced epileptiform discharges resulted in neuronal damage and eventual loss. Abnormal synapse development, function and elimination along with impairment of the excitatory-inhibitory balance was also observed.	Willoughby *et al.*, 2003 Volobouéva *et al.*,2007 Auerbach *et al.*, 2011
Inflammation	Astrogliosis and glial scar formation	During cortical injury mitochondria are fragmented in lesion core and elongated in scar region (penumbra). Pro-inflammatory stimuli increased fission, reduced respiratory capacity and increased ROS production. Restoring mitochondrial architecture requires autophagy.	Astrocytes can exert both pro- and anti-inflammatory functions. Astrocyte scars serve as critical barriers that restrict the spread of inflammatory cells away from sites of tissue damage. This serves to reduce neurodegeneration of nearby neruons	Mortori *et al.*, 2013 Sofroniew, 2005
Excitotoxicity	Dysregulated energy production	Glutamate induces a pH-mediated decrease in oxygen consumption rate i.e. disrupted ability to synthesize ATP	Spine head protrusions were inhibited by blocking astrocyte glutamate uptake. Astrocyte glutamate uptake is crucial for limiting the excitotoxic effect of glutamate on neurons	Azarias *et al.*, 2011 Verbich *et al.*, 2012 Volobouéva *et al.*,2007
Ischaemia	Restricted blood supply resulting in a build up of toxic waste, inflammation and mitochondrial damage	Long-lasting Δψm, Ca^{2+} overload, cytochrome C release and eventual cell death	Removes neuroprotective role of astrocytes compounding neuronal damage	Kintner *et al.*, 2007 Li *et al.*, 2008
Down's Syndrome	Mental retardation		Astrocytes from patients grown with wild-type (WT) neurons have abnormal spine development and reduced synaptic density and activity	Garcia *et al.*, 2010
Fragile X	Cognitive impairment, autistic characteristics, epilepsy and motor abnormalities		Astrocytes contribute to abnormal dendrite and synapse development in Fmr1 (loss induces fragile X) deficient mice. Normal astrocytes prevent effects in neurons from Fmr1-deficient mice	Jacobs *et al.*, 2010
Rett Syndrome	Loss of astrocyte methyl-CpG-binding protein 2 (MeCP2). Autism and cognitive impairment		MeCP2 deficient astrocytes shown to impair neuronal outgrowth and dendrite development	Ballas *et al.*, 2009

Table 1.1 Astrocyte dysfunction implicated in the pathogenesis of neurological disorders and diseases along with the resulting impact on neural function.

1.8 Thesis aims

1. Extensively characterise the nature of basal mitochondrial trafficking in astrocyte processes compared to neurons and establish a link, if any, between neuronal signal transmission and mitochondrial trafficking dynamics in astrocytes.

2. Define the role of Miro1 in astrocytes through the functional relevance of mutating the EF-Ca^{2+}-sensing hands of Miro1 on mitochondrial trafficking and positioning as well as the impact on cytosolic Ca^{2+} regulation and synapse formation.

3. Define the role of knocking-out astrocyte Miro1 on mitochondrial trafficking and positioning in astrocytes, as well as the functional consequences for neuronal synapse formation i.e. does this link to a potential disease phenotype?

Chapter 2

Materials and Methods

2.1 Cell culture

2.1.1 Primary neuronal cultures

Primary hippocampal neuronal cultures were isolated from E18 Sprague-Dawley rats of either sex as described previously (Banker and Goslin, 1998) with some modifications. Isolated hippocampi were incubated in 0.25 % trypsin (diluted in dissection media) for 15 minutes at 37'C. Pelleting the cells and resuspending in attachment media (Minimal Essential Media (MEM) (Gibco), 10 % heat-inactivated horse serum (HRS) (Gibco), 1 mM sodium pyruvate, 0.6 % glucose) removed the trypsin solution. Following trituration, which involved passing the tissue through a narrow fire polishes glass Pasteur multiple times until a cloudy suspension forms, cells were counted using a Neubauer Haemocytometer and cell viability was assessed by erythrosin B exclusion. 350, 000 cells were plated in 6 cm dishes containing

13 mm coverslips pre-coated with poly-L-lysine (500 mg/ml) and attachment media. Attachment media was changed the following day to maintenance media (Neurobasal Medium (NB) (Gibco), B27 supplement (Gibco), 2 mM L-Glutamine, 10 U/mL penicillin and 100 μg/mL streptomycin (Pen-Strep), 0.6 % glucose). These cultured neurons were used as mixed cultures due to the presence of astrocytes. The number of astrocytes present could be amplified or minimised by adjusting the length of time the culture initially spent in serum-containing-attachment media. Cultures were maintained at 37°C with 5 % CO_2 in a humidified incubator.

2.2.2 Preparation of primary astrocytes

Primary cultures of astrocytes were prepared from E18 Sprague-Dawley rats or transgenic Rhot1 mouse lines (E16) as previously described (Banker and Goslin, 1998, Al Awabdh et al., 2012) with some modifications. Cells were treated with 0.25 % trypsin and titurated by passing through a narrow glass Pasteur and, following pelleting, resuspended and maintained in Dulbecco's modified Eagle's medium (DMEM) (Gibco) with 20 % heat-inactivated foetal bovine serum (FBS) (Gibco) and 1 % Pen-Strep (10 U/ml, 100 μg/ml) at 37°C with 5 % CO_2 in a humidified incubator. Media was changed initially the day after plating and subsequently every 5 days until confluency was reached (7-10 days after plating). Cells were passaged after reaching 80-90 % confluency. Purity of these cultures has been previously described as being > 98 % by electron microscopy morphological studies, cell marker expression and pharmacological responsiveness (containing < 2 % OPCs and microglia) (Schildge et al., 2013).

2.2.3 Transgenic cultures

The *ras homolog family member T1* (*Rhot1*) transgenic mouse line (MBTN;EFD0066_2_F01;Allele:Rhot1$^{tm1a(EUCOMM)Wtsti}$) was obtained from the Wellcome Trust Sanger Institute as part of the International Knockout Mouse Consortium (IKMC) and were produced using the Knockout-First strategy to target *Rhot1* in JM8.F6 embryonic stem cells (C57BL/6N background) backcrossed to C57BL/6J-Tyrc-Brd. Animals were set up for breeding and were maintained by Guillermo Lopez-Domenech and Josef Kittler under controlled conditions (temperature 20 ± 2°C; 12 hour light- dark cycle). Food and water were provided *ad libitum*.

2.1.4 Preparation of transgenic cultures

For Rhot1 transgenic mouse cultures, coverslips were prepared as described in the section above. To gain *Rhot1*-/- cortical astrocytes or hippocampal neurons, heterozygous pairs were crossed and animals were taken from the pregnant female when embryos are at embryonic day 16 (E16). All pups were kept separate during the dissection stages and a tissue sample from the tail of each embryo was taken in order to allow genotyping (Table 2.1.1).

After dissecting the cortices or hippocampi in ice-cold HBSS, each embryonic cortical or hippocampal pair was incubated in 0.2 % trypsin and 5000 units/mL DNAse for 12 minutes at 37ºC. The tissue was then washed twice in HBSS before trituration in 1 mL attachment medium as described previously. Neurons were then plated at the same concentration as above (350, 000 cells plated in 6 cm dishes containing 13 mm coverslips pre-coated with poly-L-lysine (500 mg/mL)). Astrocytes were plated at roughly double the density of neurons and plated in dishes without coverslips.

2.1.5 Genotyping Rhot1 transgenic lines

To extract deoxynucleic acid (DNA) for genotyping, 65 µl of alkaline buffer (0.2 mM disodium ethylenediaminetetraacetic acid (EDTA) and 25 mM NaOH) was added to 1 mm long tissue samples (tail tips) placed in thermo cycler tubes from each pup in order to dissolve the tissue. To further aid this process, the samples were incubated in a polymerase chain reaction (PCR) machine at 94°C for 45 minutes, and then chilled to 4ºC. To neutralize the alkaline buffer, a tris(hydroxymethyl)aminomethane (Tris)-HCl based solution (65 µl, 40 mM Tris-HCl) was added to each sample.

The genotyping PCRs were then run using the components listed in table 2.1.1. Two different PCRs were run using the sample, one to detect the wildtype or mutant Rhot1 allele using forward primer 5'-TTAGGATTTGTACTTTGCCCCTG-3', reverse primer 5'-AAAACCCTTCCTGCATCACC-3' and Cassette primer 5'-TCGTGGTATCGTTATGC-GCC-3'. The first two primers anneal to the wildtype allele and give a longer PCR product of an expected band size of 546 bp, whereas the cassette primer together with the reverse primer anneal to the *Rhot1* mutant allele and give a shorter expected band of 277 bp and a separate PCR was run to detect the *lacZ* using forward primer 5'-ATCACGACGCGCTGTATC -3' and reverse primer 5'-ACATCGGGCAAATAATATCG-3'. The primer sequences were taken from the protocol supplied with the animals by Sanger. The PCR was performed in 30 cycles at an annealing temperature of 58°C and using an extension time of 45 s.

On occasion the genotyping was performed externally by Stuart Martin (UCL) using the same protocol.

PCR reaction - components:	Final concentrations:
4 μL 5x MyTaq buffer	1x
0.5 μL forward primer	0.1 μM
0.5 μL reverse primer	0.1 μM
1 μL lysate	-
13.3 or 13.8 μL milliQ water	-
0.125 μL MyTaq enzyme	0.125 U

Table 2.1.1 Genotyping Polymerase Chain Reaction

2.1.6 Passaging/splitting cells

Once grown to confluency (around 90 %) trypsin solution was added (137 mM NaCl, 2.7 mM KCL, 8 mM Na_2HPO_4, 1.5 mM KH_2PO_4, 2.5 g/L trypsin (from porcine pancreas, Sigma), 0.2 g/L EDTA, 0.0015 g/L phenol red) at 37°C with 5 % CO_2 for 5 minutes to detach cells from the dish surface. Fresh culture medium, preheated to 37°C, was applied to quench the trypsin and the cells were then pelleted by centrifugation and resuspended in the appropriate medium before being re-plated on 6 cm dishes.

2.1.7 Co-culture system

Primary cultures of cortical astrocytes were prepared from E18 transgenic mice as above and cultured on 6 cm dishes. Once grown to confluency the cells were passaged as above with additional scraping to remove any stuck cells and to yield a maximal number of cells.

Astrocyte culture medium, preheated to 37°C, was applied to quench the trypsin and following pelleting, the cells were resuspended in conditioned neuronal medium before being added to mouse neurons (prepared in the same way as the E18 Sprague-Dawley rats described above but plated at a slightly lower density to accommodate the astrocyte monolayer) at DIV 6 (unless otherwise stated) (days in vitro (DIV) refers to the age of the neurons). Astrocytes were added at a concentration of around 0.5 million cells per 6 cm dish. Prior to co-culturing, the astrocytes could be transfected (either virally transduced (see section 2.6.1) or nucleofected (see section 2.6.3)) to effectively separate the astrocyte signal from the neuronal signal.

PBS	137 mM NaCl 2.7 mM KCL 10 mM Na_2HPO_4 2 mM KH_2PO_4
Trypsin solution	137 mM NaCl 2.7 mM KCL 8 mM Na_2HPO_4 1.5 mM KH_2PO_4 2.5 g/L trypsin (from porcine pancreas) 200 mg/L EDTA
Dissection media	HBSS (Gibco) 10 mM HEPES
Attachment media	MEM (Gibco) 10% Horse Serum 1 mM sodium pyruvate 33 mM glucose
Maintanence media	Neurobasal 2% B27 supplement (Gibco) 1% Glutamine
Astrocyte culture media	DMEM (Gibco) 20% FBS 1% Pen-Strep (10 U/ml, 100 μg/ml)

Table 2.1.1 Cell culture media and reagents

2.2 Organotypic slice culturing

Slices of CNS tissue were prepared from rodent brains and maintained for a maximum of 21 days. Slices were incubated at 37°C, supplied with oxygen and frequently supplementated with culture medium (minimum of every 5 days). Under these conditions, neurons continue to differentiate and develop in a similar manner to that which is observed in an intact brain (Gahwiler et al., 1997). The Stoppini interface method allows for maintenance of the intact three-dimensional structures within the tissue. It involves culturing slices on porous membrane inserts (confetti) where tissue thinning occurs to around 5-8 layers of cells, instead of a monolayer, in the case of the roller tube technique (Stoppini et al., 1991, De Simoni and Yu, 2006). Sagittal brain slices (300 μm) were obtained from Sprague-Dawley rats or from transgenic mouse lines (in the case of mito-dendra2 experiments), at postnatal day 7-10, using a vibratome (Leica VT1200 S) in ice-cold dissection medium (HEPES (4-(2-hydroxyethyl)-1-piperazineethanesulfonic acid) buffered EBSS (Earle's Balanced Salt Solution)). Slices were cultured on sterile 0.45 μm Omnipore membrane filters (Millipore) (Koyama et al., 2007) in a humidified incubator at 37°C with 5 % CO_2. Slices were maintained for at least 7 days in culture medium (72 % MEM + glutamax (Gibco), 25 % HRS, supplemented with 20 mM HEPES, 36 mM glucose and 1.06 % Pen-Strep (10 U ml^{-1}, 100 μg ml^{-1}) with 16 % Nystatin (10, 000 U ml^{-1}) prior to transfection or transduction and imaged 3 days later. For mouse slices the culture medium was supplemented with 5 mM Tris solution. Media was changed the day after slicing and every five days after that. All steps were carried out in a laminar flow cabinet under aseptic techniques.

Organotypic slicing media	MEM (Gibco) 10% Horse Serum 1 mM sodium pyruvate 33 mM glucose
Organotypic slice culture media	MEM + Glutamax (Gibco) 25 % HRS 20 mM HEPES 36 mM glucose 1.06 % Pen-Strep (10 U/mL, 100 μg/mL) 0.16% Nystatin (10, 000 U/mL)

Table 2.2.1 Organotypic slicing media

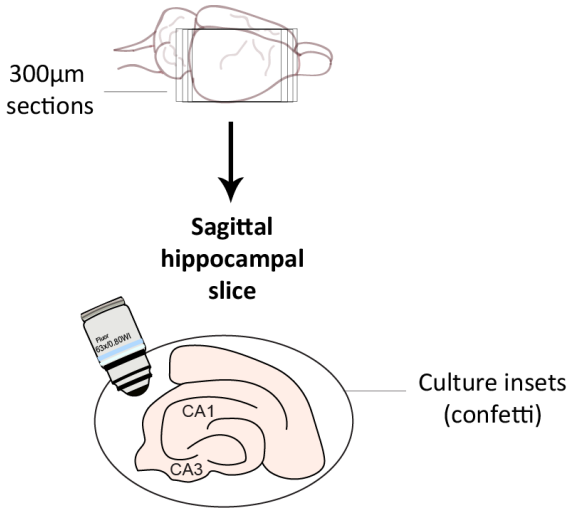

Figure 2.2.1 Organotypic hippocampal slice culturing. Once dissected the brain is sliced in the sagittal orientation as shown (300 μm thick). The hippocampus is then dissected from the rest of the tissue. These slices are kept for at least a week on culture inserts and subsequently infected before imaging.

2.3 Materials

2.3.1 Antibodies and drugs

A rabbit Miro1 antibody (Atlas, HPA010687) was used to label Miro1 and Miro2 (1:500) in organotypic slices and in western blots (1:1000). The vesicular glutamate transporter 1 (VGLUT1) guinea pig antibody (Synaptic Systems, 135-304) was used to label synapses (1:500 for slices and 1:1000 for cultures). A NeuN mouse antibody (Chemicon International (Millipore), MAB377) was used to label neuronal cell bodies (1:500). The GFAP rabbit antibody (DAKO, Z0334) was used to label astrocytes (1:500). In some cases a mouse GFAP antibody was used (DAKO, MO761) (1:500). A MAP2 mouse antibody (Sigma Aldrich, M9942) was used to label dendrites (1:500). A Homer-1 rabbit antibody (Synaptic Systems, 160-003) was used to label post-synaptic terminal (1:300). A mouse GluR2 antibody (Millipore, MAB397) was used to label AMPA receptors (1:400). A rabbit Actin (Sigma Aldrich, A2066) antibody was used at 1:1000 for western blotting experiments. Secondary antibodies Alexa-405 mouse and Alexa-633 rabbit were purchased from Invitrogen and used at 1:500. The HRP-conjugated secondary rabbit antibody was purchased from Rockland (611-1102) and used at 1:1000.

TTX (Tetrodotoxin) (used at 1 μM), D-APV ((2*R*)-amino-5-phosphonopentanoate) (used at 50 μM), MK-801 (Dizoclipine) (used at 100 μM) and MCPG (α-methyl-4-carboxyphenylglycine) (used at 1 mM) were purchased from Tocris Bioscience. 4-AP (4-

Aminopyridine) (used at 100 μM), glycine (used at 1 μM), glutamate (L-glutamatic acid) (used at 100 μM), NBQX (2,3-dihydroxy-6-nitro-7-sulfamoyl-benzo[f]quinoxaline-2,3-dione) (used at 50 μM) and EGTA (ethylene glycol tetraacetic acid) (used at 100 μM) were purchased from Sigma Aldrich.

2.3.2 Other materials

All cell culture dishes were from Techno Plastic Products (TPP) Switzerland. All chemicals were from Melford or Sigma Aldrich unless otherwise stated.

2.3.3 Plasmid constructs

mtdsRed2, encoding mitochondrially targeted dsRed2 utilises the cytochrome c subunit VIII mitochondrial targeting sequence (N-terminally attached) was obtained from Clontech (PT3633-5). Miro1^{WT}-ires-mtdsRed2 and Miro1$^{\Delta EF}$-ires-mtdsRed2 constructs were made in the lab by cloning Miro1 constucts into a bicistronic ires vector containing mtdsRed2 (Macaskill et al., 2009b). pGFAP-MyrGFP (GFAP-driven GFP) was purchased from Addgene (#22672) (Nam and Benezra, 2009). pCMV-GCaMP6s was also purchased from Addgene (#40753) (Chen et al., 2013b). Pre-synaptically targeted GCaMP5 (Sy-GCaMP5) was cloned by Victoria Vaccaro using SyGCaMP2 (#26124) (Dreosti et al., 2009) from Addgene as a target vector and inserting GCaMP5G from Addgene (#31788) (Akerboom et al., 2012) via the restriction sites SalI and NotI.

2.4 Molecular Biology

2.4.1 Polymerase Chain Reaction (PCR)

Except in the case of genotyping (see Table 2.1.1) PCR was carried out using High-fidelity Phusion DNA polymerase (Finnzymes) following the manufacturer's instructions. The PCR reaction was assembled as described in Table 2.4.1, and then subjected to a PCR programme with appropriate primer annealing temperature (calculated used Finnzymes Tm calculator) and extension time, depending on the experiment (annealing time is 30 s/kb for normal PCR and 1 min/kb for reverse PCR) (Figure 2.4.1).

Per PCR, 1 µl of DNA template (DNA concentration of ~ 50 ng/µl) was added to 49 µl of the PCR mix and temperature cycling was achieved using a GeneAmp® PCR System 2700 (Applied Biosystems) PCR machine. The PCR product was either purified directly after validating correct product length using an agarose gel or purified from the agarose gel using QIAquick purification kit (Qiagen).

PCR reaction - components:	Final concentrations:
10 μL 5x HF-buffer	1x
2.5 μL forward primer	0.5 μM
2.5 μL reverse primer	0.5 μM
1 μL dNTPs mix	2000 μM each
1 μL template DNA (50 ng/µL)	1 ng/μL
32.5 μL milliQ water	-
0.5 μL Phusion	0.02 U/μL

Table 2.4.1 Standard Polymerase Chain Reaction

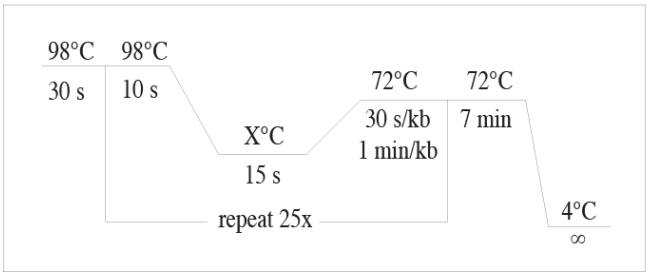

Figure 2.4.1 Standard Polymerase Chain Reaction programme. An initial melting step occurs at 95°C, where DNA is denatured. Subsequently, 25-30 cycles of a melting step (95°C, 30 s), annealing step (variable annealing temperature, 30 s) and extension step (72°C, variable time of 30 s - 1 min/ kb) take place. During the annealing step, the temperature is lowered to allow binding of the primers to the template, while the extension step allows for DNA polymerization due to the high temperature tolerance of Phusion (MyTaq). After temperature cycling, the temperature is kept at 72°C for 5 min before the samples are held at 4°C.

2.4.2 Agarose gel

Agarose gels were made melting 1 % agarose in 1x TBE buffer (10x solution purchased from National Diagnostics diluted in ddH_2O). 1 µl of ethidium bromide or 5 µl of StarSafe (Lonza) was added to visualise the DNA with UV light. Gels were let to set, and then loaded with DNA samples diluted in 6x loading buffer (0.25 % bromophenol blue and 40 % sucrose) alongside a DNA ladder (Hyperladder I, Bioline) and run at 90-100 V for the required time (approximately 1 hour).

2.4.3 Digestion and purification

5 µl of the purified insert and 1 µg of the vector were digested with the selected restriction enzymes (NEB) in the appropriate digestion buffer (NEB), supplemented with BSA for 1.5 hours at 37°C. Digests were run on an agarose gel and bands were excised and purified using Gel extraction kit (Qiagen) following the manufacturer's instructions.

2.4.4 Ligation

Purified insert and vector were combined at a 3:1 ratio and incubated with 2 µl of T4 ligase buffer and 1 µl of T4 ligase (total reaction volume 20 µl) at RT for 30 minutes and at 4°C overnight.

2.4.5 Chemically competent cells

Competent cells were prepared with Inoue method (Inoue et al., 1990) by Nathalie Higgs.

2.4.6 Transformation of competent cells

Competent cells were thawed on ice. 50 µL of cells were transferred to a 14 mL round bottom falcon tube. Following incubation for 30 minutes on ice with the appropriate amount of DNA (3 µL of ligations or 10 pg of plasmid DNA), bacteria were heat shocked at 42°C for 45 seconds. Cells were then incubated on ice for 2 minutes, 200 µL of RT LB media supplemented with 0.4 % glucose were added, and cells incubated in a bacterial shaker (230 rpm) at 37°C for 1 hour before plating onto agar plates with the appropriate resistance. Plates were then incubated overnight at 37°C.

The next day colonies were picked and grown overnight in 10 mL of LB media with the appropriate resistance. DNA was extracted with a mini prep kit (Sigma) and sequenced (Sanger sequencing, Source Bioscience). Positive bacterial clones were stored as glycerol stocks (750 µL of bacteria supplemented with 250 µl of 60 % glycerol) at -80°C.

Luria-Bertani Broth (LB)	10 g NaCl 10 g Tryptone 5 g Yeast extract H_2O up to 1 L
Luria Broth Agar (LBA)	10 g NaCl 10 g Tryptone 5 g Yeast extract 10 g Agar H_2O up to 1 L
Ampicillin	100 μg/mL
Kanamycin	30 μg/mL
TBE	89 mM Tris 89 mM Boric acid pH 8.3 2 mM Na_2EDTA
Loading dye (6x)	40% sucrose 0.25% bromophenpl blue H_2O

Table 2.4.2 Molecular biology solutions and reagents

2.4.7 Maxi preparation of plasmid DNA

Plasmid DNA was purified from bacterial cultures with Pure Yield Maxi prep Kit (Promega) following the manifacturer's instructions.

2.5 Viral construction

2.5.1 The Adenoviral Expression System

Gateway® Vector Technology (Invitrogen) was used to introduce desired construct expression in dividing and non-dividing mammalian cultured astrocytes/organotypic slice astrocytes using adenoviral vectors. Initially the gene of interest (GOI) was cloned into an

entry vector (pENTR™4A, Invitrogen, #A10465) before being transferred to a pAd/PL-DEST™ Gateway® viral vector (Invitrogen, #V494-20) using Clonase II induced AttL-AttR recombination. This technology takes advantage of the site-specific recombination properties of bacteriophage lambda (Landy, 1989). The GOI, promoter and polyadenylation (pAd) tail sequence must all be cloned between the Att sites of the entry clone to ensure proper expression of the gene within the adenovirus vector (AV). In this case the AV was a human adenovirus type 5. Subsequent amplification of the AV using ViraPower™ Adenoviral Expression System produces a replication-incompetent AV. This involved digesting the destination vector with PacI to expose the viral inverted terminal repeats (ITRs) prior to transfecting into a HEK-293A Cell Line to produce a crude adenoviral stock. This was subsequently amplified by infecting the 293A cells with the adenoviral stock. Finally, the adenoviral stock was titred to establish purity (plaque forming units) before using it to transduce cells/tissue of interest.

2.5.2 Adenovirus (AV-5)-mtdsRed2-ires-EGFP

An AV encoding mtdsred2-ires-EGFP was created using a pENTR™4A dual vector containing (3' to 5'); a CAG promoter, the mitochondrially targeted red fluorescent protein, mtdsred2, an internal ribosome entry site (ires/ir) followed by enhanced green fluorescent protein (EGFP). The entry clone pENTR-mtdsRed2-ires-EGFP was subsequently cloned into the pAd/PL-DEST vector before being amplified by the ViraPower™ Adenoviral Expression System (Invitrogen). The vector also contained a pAd tail and a Woodchuck hepatitis promoter regulatory element (WPRE) to enhance expression. Amplification of the AV-mtdsred2-ires-EGFP was performed by Nathalie Higgs.

2.5.3 Adeno-associated virus (AAV-2)-mtdsRed2-ires-egfp

A modified adeno-associated virus (AAV) was created to sparsely label neurons with transgenes of interest, long-term, with minimal cytotoxicity. The AAV backbone was modified from a pAAV vector containing EF1a-double floxed EYFP flanked by inverted terminal repeats (ITRs). Expression was driven by a CAG promoter and contained a polyadenylation tail (pAd) and a WPRE. In order to allow the insertion of constructs into the AAV backbone a sequence from the pAd/PL-DEST vector was inserted between the ITRs of the pAAV (replacing the EF1a-double floxed EYFP). This sequence consisted of AttR1-chloramphenicol resistance (Chlr)-ccdB-AttR2. This insert allows AttL-AttR recombination of entry clones into the modified AAV vector as well as negative selection of subsequent probes. Following successful recombination (with Clonase II) the AAV-mtdsRed2-ires-egfp construct was sent to Penn Vector Core (University of Pennsylvania) for production.

2.5.4 Adenovirus (AV-5)-CRE

An adenovirus encoding CRE was purchased from Penn Vector and used to induce CRE-*loxP* recombination and consequently, expression of mito-dendra2 in slices from the mouse transgenic line floxed-stop-mito-dendra2 (Pham et al., 2012).

2.6 Transfection

Transfection or transduction (viral mediated transfection) is the process by which cells are manipulated to express a specific protein of interest. Depending on the preparation, different techniques are used to transfect specific cell-types of interest.

2.6.1 Viral transduction

Slices were infected by adding 20 μl of virus diluted in slicing media (1:1000) for 3 days prior to imaging or fixing. Virus titres are as follows: AV-Cre, $1x10^{14}$ plaque forming units (PFU); AV-mtdsRed2-ires-EGFP, $2.6x10^{16}$ PFU; AAV-mtdsRed2-ires-EGFP, $2.4x10^{12}$ PFU.

2.6.2 Lipofection

Lipofectamine 2000® (Life Technologies) was used to transfect E18 hippocampal neurons (at DIV7-10) (Al Awabdh et al., 2012) with some modifications. For two 13 mm coverslips or one 25 mm coverslip, 2 μg DNA was added to 2 μl of Lipofectamine reagent, each in unsupplemented neurobasal (NB, Gibco) (100 μl or 200 μl, respectively) and incubated at room temperature for 30 minutes. Conditioned media was then added to the DNA-Lipofetamine mix (300 μl or 500 μl, respectively) before adding to cultures and allowed to complex for 2 hours after which the media was replaced with conditioned media. Lipofectamine transfection was used to transfect cultured neurons with Sy-GCaMP5, which were then co-cultured with primary cortical astrocytes. Lipofectamine transfection was also used to overexpress (OE) either Miro1^{WT}-ires-mtdsRed2 or Miro1$^{\Delta EF}$-ires-mtdsRed2 constructs with GFAP-driven GFP in E18 neuronal cultures (which contained astrocytes).

2.6.3 Nucleofection

To transfect hippocampal astrocytes (E18), before co-culturing with hippocampal neurons (E18), an Amaxa Nucleofector® was used following the manufacturer's protocol. 1 μg of DNA was added to pelleted cells, obtained using trypsinization of confluent 10 cm dish, resuspended in 100 μl WT-EM buffer solution (5 mM NaH_2PO_4, 35 mM Na_2HPO_4, 5 mM

KCl, 10 mM $MgCl_2$, 11 mM glucose, 100 mM NaCl, 20 mM HEPES). Astrocytes were transfected using the rat astrocyte program (T-020) before being co-cultured with hippocampal neurons. Transfected astrocytes were maintained with neurons for 3-4 days before live Optosplit imaging.

WT-EM	15 mM NaH_2PO_4 35 mM Na_2HPO_4 5 mM KCl 10 mM $MgCl_2$ 11 mM Glucose 100 mM NaCl 20 mM HEPES

Table 2.6.1 Transfection solutions

2.6.4 Biolistic slice transfection

Unfortunately, transfecting cells in intact tissue remains a rate-limiting factor in the study of many areas of neurobiology, including astrocyte biology. Biolistic transfection is a physical method of transfection in which the target tissue is bombarded with DNA-coated gold particles (bullets) using a gene-gun. The gene-gun uses pressurised gas to facilitate tissue penetration of the gold. Once a cell has been penetrated by the gold particles the DNA is likely to be taken up by the cell. In this way, cells of interest can be labelled with fluorescent molecules or proteins of interest can be overexpressed or knocked-down.

Organotypic slice cultures (rat P7, 300 μm thick) were biolistically transfected at 7 DIV using a Helios gene gun (BioRad) (Woods and Zito, 2008). Slices greater than 300 μm thick display lower transfection efficiency (Benediktsson et al., 2005). Biolistic transfection involved

coating small (0.6 μm) gold particles (Benediktsson et al., 2005) with up to 40 μg of DNA (a maximum of 20 μg for each construct if more than one was used). This allowed sparse transfection of astrocytes in organotypic slices. For optimal transfection of astrocytes gene gun bullets were prepared with 9–12 mg of gold per 75 cm of tubing, compared to 7–9 mg of gold for optimal labelling of neurons. The distance of the gene gun tip to the tissue slice was another variable that affects astrocyte transfection efficiency. If the tip was too close (< 1 cm), cells located at the edges of the slice were primarily transfected. Another important variable was the health of the slice at the time of transfection, affected by the angle at which the tissue was initially cut as well as the frequency at which cultures were fed. Slicing off-axis (i.e. at an angle) increases neuronal damage and results in low tissue viability (Benediktsson et al., 2005). Feeding cultures more frequently (i.e. every 2-3 days) promotes tissue viability.

Transfection typically yielded 20–100 labelled cells per slice. Slices were maintained for 2 days, following shooting, before imaging to improve visibility. Labelled cells were present several days after transfection. Post-imaging immunohistochemistry (IHC) staining with GFAP and MAP2 was used to confirm cell-type specificity. The triple expression system involved coating bullets with Miro1$^{WT/\Delta EF}$-ir-mtdsRed2 and GFAP promoter driven GFP DNA or GCaMP6s DNA.

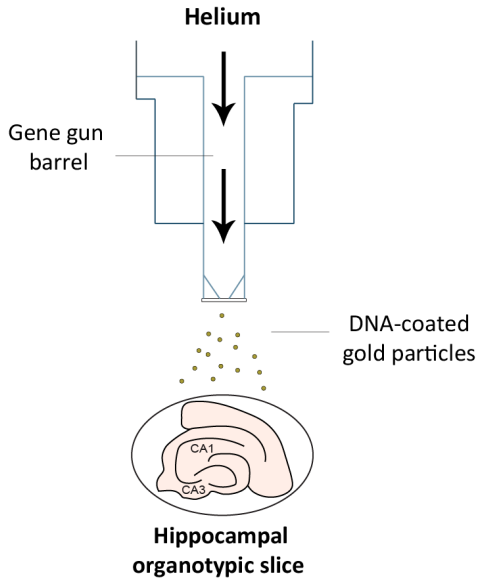

Figure 2.6.4 Biolistic slice transfection. Once cultured for at least a week and allowed to recover from the insult of slicing, the tissue can be transfected using DNA-coated gold particles and a Helios gene-gun (Bio-rad). Helium gas is pressurised to 180 mmHg, which forces the DNA-coated gold particle through a filter to lessen the impact and into the tissue below. Expression takes around 1-2 days following shooting.

2.7 Treatment of organotypic hippocampal slice cultures for fixed imaging

Slices were treated 3 days post infection. Slices were placed in a well containing organotypic media supplemented with the relevant drugs for 10 minutes at 37°C. The slices were then washed with organotypic media before fixing with 4 % PFA (4 % paraformaldehyde, 4 % sucrose, 50 % PBS (137 mM NaCl, 2.7 mM KCL, 10 mM Na_2HPO_4, 2 mM KH_2PO_4, pH 7). Depending on the mechanism of action drugs were added for sufficient time for required activation. For experiments using EBSS + Ca^{2+} the composition was as follows: EBSS (no Ca^{2+}, GIBCO) supplemented with 1.8 mM $CaCl_2$, 1 mM $MgCl_2$ and 5.56 mM D-glucose. For experiments with 0$[Ca^{2+}]_e$, EBSS (no Ca^{2+}, GIBCO) was supplemented with 1 mM $MgCl_2$, 5.56 mM D-glucose and 100 μM EGTA.

2.8 Imaging

2.8.1 Live imaging

2.8.1.1 Confocal imaging

Hippocampal slices (imaging was confined to the CA3 where possible) or cultured astrocytes were imaged using an upright Zeiss LSM700 confocal with a 63x 1 NA water objective. Upon live imaging, cells/slices were transferred to a recording chamber, perfused at 5 ml/min with imaging solution (ACSF) at pH 7.4 (125 mM NaCl, 10 mM D-glucose, 10 mM HEPES, 5 mM KCl, 2 mM $CaCl_2$, 1 mM $MgCl_2$) and heated to 35-37°C. Perfusion was supplemented

with drug combinations as indicated in the text for 5 minutes, slices were then washed for 5 minutes. Images were acquired at 1 frame every 5 seconds, except for imaging GCaMP6s where images were acquired at a frame rate of 2 seconds. Excitation was achieved via diode lasers at wavelengths of 488 m and 555 nm.

2.8.1.2 Custom optosplit imaging

An inverted Zeiss Axiovert 200 microscope (63x 1.4 NA oil objective), attached to an Evolve (EMCCD) camera (Photometrics), fitted with an image splitter (Optosplit II, Cairn Research), allowed simultaneous acquisition of images at two separate emission wavelengths. Images were acquired with 30 ms exposure at 1 frame every 2 seconds using Micro-manager software (Edelstein et al., 2010). Excitation was achieved through a D470/40X filter (Chroma) and emission was split using a 565DCXR dichroic beam-splitter (Chroma), subsequently collecting with HQ522/40M and HQ607/75M (Cairn Research) filters for SyGCaMP5 and mtdsRed2, respectively. A Grass S9 stimulator and a stimulation bath (Warner Instruments) allowed field stimulation (20 Hz for 10 s) of 25 mm coverslip-plated neuron-astrocyte enriched cultures.

2.8.2 Immunofluorescence

Cultures for immunocytochemistry were fixed with PFA for either 5 min for surface staining or 10 min for whole cell staining. Coverslips were washed with PBS and subsequently incubated with block solution (PBS containing 10 % HRS, 0.5 % BSA (bovine serum albumin), 0.2 % Triton-100) at room temperature (RT) for 1 hour. Coverslips were then incubated with primary antibody, diluted in block solution, for 2 hours at RT. Following washing with PBS the cells were incubated for a further hour at RT with secondary

antibodies, diluted in block solution at 1:800 (AlexaFluor, Invitrogen). The coverslips were washed several times and then mounted on microscope slides using Pro-Long Gold antifade reagent mounting medium (Invitrogen). For organotypic slice immunohistochemisty, slices were incubated with block solution with 0.4 % Triton for 4-6 hours before incubating in primary antibody overnight at 4°C. The following day the slices were washed (with PBS) and blocked for a further 4-6 hours before being incubated with secondary antibodies (diluted in block solution, 0.4 % Triton) overnight at 4°C. Slices were then mounted on microscope slides with Vectorshield hard set mounting medium (Vector Labs) and then covered with 18 mm coverslips. Images of fixed cultures or slices were taken on a Zeiss LSM700 confocal using a 63x oil objective (1.4 NA).

PFA solution	4% PFA 4% sucrose in 1x PBS pH 7.0
IF blocking solution	10% Horse serum 0.5% BSA 0.2% Triton X-100 in 1x PBS
Imaging solution (ACSF)	125 mM NaCl 10 mM HEPES 10 mM glucose 5 mM KCl 2 mM $CaCl_2$ 1 mM $MgCl_2$

Table 2.8.1 Immunohisto/cytochemistry and imaging solutions

2.8.3 Image Processing

2.8.3.1 Mitochondrial morphology

Mitochondrial morphology was analysed by manually calculating mitochondrial length in a maximum intensity projection of regions of interest, using ImageJ. This was achieved by tracing the longest line along each mitochondrion and establishing the output length in μm.

2.8.3.2 Mitochondrial mobility

Mitochondrial mobility was assessed by counting the percentage of mitochondria moving during an imaging period (5 min). Mitochondria in a field of view were manually classed as moving if they moved more than 2 μm. Oscillating mitochondria were identified as moving back and forth no more than 2 μm. Immobile mitochondria were manually identified as not moving and not oscillating.

2.8.3.3 Kymograph creation

Kymographs were created as described previously (Macaskill et al., 2009b, Muir et al., 2010, Twelvetrees et al., 2010). Curved processes were straightened using the Straighten macro in ImageJ and kymographs created using the Multiple Kymograph plugin (ImageJ) (with a line width of 1). Resultant kymographs show the process along the x-axis and time projected down the y-axis. Height of the kymographs is 15 min, unless otherwise stated, and time increases down the page. Immobile mitochondria can be identified as straight lines, diagonal lines represent moving mitochondria and oscillating mitochondria can be seen as zigzag lines.

2.8.3.4 Mitochondrial velocity analysis

The average velocities (μm/s) of moving mitochondria were quantified using the ImageJ Manual Tracking plugin. Since mobility was usually accompanied by brief pauses, along with changes in direction, stops greater than 5 seconds were omitted. Again, mitochondria were only included in the analysis if they moved more than 2 μm, with the aim of avoiding the data being dominated by mitochondria that did not move throughout the experiment and excluded oscillating mitochondria.

2.8.3.5 Synaptic recruitment of astrocyte mitochondria

For synaptic recruitment experiments, mtdsRed2 labelled mitochondria distributed along astrocytic processes were assessed in relation to VGLUT1 labelled pre-synaptic vesicles (used to label synapses). Images were manually thresholded and using the ImageJ plugin JACoP (Objects based methods of co-localisation) (Bolte and Cordelieres, 2006) the distance from the centre of each mitochondrion to the centre of each VGLUT1 puncta in the proximal axon was calculated. For each mitochondrion, the distance to its nearest synapse was then extracted using Excel (Microsoft). From the JACoP data the number of synapses and mitochondria was also calculated per μm of astrocyte process.

2.8.3.6 Mitochondrial fusion rate analysis

In each experiment, an 80x80 μm region in the distal processes was switched with 405 nm confocal laser light (200 iterations ~ 0.6 mW). This switched the green mito-dendra2-labelled mitochondria to red in the region exposed to 405 nm light. To calculate the mitochondrial fusion rate, an automated approach was used to measure co-localisation (Pearson's R-value, JACoP, ImageJ) of the manually thresholded red and green mito-dendra2 channels. This

represents overlap between the switched red mito-dendra2 signal and green mito-dendra2 signal redistributing into the switched area. Results were normalised to the R-value of the pre-switched region in each experiment to account for any noise in the system.

2.8.3.7 Particle analysis

The ImageJ plugin Analyse Particles was used for automated calculations of synapse number and size (VLGUT1, homer puncta or GluR2 puncta) following manual thresholding.

2.8.3.8 Sholl analysis

The ImageJ Sholl analysis plugin (Gensel et al., 2010) was used to calculate the number of astrocyte process intersections contained within concentric circles radiating out from the soma at 10 μm increments with a cut off at 100 μm. Images were manually thresholded prior to Sholl analysis and all if applicable the processes of other cells removed manually.

2.9 Western Blotting

Nitrocellulose membranes with transferred cells (pure astrocyte cultures) were blocked in block solution (4 % Marvel Milk powder, 0.1 % Tween-20 in PBS) for 1 hour prior to addition of primary antibody (Miro1 rabbit Atlas antibody (1:1000) and Actin rabbit Sigma antibody (1:1000)). Primary antibodies were incubated overnight in a sealed plastic bag at 4°C. Residual antibody was then removed by washing 3 times for 5 minutes (with block solution) before incubating with HRP conjugated secondary antibody (Rockland HRP-conjugated rabbit antibody in block solution) for 1 hour at room temperature. Membranes were washed 4 times for 10 minutes with block solution and rinsed with 1x PBS. Membranes

were then allowed to dry on 3 mm blotting paper and incubated for 5 minutes with super signal enhanced chemiluminescent Crescendo substrate (Milipore) to allow detection of signal with a LAS 4000 imager (GE Healthcare).

10% resolving gel	10% Protogel (acrylamide solution) 375 mM Tris pH 8.8 1% SDS 1% ammonium persulphate (APS) 0.04% TEMED
Stacking gel	5% Protogel (acrylamide solution) 125 mM Tris pH 6.8 1% SDS 1% APS
10x Running buffer	250 mM Tris 1.92 M Glycine 1% SDS
10x Transfer buffer	250 mM Tris 1.92 M Glycine 20% methanol 0.35% SDS
Ponceau stain	5% acetic acid 0.1% Ponceau S
Membrane blocking solution	4% non fat milk 0.05% Tween in 1x PBS
Stripping buffer	6.25 mM Tris pH 6.8 2% SDS 0.7% mercapto-ethanol in 1x PBS

Table 2.9.1 Biochemistry buffers and reagents

2.10 Statistical Analysis

All data were obtained using cells from at least three different animals/preparations. Results are presented as mean ± SEM. Statistical analysis was performed using student's unpaired, two-tailed, two-sample t-test (homoscedastic variance) in Excel. One-sample t-tests were performed in Mathematica. Statistical significance is indicated by: $p < 0.05$, *; $p < 0.01$, **; $p < 0.001$, ***. Significance was corrected for multiple comparisons, where applicable, by dividing the p-value required for significance by the number of comparisons made (Bonferroni correction) and n's are indicated in the figure legends. For mitochondrial mobility, velocity and length analysis, p-values indicated in the text reflect comparisons made to their corresponding pre-treatment values, where possible (in the case of TTX treatment and $0Ca^{2+}$ p-values reflect comparisons made across all pre-treatments excluding TTX and $0Ca^{2+}$ pre-treatments).

Chapter 3

Neuronal activity induces stopping of astrocyte mitochondria close to synapses.

3.1 Introduction

The processes of astrocytes that ensheath synapses have been shown to contain a significant number of mitochondria (Grosche et al., 1999, Lovatt et al., 2007, Oberheim et al., 2009). Here, their positioning could be of particular importance for intracellular Ca^{2+} regulation, which influences Ca^{2+}-dependent gliotransmission. However, whether and how astrocyte mitochondria are able to respond to neuronal activity and position themselves accordingly remains to be addressed. Reciprocally, how their positioning may regulate aspects of neuronal signalling is also an important unanswered question.

A study by Kremneva and colleagues addressed the regulation of mitochondrial mobility in cultured astrocytes (Kremneva et al., 2013). Mitochondria were highly motile in regions of low intracellular Ca^{2+}. This motility and velocity was significantly reduced in response to low

(1 μM) and high (5 μM) doses of ionomycin, which raises intracellular Ca^{2+}. In addition, the reduction in motility corresponded to a significant rise in (Fura2 labelled) intracellular Ca^{2+}. ATP (100 μm) also induced a significant rise in intracellular astrocyte Ca^{2+}, alongside a decrease in mitochondrial motility (Kremneva et al., 2013). Astrocyte mitochondrial mobility was concluded to be mainly microtubule dependent when intracellular Ca^{2+} was low (baseline signalling), where they were highly motile. However, during elevations in intracellular Ca^{2+} mitochondrial movement ceased as they become anchored to actin filaments, dependent on Ca^{2+} induced interactions (Kremneva et al., 2013). Human astrocytes also respond to ATP (100 μM-5 mM) by increasing their intracellular Ca^{2+} (Oberheim et al., 2009). Furthermore, electrical stimulation of CA3-CA1 projecting Schaffer collateral (SC) axons (50 Hz, 2 s) increased intracellular astrocyte Ca^{2+} in hippocampal slices (Porter and McCarthy, 1996). The astrocyte response to electrical stimulation was enhanced by 4-AP (100 μM) (K^+ channel antagonist that stimulates neuronal activity) and blocked by TTX (1 μM) (Na^+ channel blocker that decreases neuronal firing) and the mGluR antagonist MCPG (1 mM). Inhibiting the response of astrocytes to electrical stimulation and 4-AP required not only MCPG but also the iGluR antagonist kynurenic acid. Porter and McCarthy conclude from this that higher levels of neuronal activity (in the case of combining electrical stimulation with 4-AP) activate astrocyte mGluRs and iGluRs (Porter and McCarthy, 1996). These results indicate that rises in astrocyte intracellular Ca^{2+} reduce mitochondrial mobility and that neuronal activity regulates intracellular Ca^{2+} in astrocytes via mGluR and iGluR activation in the hippocampus. This provides a likely link between stimulation of neuronal activity and alterations in mitochondrial mobility in astrocytes. However, exactly how this regulation occurs remains to be resolved.

Jackson and colleagues found that although astrocyte mitochondria were mobile in astrocyte processes, they moved significantly slower and covered shorter distances than in dendrites (Jackson et al., 2014). Average displacement was around 5 μm for astrocyte mitochondria and 25 μm for neuronal mitochondria. In neurons, the mean maximal instantaneous velocity was 0.65 μm/s, in the retrograde direction and 0.55 μm/s, in the anterograde direction. In astrocytes, the mean maximal instantaneous velocity was 0.2 μm/s in the retrograde direction and 0.15 μm/s in the anterograde direction. However, the length of individual mitochondria in astrocytes and neuronal dendrites were similar. This suggests that different mechanisms may regulate mitochondrial trafficking in astrocytes.

Under basal conditions, astrocyte mitochondria undergo fission and fusion events, where 50 % of events were fusion and 50 % where fission events in acute cortical slices (Motori et al., 2013). Pharmacologically elevating intracellular Ca^{2+} in astrocytes resulted in remodelling or rounding of mitochondria (Tan et al., 2011). Although the functional relevance of altering mitochondrial morphology is not clear, it may affect their ability to buffer Ca^{2+} and release ATP. Longer mitochondria, perhaps, might allow a greater area for ATP production and Ca^{2+} buffering, while it may be easier for shorter, more rounded mitochondria to position themselves in spatially restricted regions of the cell (i.e. very fine astrocyte processes known as perisynaptic astrocytes processes (PAPs)) (Chang et al., 2006). Interestingly, cellular injury alters the balance between mitochondrial fission and fusion events in astrocytes (Motori et al., 2013).

There is evidence suggesting that astrocytes can spatially regulate mitochondria in order to regulate their function. Astrocyte mitochondria have been shown to localise at sites of glutamate uptake in astrocytes (Chaudhry et al., 1995, Bezzi et al., 2004). In addition, the Na^{+}

channel blocker TTX (which blocks neuronal activity) decreased the positioning of mitochondria at GLT-1. It has not been investigated whether astrocyte mitochondria position themselves near synapses with stimulation of neuronal activity. Thus, investigating whether mitochondria respond to neuronal activity stimulation, which increases their presence near synapses is the main aim of this section.

3.2 Results

3.2.1 Labelling mitochondria in neurons and astrocytes in organotypic slices.

Slices of CNS tissue prepared from rodent brains can be maintained in culture for many weeks or even months. Under these conditions, neurons continue to differentiate and develop in a similar manner to that which is observed in an intact brain (Gahwiler et al., 1997). The interface method allows for maintenance of the intact three-dimensional structures within the tissue. Organotypic slice culturing incorporates several advantages over acute slices. For example, most debris and dead cells, ensuing from the slicing itself disappear after 2 weeks in vitro (Gahwiler, 1981). In addition, organotypic slices have the time to accommodate/recover from the alterations in metabolic state resulting from physically the cutting of the tissue. In addition, astrocytes maintain much of their three-dimensional morphology in organotypic slice cultures, with many thin processes radiating from the cell body and the presence of numerous branchlets (Benediktsson et al., 2005).

In conjunction with organotypic slice cultures, adenoviral vectors were used to label astrocytes. Serotype 5 human adenoviruses, in particular, preferentially transduce astrocytes, due to the high levels of coxsackievirus and adenovirus receptor (CAR) expression in

astrocytes, to which the AV binds (Duale et al., 2005). This was confirmed using glial fibrillary acidic protein (GFAP), a marker of astrocytes commonly detectable by immunohistochemistry in many astrocytes throughout the healthy CNS (Figure 3.2.1A and B). However, it is important to note that many mature astrocytes in healthy CNS tissue do not express GFAP. Astrocyte GFAP expression exhibits regional variability that is dynamically regulated by a large number signalling molecules (inter- and intra-cellular) (Sofroniew, 2009). A serotype-5 human adenovirus (AV) was used to transduce astrocytes with mitochondrially-targeted dsRed2 (mtdsRed2) and EGFP (Figure 3.2.1A and B).

Neurons were transduced with a serotype-2 adeno-associated virus (AAV), also encoding mtdsRed2 and EGFP (Figure 3.2.1D and E). Adeno-associated viruses, in particular serotype-2, preferentially transduce neurons via their selective binding to integrin receptors, more highly expressed by neurons (Bartlett et al., 1998). 75 % of AV transduced cells co-localised with GFAP (Figure 3.2.1B and C), while 82 % of cells transduced with the AAV co-localised with MAP2 (a marker of neuronal dendrites) (Figure 3.2.1E and F). Thus correct viral tropism was confirmed in this system and throughout this thesis the AV encoding mtdsRed2 and EGFP will be used to selectively transduce astrocyte mitochondria (unless otherwise stated).

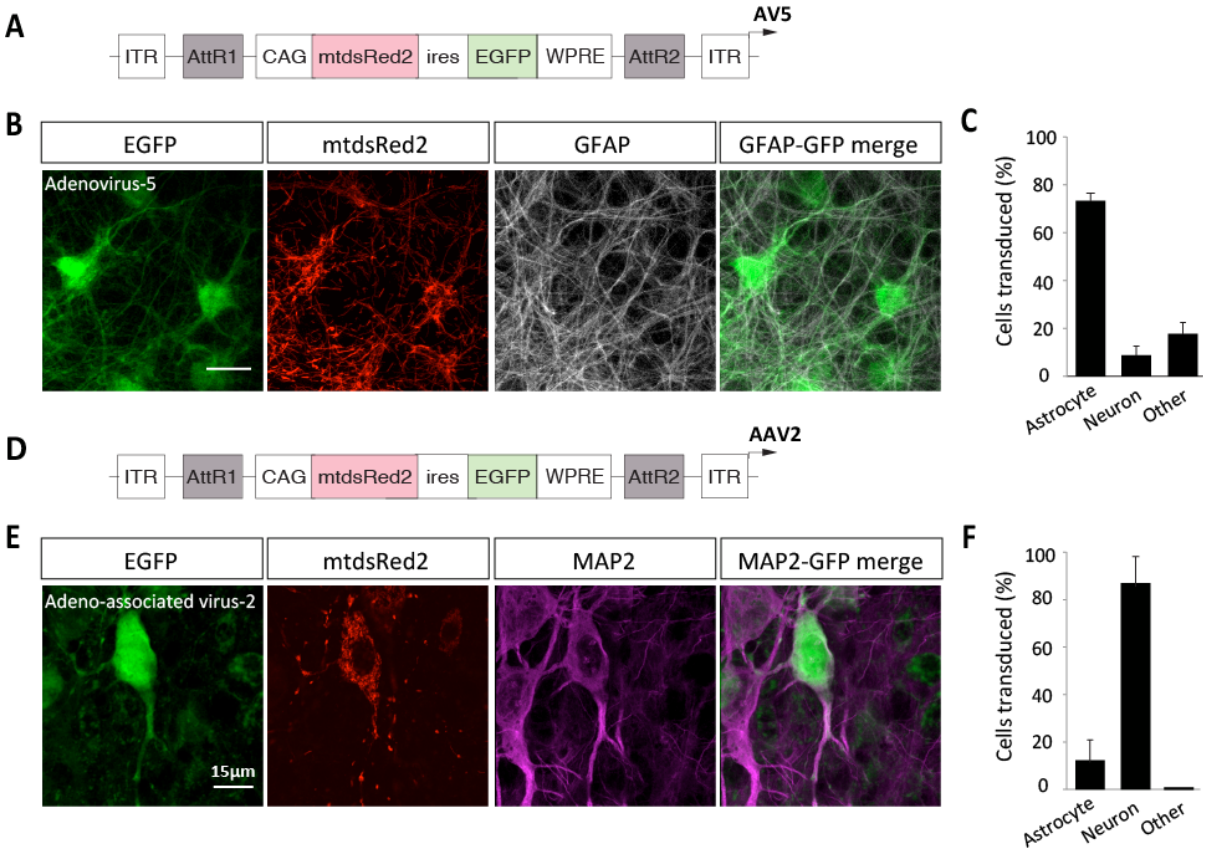

Figure 3.2.1 Viral tropism of AV-mtdsRed2-ir-EGFP and AAV-mtdsRed2-ir-EGFP. **A.** The AV consists of a CAG promoter, the mitochondrially-targetd fluorophore mtdsRed2, enhanced green fluorescent protein (EGFP) and a Woodchuck Hepatits Virus Post-transcriptional Regulatory Element (WPRE) to enhance expression. **B**. An example of AV labelling, in hippocampal organotypic slices, along with immuno-labelled GFAP, a marker of astrocytes. Scale bar, 15 μm. **C**. Quantification of the percentage of AV transduced cells positive for GFAP and MAP2 as well as cells negative for both GFAP and MAP2 (other). **D**. The AAV also consists of a CAG promoter, mtdsRed2, EGFP and a WPRE. **E**. Example AAV labelling, in hippocampal organotypic slices, along with immuno-labelled MAP2, a marker of neuronal dendrites. Scale bar, 15 μm. **F**. Quantification of the percentage of AAV transduced cells positive for GFAP and MAP2 as well as cells negative for both GFAP and MAP2 (other).

3.2.2 Mitochondria are present in the finer processes of astrocytes *in situ*.

Using the viral approach described above to label astrocytes in hippocampal slices, it was possible to visualise the distribution of mitochondria in their processes *in situ*. With this approach it was evident that mitochondria were non-uniformly distributed throughout the processes of astrocytes, including the finer processes and end-feet, with an accumulation in soma (Figure 3.2.2A-B). It has been reported that astrocyte mitochondria can be found in the thinner processes *in situ* (~ 600 nm in diameter) (Jackson et al., 2014). In this thesis, mitochondria were found in processes around 250 nm wide (Figure 3.2.2C).

A recent study by Derouiche and colleagues revealed that a substantial proportion of astrocyte mitochondria are present in PAPs, which ensheath synapses (Derouiche et al., 2015). PAPs are the astrocytic compartments implicated in buffering glutamate, where it is subsequently converted to non-toxic glutamine and supplying glutamate to axon terminals (Hertz et al., 2007, Dienel, 2013). On average, mitochondria were smaller in these PAPs than the stem (wider) processes. They find that in general, the majority of astrocyte mitochondria are small (0.2-0.4 μm), spherical and not elongated. The density of mitochondria in PAPs is much lower than in the stem processes. Thus, PAPs are not devoid of mitochondria as previously thought, but contain a large amount of mitochondria (Derouiche et al., 2015). These results are supported here, as finer processes (which included end-feet had an average width of ~ 600 nm) contained significantly more spherical, smaller mitochondria (~ 0.5 μm) while wider processes (which, on average had a width > 800 nm) contained more elongated mitochondria (~ 2.6 μm) (Figure 3.2.2D). This is likely to be because smaller mitochondria can more easily invest into the spatially restricted regions of the finer processes and end-feet.

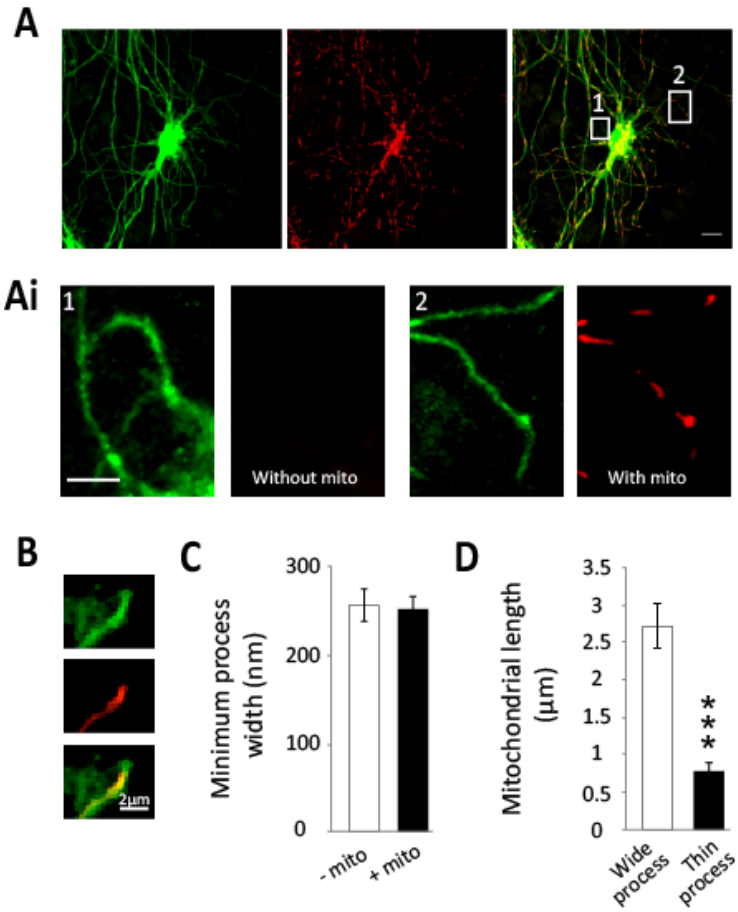

Figure 3.2.2 Mitochondria are present in the thinner processes of astrocytes in hippocampal slices. **A.** Representative live confocal images of astrocyte processes transduced with mtdsRed2 and EGFP (AV infected hippocampal slices) with zooms of regions of interest (ROI's) 1 and 2. Scale bar, 15 μm. **Ai**. ROIs show example astrocyte processes containing and lacking mitochondria in the same cell. Scale bar, 5 μm. **B**. Example end-foot containing mitochondria. Scale bar 2 μm. **C**. Minimum process width of process containing and lacking mitochondria. It is important to note that this analysis overestimated the minimum process width due to resolution limitations (resolution of the confocal is around 200-250 nm). D. Mitochondrial length in wide (< 800 nm) and thin (> 800 nm) processes (wide processes n=15 processes; thin processes n=16 processes).

3.2.3 Basal mitochondrial trafficking dynamics differs in astrocytes compared to neurons.

Initially, the nature of mitochondrial trafficking in hippocampal astrocytic processes was compared to hippocampal neurons, *in situ*. Under basal conditions, significantly more mitochondria were moving in neuronal dendrites (53.6 ± 1.3 %) compared to the processes of astrocytes (31.3 ± 3.2 %) (Figure 3.2.3C, p = 0.0007). In astrocyte processes, a significant percentage of mitochondria were also found to exhibit oscillating (back and forth) movements (36.8 ± 5.8 %), in contrast to neurons, where this type of movement was almost absent (2.5 ± 0.4 %) (Figure 3.2.3C, p = 0.002). The function of these oscillating movements is not known. Neuronal mitochondria moved significantly faster (0.28 ± 0.02 μm/s) than astrocytic mitochondria (0.12 ± 0.01 μm/s) (Figure 3.2.3D, p = $1x10^{-7}$). Maximum instantaneous speed was significantly greater in dendrites (0.66 ± 0.04 μm/s) compared to astrocyte processes (0.38 ± 0.04 μm/s) (Figure 3.2.3E, p = 0.0001). Mitochondrial length was also seen to be significantly greater in dendrites (4.7 ± 0.3 μm) than in astrocyte processes (2.4 ± 0.2 μm) (Figure 3.2.3F, p = 0.002). It can therefore be concluded that, although mitochondria are mobile in the processes of astrocytes, their trafficking dynamics are slower than that observed in neurons. This may be due to different adaptors and transport machinery in astrocytes. It may also be due to the slower signalling cascades that exist in astrocytes (Wang et al., 2006, Shigetomi et al., 2013). Astrocyte mitochondria were nevertheless capable of covering similar distances (9.8 ± 1.1 μm) compared to mitochondria in neuronal dendrites (11.9 ± 1.2 μm) (Figure 3.2.3G, p = 0.15). Thus, the spatial extension of their neuromodulatory role may not be limited.

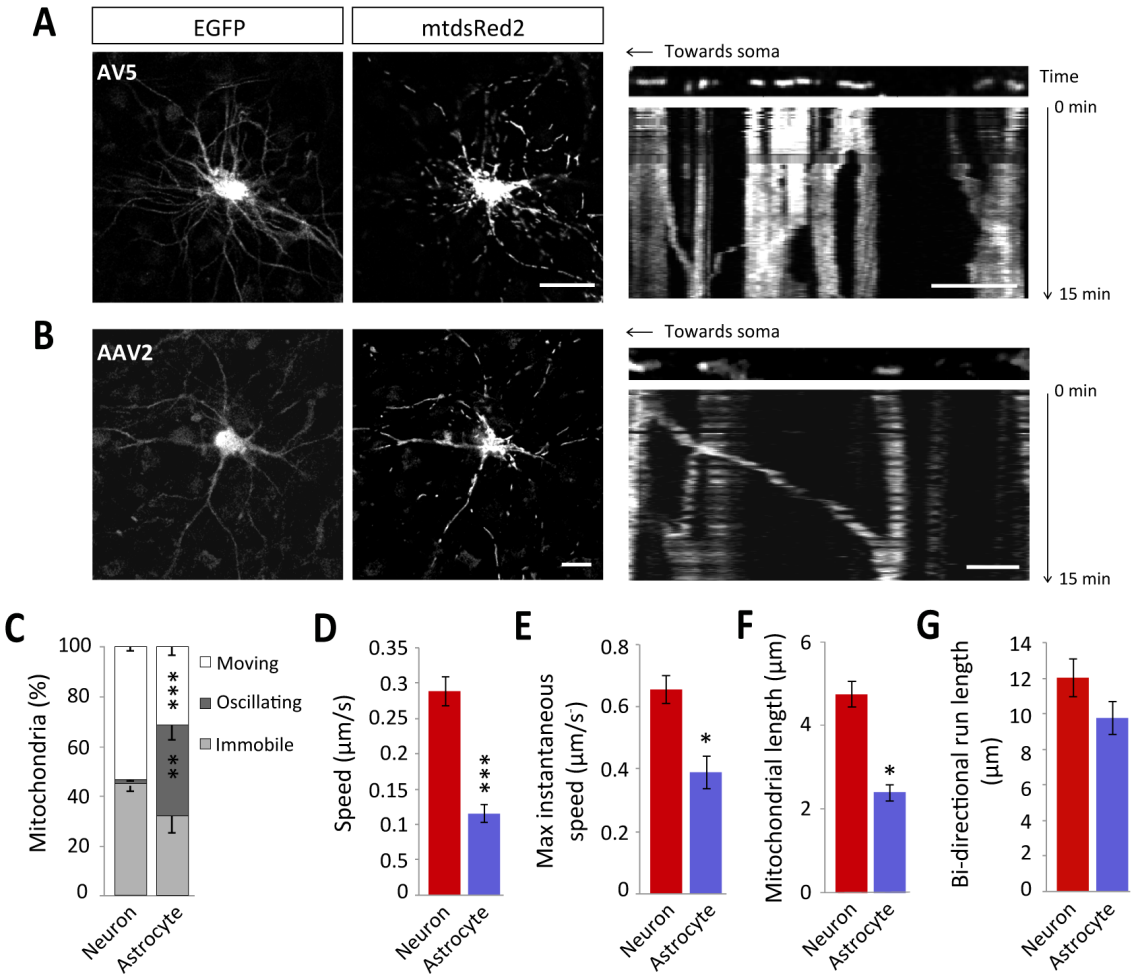

Figure 3.2.3 Basal mitochondrial trafficking dynamics differs in astrocyte processes compared to neuronal dendrites *in situ*. **A**. Representative confocal image of an organotypic slice hippocampal (HPC) astrocyte transduced with an AV expressing mtdsRed2 and EGFP. Scale bar, 15 μm. Inset example kymograph of basal mitochondrial trafficking over a 15-minute period. Scale bar, 5 μm. **B**. Example HPC neuron transduced with an AAV expressing mtdsRed2 and EGFP. Scale bar, 15 μm. Inset example kymograph of basal mitochondrial trafficking over a 15-minute period. Scale bar, 5μm. **C**. Basal mitochondrial mobility in astrocyte processes and dendrites, defined as moving, oscillating or immobile (neurons n = 4 cells, 4 slices; astrocytes n = 7 cells, 7 slices). **D**. Basal speed of moving mitochondria in astrocyte processes and neuronal dendrites (neurons n = 21 mitochondria, 8 cells, 8 slices; astrocytes n = 20 mitochondria, 9 cells, 9 slices). **E**. Maximum instantaneous speed of moving mitochondria in astrocyte processes and dendrites (neurons n = 21 mitochondria, 8 cells, 8 slices; astrocytes n = 20 mitochondria, 9 cells, 9 slices). **F**. Mitochondrial length in astrocyte processes and dendrites (neurons 3 cells, 3 slices; astrocytes 3 cells, 3 slices). **G**. Bidirectional run length of moving mitochondria in astrocyte processes and dendrites (neurons n = 21 mitochondria, 8 cells, 8 slices; astrocytes n = 20 mitochondria, 9 cells, 9 slices).

3.2.4 Mitochondrial trafficking in astrocytes is regulated by neuronal activity

An important question that required investigation was whether astrocyte mitochondria are spatially regulated by neuronal activity. A study by Jackson and colleagues revealed that inhibiting neuronal activity increased mitochondrial mobility (Jackson et al., 2014) and from this they infer that neuronal activity regulates mitochondrial trafficking in astrocyte processes. To build on this finding it was essential to investigate whether stimulating neuronal activity influenced mitochondrial trafficking dynamics in astrocyte processes. This was addressed using hippocampal organotypic slices transduced with AV-mtdsRed2-ir-EGFP.

An acute (5 minute) treatment of 4-AP (100 μM), which stimulates neuronal activity, significantly (by non-specifically blocking K^+ channels) reduced mitochondrial mobility (Figure 3.2.4B, p = < 0.0001) and speed (Figure 3.2.4C, p = 0.0003) in the processes of astrocytes. The reduction in mitochondrial mobility and speed induced by 4-AP recovered to basal levels 30 minutes following treatment showing that these alterations are transient (Figure 3.2.4B, p = 0.7 and C, p = 0.7). In addition, omitting extracellular Ca^{2+} from the perfusion media, along with EGTA (100 μM) to chelate any existing Ca^{2+}, blocked the reduction in mitochondrial mobility and **speed** induced by 4-AP (Figure 3.2.4B, p = 0.5 and C, p = 0.1), which suggests that neuronal activity induces astrocyte Ca^{2+} elevations. Conversely, blocking neuronal activity with TTX (1 μM) (which blocks Na^+ channels) for 30 minutes significantly increased astrocyte mitochondrial mobility and speed (Figure 3.2.4B, p = 0.04 and C p = 0.04). This reveals that mitochondrial trafficking is regulated by neuronal activity and confirms that blocking neuronal activity increases mitochondrial mobility in astrocytes (Jackson et al., 2014).

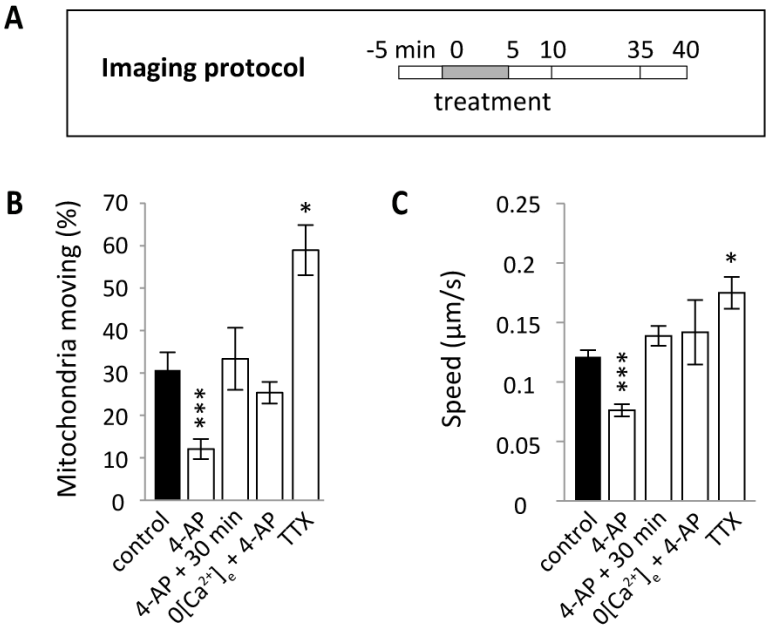

Figure 3.2.4 Neuronal activity induces mitochondrial stopping in astrocyte processes *in situ*. **A**. Schematic explanation of the imaging protocol, whereby mitochondria were imaged for 5 minutes before being perfused with ASCF containing 4-AP or TTX and subsequently washed during the remaining imaging period. **B**. Mitochondrial moving during the 5 minutes post treatment (except 4-AP + 30 minutes) (control (combined pre) n = 7 cells, 7 slices; 4AP (100 μM) n = 7 cells, 7 slices; 4-AP + 30 min n = 3 cells, 3 slices; 0$[Ca^{2+}]_e$ + 4-AP n = 4 cells, 4 slices; TTX (1 μM) n = 3 cells, 3 slices). **C**. Speed of mitochondria moving post treatment (except 4-AP + 30 minutes) (control (all pre) n = 13 mitochondria, 4 slices; 4AP n = 11 mitochondria, 4 slices; 4-AP + 30 min n = 18 mitochondria, 4 slices; 0$[Ca^{2+}]_e$ + 4-AP n = 12 mitochondria, 4 slices; TTX n = 16 mitochondria, 3 slices).

3.2.5 Neuronal activity induces intracellular Ca^{2+} signalling in astrocyte processes

Pharmacologically elevating neuronal activity (4-AP, 100 μM) *in situ* has been shown to induce significant Ca^{2+} transients in astrocytes, detected using Calcium Green-1 AM (an ester-bound dye that is lipophilic and can easily be taken up by cells where esterases cleave the ester bonds to allow indicator function) (Porter and McCarthy, 1996). However, according to Srinivasan and colleagues, many issues exist with dye loading and it is therefore important to bare this in mind when analysing astrocyte Ca^{2+} dynamics (Srinivasan et al., 2015). Previous studies using bulk loading of organic Ca^{2+} indicator dyes have underestimated astrocyte Ca^{2+} signalling and potentially miss the vast majority of fluctuations that occur in their processes (Srinivasan et al., 2015). Therefore, hippocampal astrocytes were biolistically transfected with the slow variant of the cytosolic genetically encoded calcium indicator (GECI) GCaMP6s along with mtdsRed2 (Figure 3.2.5A).

GECIs are excellent tools for studying Ca^{2+} signalling in astrocytes and they have shed new light on areas such as the processes that have previously been difficult to explore (Srinivasan et al., 2014). It is necessary to monitor Ca^{2+} fluctuations in astrocyte compartments in order to understand how astrocytes contribute to brain function, akin to the need to understand signalling in dendritic spines and nerve terminals (Srinivasan et al., 2015). It is conceivable that cytosolic GECIs might miss Ca^{2+} signals in fine astrocyte processes (Srinivasan et al., 2015). However, astrocytes in the CA3 region of the hippocampus reported fewer spontaneous Ca^{2+} signals with membrane-bound (Lck) GCaMP3 than cytosolic GCaMP3 (Haustein et al., 2014). This suggests that fewer signals are mediated by near-membrane Ca^{2+}

signals in the CA3 of the hippocampus *in situ*. More recently, more optimised forms of GCaMP have been developed, including GCaMP6 fast, slow and medium (GCaMP6f, GCaMP6s and GCaMP6m) (Chen et al., 2013b). These improved GCaMPs were produced by non-selective mutagenesis and screening to select the brightest and most sensitive variants. GCaMP6s allows for increased sensitivity of cytosolic Ca^{2+} sensing (Chen et al., 2013b) with more suitable decay dynamics for monitoring astrocyte signalling (i.e. slower) (Fiacco and McCarthy, 2006).

The method of biolistic transfection of astrocytes used here has been shown previously to label more glial cells than neurons (typically 3 glial cells to 1 neuron) (Benediktsson et al., 2005). Additionally, labelling was confirmed by the fact that the GCaMP6s signal co-localised with the astrocyte marker GFAP (Figure 3.2.5B). Astrocyte process Ca^{2+} transients were elevated with ATP treatment and when neuronal activity was stimulated with 4-AP (Figure 3.2.5C-F). Compared to basal signalling, ATP and 4-AP significantly increased the amplitude (Figure 3.2.5D, $p = 1.9x10^{-7}$ and $9.4x10^{-7}$, respectively) and frequency (Figure 3.2.5E, $p = 1.3x10^{-5}$ and 0.002, respectively) of process Ca^{2+} transients. The duration of the response to ATP and 4-AP was unchanged (Figure 3.2.5D, $p = 0.3$). This supports the literature showing that pharmacologically elevating neuronal activity activates astrocyte Ca^{2+} signalling in their processes and indicates that neuronal activity elevates astrocyte Ca^{2+}, which is responsible for altering their mitochondrial dynamics.

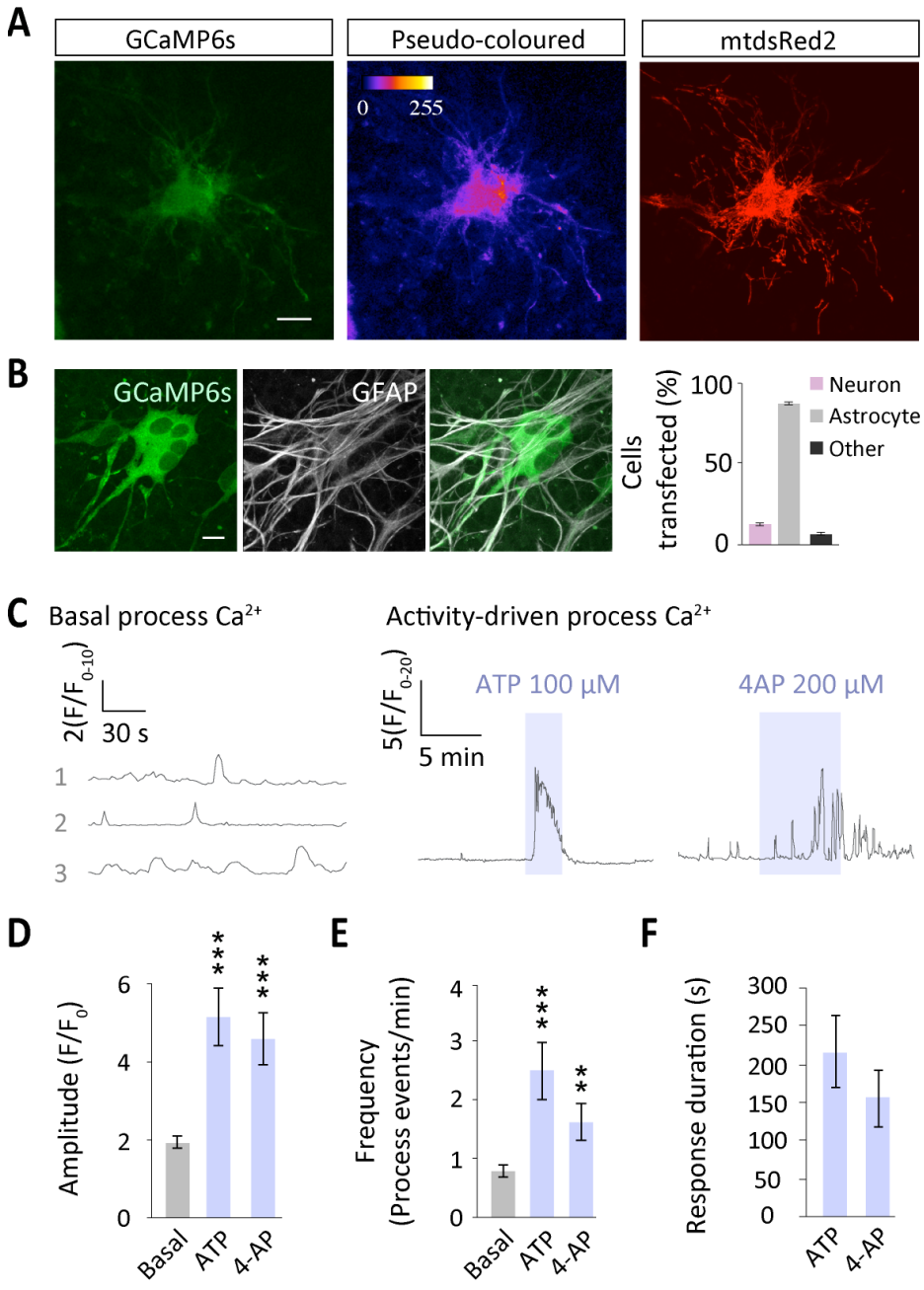

Figure 3.2.5 Neuronal activity and ATP stimulates Ca^{2+} entry in astrocyte processes in hippocampal slices. **A.** Example astrocyte biolistically transfected with GCaMP6s and mtdsRed2. Scale bar, 15 μm. **B**. GCaMP6s co-localises with GFAP confirming transfection specificity for astrocytes. Scale bars, 15 μm. **C**. Example normalised GCaMP6s fluorescence under basal conditions (normalised to the first 10 seconds) and 100 μM ATP for 2 minutes or 200 μM 4-AP for 5 minutes (normalised to the first 20 seconds). **D**. Amplitude of the response to ATP and 4-AP compared to basal signalling (GCaMP6s normalised fluorescence) (Basal n = 27 ROIs; ATP n = 10 ROIs; 4-AP n = 9 ROIs). **E**. Frequency of the response to ATP and 4-AP compared to basal signalling (Basal n = 27 ROIs; ATP n = 10 ROIs; 4-AP n = 9 ROIs). **F**. Duration of the response to ATP and 4-AP (ATP n = 10 ROIs; 4-AP n = 9 ROIs).

3.2.6 Ca^{2+} entry plays a role in regulating mitochondrial trafficking dynamics in astrocyte processes.

Exogenous glutamate (100 μM + 1 μM glycine), used at high levels to activate glutamate receptors in organotypic slices, induced mitochondrial stopping in astrocyte processes, as indicated by the kymograph, where straight lines represent immobile mitochondria following glutamate treatment (Figure 3.2.6A). Glutamate significantly reduced mitochondrial mobility (Figure 3.2.6B, $p = < 0.0001$) and speed (Figure 3.2.6C, $p = 0.001$) in astrocyte processes. The reduction in mobility and speed, induced by glutamate, was transient as recovery was visable roughly 15 minutes following treatment (Figure 3.2.6B, $p = 0.4$ and C, $p = 0.3$).

Subsequently, the glutamate receptors that are involved in regulating glutamate receptor dependent mitochondrial stopping in astrocytes were investigated. AMPA receptors and mGluRs have been shown to play an important role in increasing astrocytic Ca^{2+} (Araque et al., 2001, D'Ascenzo et al., 2007, Srinivasan et al., 2015). Mitochondrial mobility was significantly reduced when glutamate was added together with the broad spectrum mGluR blocker MCPG (1 mM) (Figure 3.2.6B, $p < 0.0001$), however, not to the same degree as with glutamate alone (Figure 3.2.6B, $p = 0.02$), suggesting a partial role for mGluRs in mediating glutamate-dependent stopping of mitochondria in astrocyte processes. With the addition of the AMPA receptor blocker NBQX (50 μM), glutamate treatment still caused a significant reduction in mitochondrial mobility (Figure 3.2.6B, $p < 0.0001$) that was not significantly different to the reduction observed upon glutamate treatment alone (Figure 3.2.6B, $p > 0.9$). In contrast, the NMDAR antagonist, D-APV (50 μM) did prevent glutamate-induced alterations in mitochondrial mobility (Figure 3.2.6B, $p = > 0.9$), demonstrating that activation

of NMDARs is a major pathway in the glutamate-dependent control of astrocyte mitochondrial mobility. Removing extracellular Ca^{2+} (omitting Ca^{2+} from the perfusion media, in addition to supplementing with the Ca^{2+} chelator EGTA, 100 μM), in the presence of glutamate, blocked the alterations in mobility (Figure 3.2.6B, $p = 0.6$) and significantly increased mitochondrial speed (Figure 3.2.6C, $p = 0.04$).

This reveals that the changes in mitochondrial trafficking induced by glutamate are dependent on the influx of extracellular Ca^{2+} and suggests that mGluRs play a partial role in regulating mitochondrial trafficking in hippocampal astrocyte processes *in situ*, supporting other investigations (Porter and McCarthy, 1995).

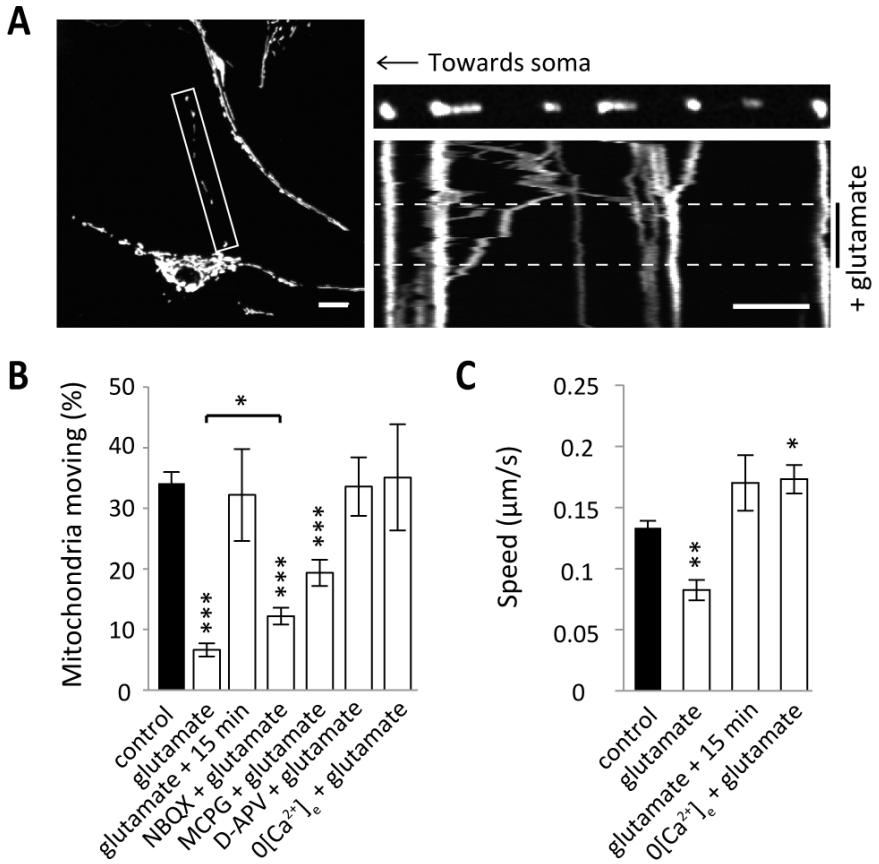

Figure 3.2.6 Glutamate reduces mitochondrial trafficking dynamics in astrocyte processes in hippocampal slices. **A**. Example slice astrocyte transduced with AV-mtdsRed2-ir-EGFP (image shows just mtdsRed2). Inset kymograph shows the effects of mitochondrial mobility with glutamate treatment (100 μM + 1 μM glycine). Scale bar, 15 μm. **B**. Basal mitochondrial mobility 5 minutes post treatment (except glutamate + 15 minutes) (control (combined pre) n = 32 cells, 29 slices; glutamate n = 8 cells, 8 slices; glutamate + 15 min n = 3 cells, 3 slices; MCPG (1mM) + glutamate n = 12 cells, 7 slices; NBQX (50 μM) + glutamate n = 11 cells, 11 slices; D-APV (50 μM) + glutamate n = 5 cells, 3 slices; $0[Ca^{2+}]_e$ (100 μM EGTA) + glutamate n = 4 cells, 3 slices). **C**. Speed of moving mitochondria 5 minutes post treatment (except glutamate + 15 minutes) (control (combined pre) n = 12 mitochondria, 4 slices; glutamate treatment n = 13 mitochondria, 4 slices; glutamate + 15 min n = 23 mitochondria, 3 slices; $0[Ca^{2+}]_e$ + glutamate n = 11 mitochondria, 4 slices).

3.2.7 Cessation of mitochondrial trafficking is coupled to alterations in morphology in culture and involves astrocyte NMDAR activation.

In cultured neurons, glutamate arrests mitochondrial trafficking and decreases their length (with recovery after 2 hours) (Rintoul et al., 2003). A decrease in mitochondrial length is indicative of fission and indeed these spherical mitochondria associate with the pro-fission protein Drp-1 (Frank et al., 2001). However, these changes in mitochondrial morphology can occur independent of fission-mechanisms. Mitochondria can contract or undergo rounding where they change from elongated to spherical mitochondria (Tan et al., 2011), resulting in a reduction in mitochondrial length. This process is often referred to as remodelling. The morphological state of mitochondria has been linked to their capacity to produce energy, as well as cell death mechanisms (Chen et al., 2005, Benard and Rossignol, 2008). Elevating astrocyte Ca^{2+} has been shown to induce mitochondrial swelling (Kristal and Dubinsky, 1997) and because glutamate has been shown to induce Ca^{2+}-dependent changes in mitochondrial trafficking, the effects of glutamate on astrocyte mitochondrial morphology were examined.

Isolated pure astrocyte cultures (> 98 %) were AV-transduced to label mitochondria with mtdsRed2 (Figure 3.2.7A) and following glutamate (100 μM + 1 μM glycine) mitochondrial length was greatly reduced (Figure 3.2.7B and C, $p = 0.002$). Interestingly, the active NMDAR antagonist MK-801 (100 μM) blocked the reduction in mitochondrial length in the absence of neurons (Figure 3.2.7C, $p = 0.002$). Previously, it was clear that NMDARs mediated the alterations in mitochondrial trafficking induced by glutamate (Figure 3.2.6), but the origin of the receptors was unclear. This result suggests that astrocyte NMDARs are involved in mediating the Ca^{2+}-dependent effects of glutamate on mitochondrial trafficking and morphology.

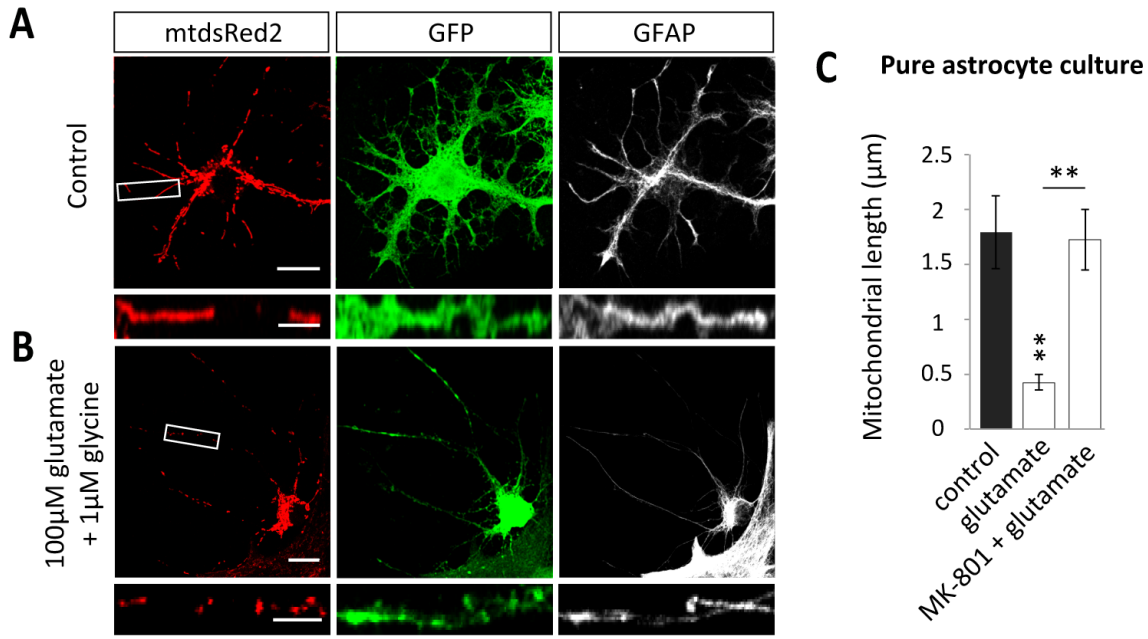

Figure 3.2.7 Glutamate alters mitochondrial morphology in astrocyte processes in culture. **A.** Example hippocampal astrocyte transduced with AV-mtdsRed2-ir-EGFP and co-immunolabelled with GFAP. Inset shows long, elongated mitochondria. Scale bar, 15 μm, inset 5 μm. **B**. Example astrocyte AV-transduced post glutamate treatment (100 μM glutamate + 1 μM glycine, 10 minutes). Inset shows round, spherical mitochondria. Scale bar 15 μm, inset 5 μm. **C**. Quantification of mitochondrial length post-glutamate treatment and glutamate + MK-801 (100 μM) (control and glutamate treatment n = 7 cells; glutamate + MK-801 n = 10 cells).

3.2.8 Mitochondria become fragmented upon stimulation *in situ*.

In situ, hippocampal astrocytes were AV-transduced to label mitochondria with mtdsRed2 and EGFP (Figure 3.2.8A). Following glutamate treatment (100 μM + 1 μM glycine, 10 minutes), mitochondria change from elongated to round (Figure 3.2.8A and B). This can be seen as a dramatic shift in the cumulative distribution of mitochondrial length (Figure 3.2.8C). To establish whether glutamate treatment induced mitochondrial remodelling or fission, the total number of mitochondria along the process was quantified before, during and after glutamate treatment, within the same cell. Glutamate treatment did not appear to alter the average number of mitochondria suggesting mitochondrial remodelling is occurring and not fission (Figure 3.2.8D, p = 1).

Stimulating neuronal activity with 4-AP (100 μM) also dramatically decreased mitochondrial length (Figure 3.2.8E p = $3x10^{-5}$), while decreasing neuronal activity with TTX (1 μM) did not alter mitochondrial length (Figure 3.2.8E p = 0.8). Where glutamate greatly reduced mitochondrial length (Figure 3.2.8E, p = $7x10^{-35}$), mitochondria were significantly elongated after 24 hours without glutamate (Figure 3.2.8E, p = 0.02). This reveals that the changes in mitochondrial morphology are not cytotoxic. The effects of glutamate treatment were blocked when extracellular Ca^{2+} chelated with EGTA (100 μM) (Figure 3.2.8E, p = 0.1). MK-801 (100 μM) also blocked the effects of glutamate (Figure 3.2.8E, p = 0.3). However, NBQX (50 μM) did not block the effects of glutamate treatment on morphology (Figure 3.2.8E p = $3x10^{-11}$). Taken together it can be concluded that neuronal activity, via glutamate release, regulates mitochondrial morphology in astrocytes where glutamate could be acting on NMDARs to mediate these alterations.

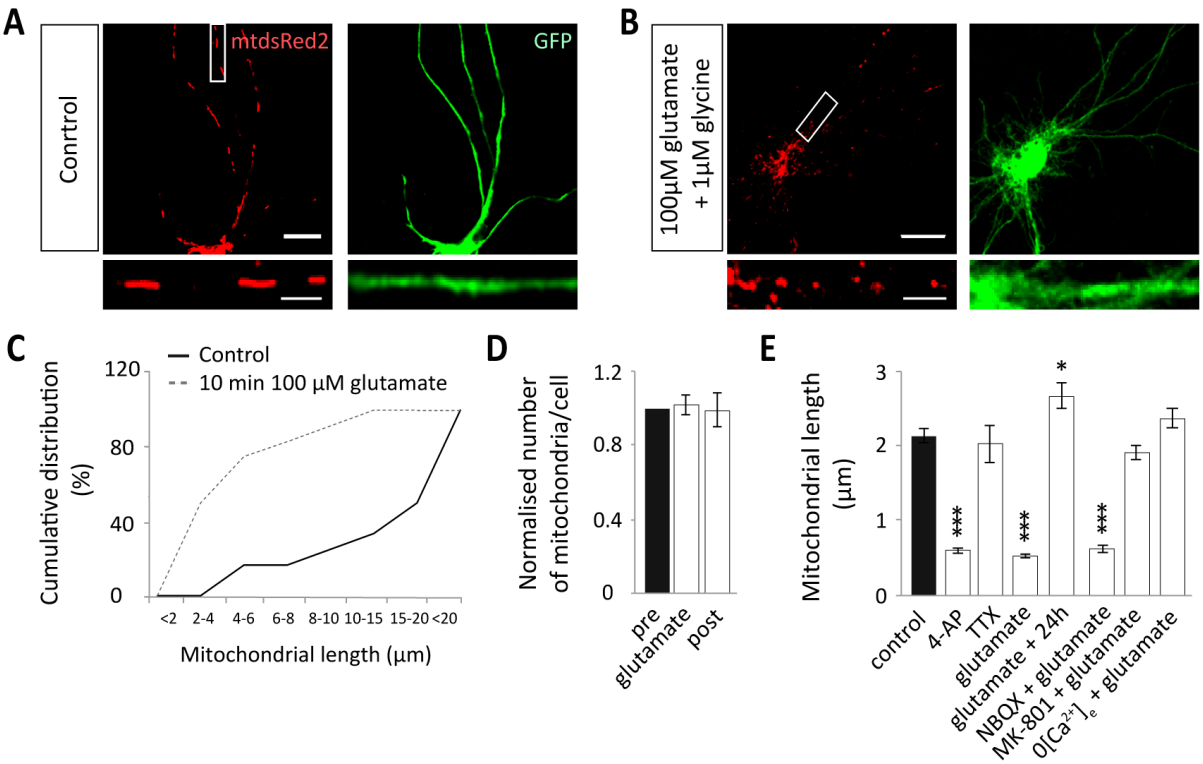

Figure 3.2.8 Stimulation alters mitochondrial morphology in astrocyte processes in hippocampal slices. **A**. Example astrocyte transduced with AV-mtdsRed2-ir-EGFP. Inset shows long elongated mitochondria within the processes. Scale bar, 15 μm, inset 5 μm. **B**. Example astrocyte AV-transduced post glutamate treatment (100 μM glutamate + 1 μM glycine, 10 minutes). Inset shows round, spherical mitochondria. Slices were treated for 10 minutes after culturing for 7-10 days (3 days following AV infection). Scale bar, 15 μm, inset 5 μm. **C**. Cumulative distribution of mitochondrial morphology in control conditions (solid line) and following glutamate treatment, 15 min post (broken line). **D**. Normalised number of mitochondria before, during and after glutamate treatment (pre n = 3 cells; glutamate n = 3 cells; post n = 3 cells). **E**. Quantification of mitochondrial length post-treatment (control n = 53 cells, 53 slices; 4AP (100 μM) n = 11 cells, 11 slices; TTX (1 μM) n = 3 cells, 3 slices; glutamate n = 58 cells, 58 slices; glutamate + 24 hours n = 10 cells, 10 slices; NBQX (50 μM) + glutamate n = 25 cells, 25 slices; MK-801 (100 μM) + glutamate n = 24 cells, 24 slices; 0[Ca^{2+}]$_e$ + glutamate n = 24 cells, 24 slices).

3.2.9 Glutamate reduces mitochondrial fusion in astrocyte processes.

To further investigate mitochondrial dynamics in astrocytes a fusion assay was set up in organotypic slices, using time-lapse confocal microscopy and the photo-switchable fluorescent protein, Dendra2 (Gurskaya 2006}, targeted to the mitochondrial matrix (mito-dendra2). Dendra2 fluoresces green and switches to red when photo-activated with 405 nm (UV) light. The photo-conversion is irreversible, non-toxic and stable, making mito-dendra2 ideal for observing fusion of labelled mitochondria when a small subset is photo-converted (Magrane et al., 2012, Pham et al., 2012). Fusion events between the red and the green mitochondria result in the transfer of fluorescence, which indicates mitochondrial matrix exchange (seen as a mixing of red and green- forming orange mitochondria) (Pham et al., 2012). Expression of mito-dendra2 does not adversely affect mitochondrial morphology (Pham et al., 2012; Magrane et al., 2012).

A transgenic mouse line expressing a *loxP*-flanked termination signal upstream of the mito-dendra2 (*loxP*-stop-*loxP*-mito-dendra2) only allows mito-dendra2 expression when CRE is present (Pham et al., 2012). CRE binds to the floxed region and removes the stop cassette, subsequently allowing mito-dendra2 expression. The CRE protein is a site-specific DNA recombinase, and if the loxP sites are parallel, it forms dimers of the signal between them. These are then cut and the sequence between the loxP sites is removed. The downstream signal can then be transcribed (Figure 3.2.9A).

Specific mito-dendra2 expression in astrocytes was induced with infection of an AV encoding CRE (AV-CRE). Expression was specific to astrocytes as the mito-dendra2 signal co-localised with GFAP and not NeuN (a marker of neuronal cell bodies) (Figure 3.2.9B). Upon photo-conversion of a small subset of mito-dendra2 labelled mitochondria, fusion events between the red and the green mitochondria result in the transfer of fluorescence, which indicates mitochondrial matrix exchange (seen as a mixing of red and green- forming orange mitochondria) (Figure 3.2.9C) (Magrane et al., 2012, Pham et al., 2012). In this system, mitochondrial fusion remained unchanged with glutamate treatment (100 μM + 1 μM glycine) (Figure 3.2.9C, 2-10 min compared to pre-switch, p = 0.5, 0.7, 0.2, 0.1 and 0.6, respectively), where the fusion rate significantly increased in untreated controls (Figure 3.2.9D, 2-10 min compared to pre-switch, p = 0.02, 0.005, 0.02, 0.01 and 0.002, respectively). This suggests that glutamate alters mitochondrial morphology in astrocyte processes *in situ*. A reduction in the fusion rate could be a consequence of a reduction in mitochondrial mobility induced by glutamate.

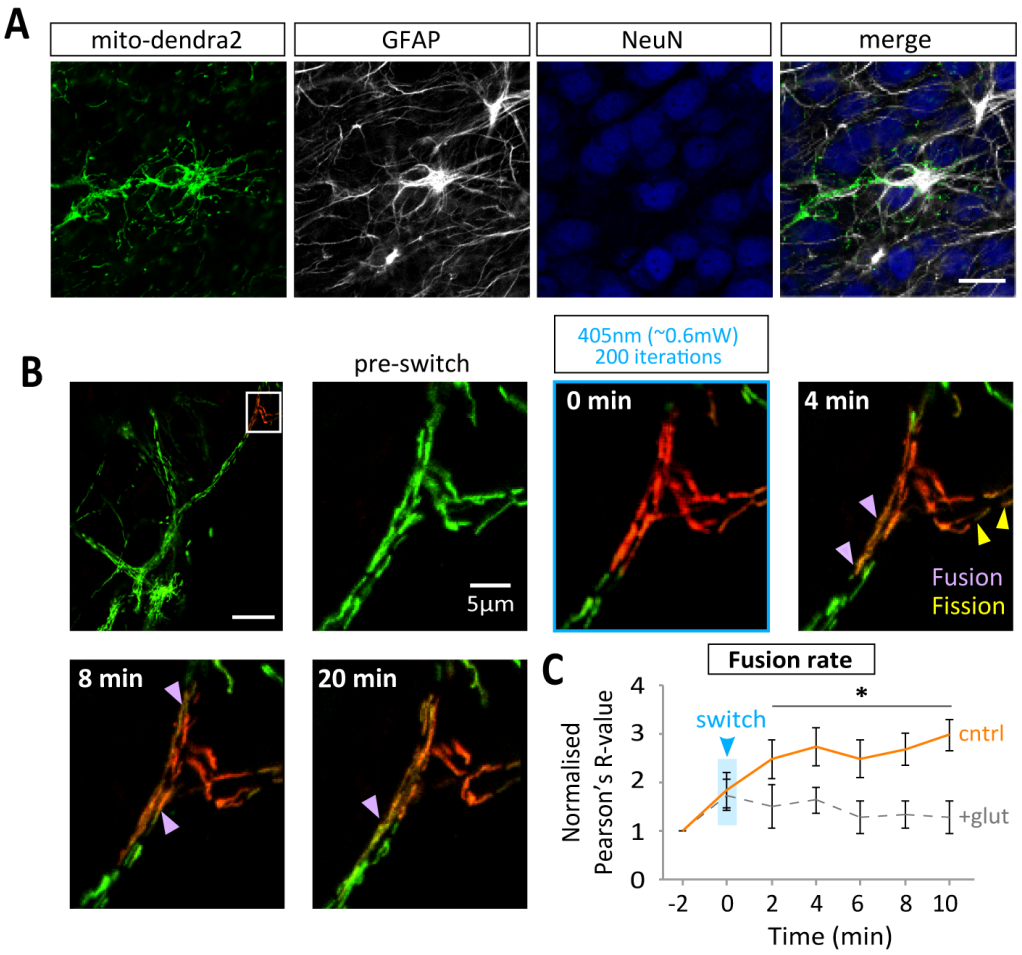

Figure 3.2.9 Glutamate reduces mitochondrial fusion in astrocyte processes in hippocampal slices. **A.** The mito-dendra2 transgenic mouse line is constructed so that the mito-dendra2 signal is downstream of a floxed (loxP flanked) stop cassette, under a ubiquitous CAG promoter. With addition of and adenovirus (AV) encoding encoding CRE, the stop cassette is removed and subsequently mito-denra2 is expressed in astrocytes. **B**. Mito-dendra2 is expressed in astrocytes in organotypic slices. This induced mito-dendra2 signal overlapped with the astrocyte marker GFAP and not NeuN (a marker of neuronal cell bodies). Scale bar, 15 μm. **C**. Mito-dendra2 was then switched with 405 nm laser light in a small region of the distal astrocyte process and the rate of fusion was analysed. Upon switching, green mitochondria can be seen to change to red and over time new, green mitochondria move into the switched region creating orange mitochondria. Scale bars, 5 μm. **D**. Quantification of the overlap of green and red mitochondria over a 10-minute period post switching in untreated controls and with glutamate treatment (control n = 5 cells, 5 slices; glutamate n = 4 cells, 4 slices).

3.2.10 Mitochondrial trafficking in astrocytes is regulated by intracellular Ca^{2+}.

Astrocytes were biolistically transfected with GCaMP6s along with mtdsRed2 in order to establish the relationship between mitochondrial trafficking and intracellular Ca^{2+}. GCaMP6s expression was previously confirmed to be astrocyte specific by increased co-localisation with the astrocyte marker GFAP (Figure 3.2.5). Using kymographs, mitochondria were overlaid with the GCaMP6s signal that corresponded to the levels of intracellular Ca^{2+} within the region of interest (ROI) (Figure 3.2.10A).

Stationary mitochondria corresponded more often with regions of high intracellular Ca^{2+} (pseudo-coloured red-orange GCaMP6s), while more mobile mitochondria were observed in regions of low Ca^{2+} (blue-black) within the same cell (Figure 3.2.10A). In addition, mitochondrial speed was elevated (0.42 ± 0.05 μm/s) in these regions of low Ca^{2+} (defined as $F/F0 < 5$) compared to regions of high Ca^{2+} (0.01 ± 0.01 μm/s) (defined as $F/F0 > 5$) (Figure 3.2.10B, $p = 0.01$). This suggests that intracellular Ca^{2+} in astrocytes regulates mitochondrial trafficking and that they stop more frequently within regions of elevated intracellular Ca^{2+}.

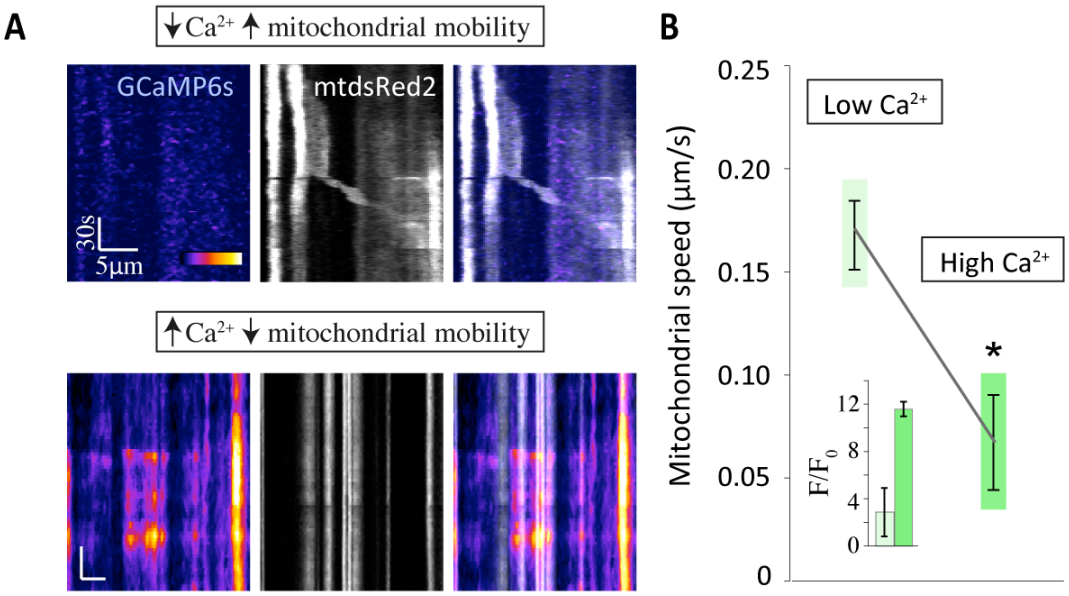

Figure 3.2.10 Mitochondria within regions of elevated intracellular Ca^{2+} are less mobile than in regions of low intracellular. **A**. Kymogaphs of GCaMP6s (pseudo-coloured) along with corresponding mitochondrial trafficking. Overlays show that mitochondria are mobile when GCaMP6s signal is relatively low and are immobile at regions of elevated Ca^{2+} in the same cell. Scale bars, 5 μm. **B**. Quantified mitochondrial speed in regions of the cell where Ca^{2+} is low and high. Inset shows the fluorescence intensity defined as low and high Ca^{2+}, respectively (Low Ca^{2+} n = 4 cells, 3 slices; High Ca^{2+} n = 5 cells, 3 slices).

3.2.11 Field stimulation induces astrocyte mitochondrial stopping

The relationship between electrical field stimulation (a more physiological form of inducing neuronal firing) and astrocyte mitochondrial dynamics was subsequently investigated. Hippocampal neurons were transfected with synaptically targeted GCaMP5 (Sy-GCaMP5), to label active synapses, and co-cultured with hippocampal astrocytes pre-transfected with mtdsRed2 (Figure 3.2.11A). This allowed separation of the astrocyte mtdsRed2 signal and the neuronal Sy-GCaMP5 signal in order to observe the effects of stimulating neuronal activity specifically on astrocyte mitochondrial dynamics.

Upon field stimulation (20 Hz for 20 s), a four-fold increase was observed in the Sy-GCaMP5 signal, confirming that field stimulation drives increased neuronal synaptic activity (Figure 3.2.11B). In addition, field stimulation rapidly decreased (< 30 s delay) the trafficking of astrocyte mitochondria (% moving) compared to pre-stimulated controls (Figure 3.2.11C, $p = 0.001$ and $p = 7x10^{-12}$, respectively). This decrease in mitochondrial mobility recovered 5 minutes following stimulation (Figure 3.2.11C, $p = 0.2$). Field stimulation also reduced the speed of astrocyte mitochondria compared to pre-stimulated controls (Figure 3.2.11D, $p = 0.001$ and $6x10^{-5}$, respectively). There was also recovery in the decrease in speed 5 minutes after stimulation (Figure 3.2.11D, $p = 0.4$).

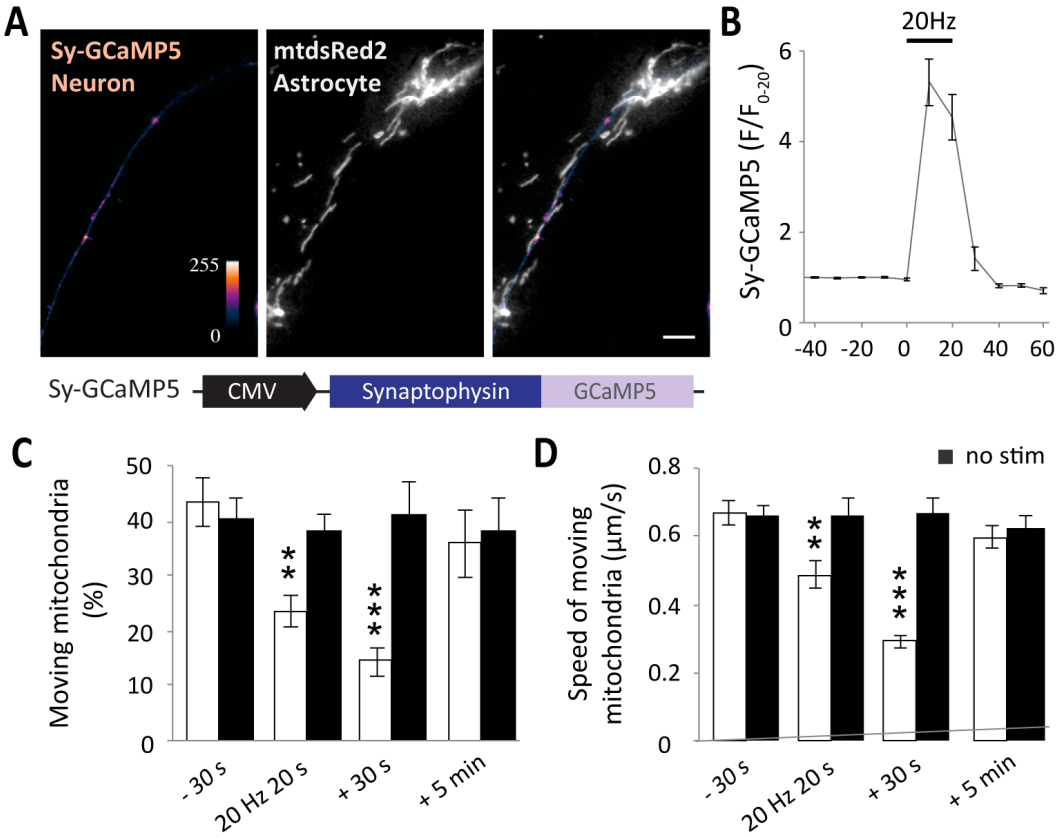

Figure 3.2.11 Electrical field stimulation reduces mitochondrial trafficking in astrocyte processes. **A.** Cultured neurons were transfected with synaptically targeted GCaMP5 (Sy-GCaMP5, whereby a synaptophysin tag was inserted upstream of GCaMP5) and co-cultured with astrocytes pre-transfected with mtdsRed2. Scale bar, 10 μm. **B**. Upon field stimulation, 20 Hz for 20 s, an increase was seen in the Sy-GCaMP5 signal, confirming synaptic activation. **C**. Mitochondrial mobility (% moving) before, during stimulation, 30 s post stimulation and 5 minutes post stimulation compared to pre-stimulated controls (-30 s and stim n = 11 cells; 30 s post n = 9 cells; 5 min post n = 6 cells; -30 s and no stim n = 9 cells; 30 s post no stim n = 7 cells; 5 min post no stim n = 5 cells). **D**. Speed of moving mitochondria before, during stimulation, 30 s post stimulation and 5 minutes post stimulation compared to pre-stimulated controls (-30 s stim n = 30 mitochondria; stim n = 27 mitochondria; 30 s post stim n = 24 mitochondria; 5 min post stim n = 21 mitochondria; -30 s no stim n = 24 mitochondria; no stim, 30s post no stim and 5 min post no stim n = 18 mitochondria).

3.2.12 Astrocyte mitochondria position themselves near synapses in culture, with activation of glutamate receptors.

The relationship between mitochondria, within the processes of astrocytes, and synaptic regions remains to be clarified. In light of this, the question of whether activity-driven mitochondrial immobilisation occurs at regions within astrocyte processes in close proximity to synapses was addressed. Initially, hippocampal cultured astrocytes, in the presence of hippocampal neurons, were AV-transduced to label astrocyte mitochondria and synapses were immuno-labelled with VGLUT1 (a marker of pre-synaptic terminals) (Figure 3.2.12A).

Following glutamate treatment (5 minutes, 100 μM + 1 μM glycine), a significant decrease was seen in the distance between the centre of each astrocyte mitochondrion and the centre of its nearest VGLUT1 puncta (synapse) compared to untreated controls (Figure 3.2.12B, $p = 0.04$). In addition, the distance between each mitochondrion pixel and each synapse pixel was established to account for the change in mitochondrial morphology following glutamate treatment (Figure 3.2.12C, $p = 0.03$). Importantly, there was no change synapse number (per μm) (Figure 3.2.12D, $p = 0.2$). There was, however, a significant increase in the number of mitochondria (per μm), which suggests that mitochondrial fission might be occurring (i.e. the existing mitochondria are breaking/splitting apart) (Figure 3.2.12.E, $p = 0.02$). This may allow them to move into the smaller PAPs that are in close proximity to synapses. Taken together, this reveals that glutamate triggers mitochondrial retention near synapses in culture.

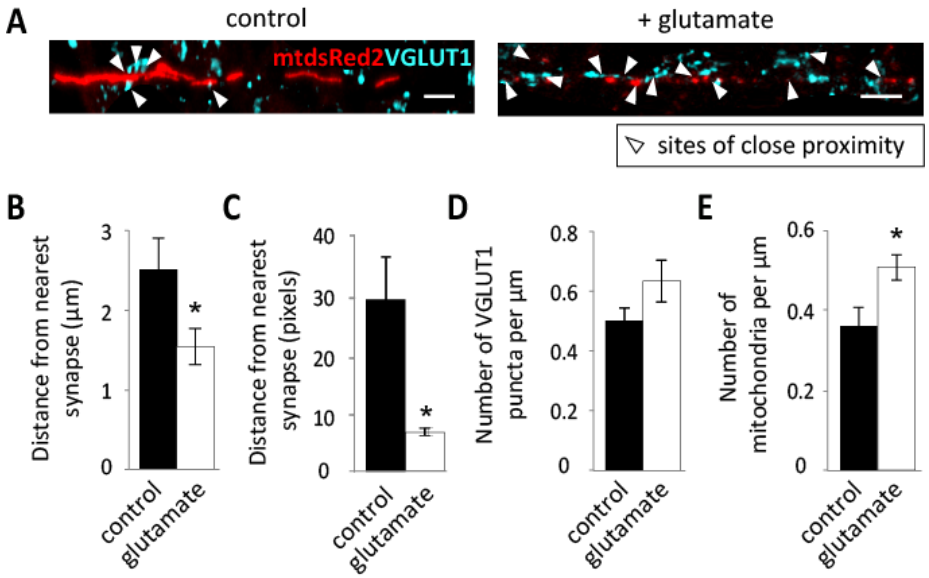

Figure 3.2.12 Glutamate induces mitochondrial confinement within astrocyte processes in close proximity to synapses in culture. **A**. Astrocyte mitochondria labelled with mtdsRed2 (AV-mtdsRed2-ir-EGP transduced) and co-immunolabelled with VGLUT1 (a marker of pre-synaptic terminals) under control (untreated conditions) and with application of glutamate (5 min, 100 μM + 1 μM glycine). Scale bars, 5 μm. **B**. The distance between each mitochondrion (centre of mass) and its nearest synapse (centre of mass) under control conditions and with glutamate treatment. **C**. The distance of each mitochondrion pixel to its nearest synaptic pixel under control conditions and with glutamate treatment. **D**. Number of VGLUT1 positive synapses per μm in untreated controls and following glutamate treatment. **E**. Number of mitochondria per μm in untreated controls and following glutamate treatment. Control n = 6 ROIs, 6 cells; glutamate n = 7 ROIs, 7 cells.

3.2.13 Field stimulation induces astrocyte mitochondrial confinement near active synapses.

Analysing the effects of field stimulation on astrocyte mitochondria revealed that along with a rapid decrease in mitochondrial trafficking (Figure 3.2.11), they localise near active Sy-GCaMP5-labelled synapses (3.2.13A). Mitochondrial retention near synapses is reflected by a decrease in the distance between astrocyte mitochondria and their corresponding nearest activated synapse, which is seen to occur within the first 30 seconds following stimulation (20 Hz 20 s) (Figure 3.2.13B, $p = 0.003$, 0.007, 0.009, 0.005 and 0.008, respectively). Mitochondria remain confined within close proximity to their nearest activated synapse for around 50 seconds and then begin to move away roughly 80 seconds following stimulation. Interestingly, electrical stimulation of neuronal-astrocyte co-cultures resulted in a similar recruitment of astrocyte mitochondria near synapses as observed for exogenously applied glutamate (Figure 3.2.12). Furthermore, the response was shown to be transient as the decrease in distance between astrocyte mitochondria and their nearest activated synapse increased around 80 seconds following stimulation. This result also reveals a fairly fast timescale in which astrocyte mitochondria become confined near synapses (~ 30 s) (Figure 3.2.13B). This is comparable to the timescale in neurons (MacAskill et al., 2009a) where mitochondria are recruited to synapses in dendrites within 60 s. However, confinement seemed to persist for longer in dendrites than in astrocytes (around 120 s vs 50 s, respectively).

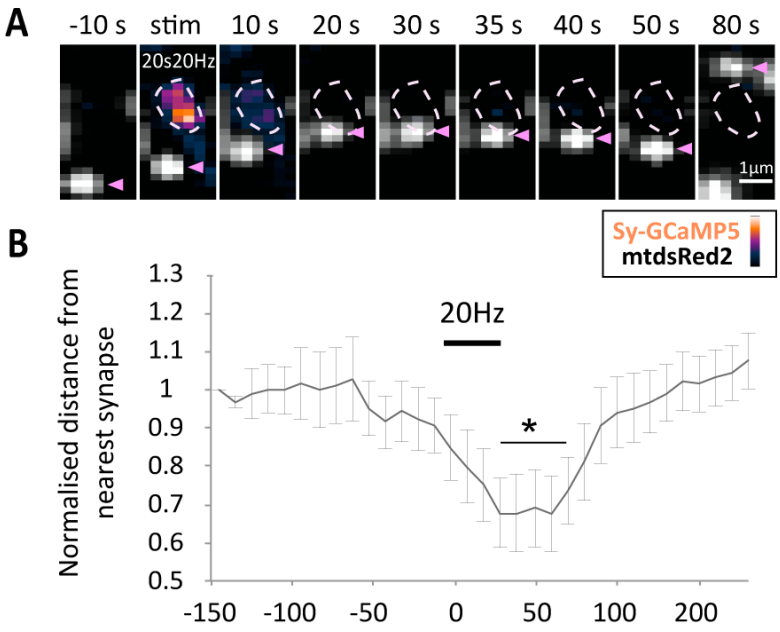

Figure 3.2.13 Electrical field stimulation transiently induces mitochondrial confinement within astrocyte processes close to synapses. **A.** An example of a synapse transfected with Sy-GCaMP5 and nearby astrocyte mitochondria transfected with mtdsRed2. Following stimulation the nearby mitochondrion moves closer to the marked synapse (within 30 s) where it remains for around 20 seconds. Around 50 seconds following stimulation the mitochondrion begins to move away. Scale bar, 1 μm. **B**. Quantification of mitochondria near synapses (< 15 μm) move even closer to their nearest synapse, temporarily, following field stimulation (20 Hz 20 s) (n = 12 mitochondria, 8 ROIs from 8 cells).

3.2.14 Astrocyte mitochondria position themselves near synapses *in situ*, with pharmacological elevation of neuronal activity.

The influence of pharmacologically elevating neuronal activity on astrocyte mitochondrial confinement was investigated in an intact, more physiological system (organotypic brain slices). AV-mtdsRed2-ir-EGFP was used to label mitochondria and synapses were immuno-labelled with VGLUT1, in hippocampal slices (Figure 3.2.14A). Similar to astrocytes in culture, mitochondria *in situ* became confined near synapses when neuronal activity was stimulated with 4-AP (5 minutes, 100 μM) (Figure 3.2.14B, $p = 0.02$), without causing a significant change in mitochondrial or synapse number (per μm) (Figure 3.2.14C, $p = 0.7$ and $p = 0.7$, respectively).

These data indicate that, in addition to a decrease in mitochondrial trafficking dynamics, stimulating neuronal activity recruits astrocyte mitochondria near synapses. This novel finding highlights that neuronal signalling alters mitochondrial dynamics within the processes of astrocytes, recruiting them to areas of activity where they can provide metabolic support.

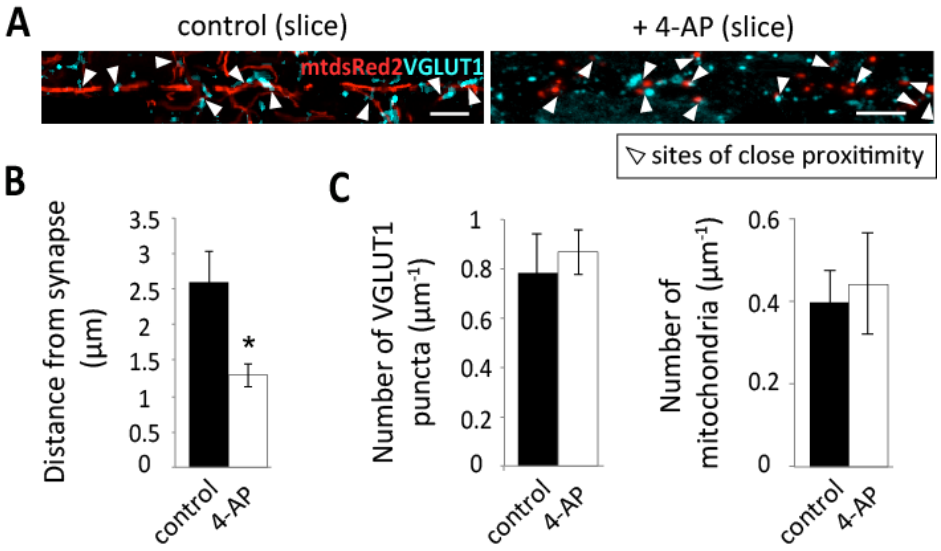

Figure 3.2.14 Neuronal activity induces mitochondrial confinement within astrocyte processes near synapses, *in situ*. **A**. Astrocyte mitochondria labelled with mtdsRed2 (AV-mtdsRed2-ir-EGP transduced) along with immuno-labelled VGLUT1 in untreated slices and following application of 4-AP (5 min, 100 μM). Arrows indicate mitochondria in close association with VGLUT1 labelled synapses. Scale bars, 5 μm. **B**. The distance between mitochondria (centre of mass) and their nearest synapse (centre of mass) under control conditions and following treatment with 4-AP. **C**. Number of VGLUT1 positive synapses and mitochondria per μm in untreated controls and following 4-AP treatment. Control n = 6 ROIs, 6 cells, 3 slices; 4-AP n = 5, 5 cells, 3 slices.

3.3 Discussion

Here, further insights are gained into the regulation of activity-dependent trafficking and positioning of mitochondria in astrocytes. The results in this chapter support the well-established idea that astrocytes can sense neuronal activity by raising their intracellular Ca^{2+} and add that this alters their mitochondrial trafficking dynamics, inducing transient docking of mitochondria near synapses.

Firstly, the recent finding by Derouiche and colleagues, showing that PAPs are not devoid of mitochondria, is supported here. Mitochondria were smaller in these finer processes (< 800 nm) supporting the study by Derouiche and colleagues (Derouiche et al., 2015). Interestingly, the number of mobile mitochondria was decreased in astrocytes, as well as the speed at which they were capable of moving, compared to dendrites, supporting previous observations by Jackson and colleagues (Jackson et al., 2014). However, astrocyte mitochondria were still capable of covering the same distances as neuronal mitochondria (9.8 ± 1.1 μm vs 11.9 ± 1.2 μm, respectively). These differences in trafficking dynamics could be due to differences in the trafficking machinery utilised by neurons and astrocytes.

Synaptic activity can evoke feedback Ca^{2+} transients in astrocytes, which may alter their ability to release gliotransmitters (Perea and Araque, 2005, Serrano et al., 2006, Di Castro et al., 2011, Navarrete et al., 2013). Here, enhancing neuronal activity alters mitochondrial trafficking dynamics and morphology in astrocyte processes in a Ca^{2+}-dependent manner.

Mitochondria became shorter with a concomitant reduction in mobility and speed when synaptic activity was stimulated (with field stimulation, glutamate and 4-AP the reduction in mobility and speed persisted for 5 minutes, 15 minutes and 30 minutes, respectively). Alterations in mitochondrial morphology can be accompanied by a marked increase in ROS and autophagy (Motori et al., 2013). However, in this study, mitochondria were significantly more elongated after 24 hours, showing that these changes in morphology are reversible.

The response to glutamate involved NMDARs and partially involved mGluRs but not AMPARs. However, it should be noted that it is difficult to separate the inhibition of neuronal NMDARs and astrocytic NMDARs, *in situ*. This was overcome by stimulating pure astrocyte cultures in the presence of an NMDAR antagonist, which blocked the glutamate-induced reduction in mitochondrial length. There is evidence to suggest that hippocampal astrocytes *in situ* express functional iGluRs of the NMDAR sub-type (Porter and McCarthy, 1995, Latour et al., 2001, Verkhratsky and Kirchhoff, 2007). For example, Porter and McCarthy show that in 45 % of astrocytes TTX (1 μM) was unable to block NMDA induced astrocyte Ca^{2+} elevations. In addition, some of these astrocyte Ca^{2+} responses to NMDA in the presence of TTX might have been missed due to the use of bulk-loaded Ca^{2+} dye imaging (Ca^{2+} Green-1 AM), which is not sufficient for observing all astrocyte Ca^{2+} fluctuations (especially within their processes) (Srinivasan et al., 2015). NMDAR expression (NR2B) in astrocytes has also been observed in the hippocampus following ischaemia (Krebs et al., 2003). Porter and McCarthy also show that 80 % of astrocytes responded to the mGluR agonist t-ACPD, where a larger percentage of astrocytes responded to t-ACPD than glutamate (Porter and McCarthy, 1995).

Another possible route for Ca^{2+} entry could be activation of the reverse mode of the Na^{+}/Ca^{2+} exchanger (NCX), which removes Na^{+} that enters with glutamate uptake via glutamate transporters in exchange for Ca^{2+} (Goldman et al., 1994). Here, the proposed route for astrocyte Ca^{2+} entry, occurring during stimulation of neuronal activity, partially involves mGluRs and NMDARs but confirming this absolutely requires further investigation. It could be that these two receptor sub-types co-ordinate the uptake of astrocyte Ca^{2+}, providing astrocytes a greater arsenal for dealing with extracellular glutamate. Overall, astrocyte mitochondrial dynamics are shown here to be tightly coupled to neuronal activity.

Previously, it has been proposed that mitochondria localise within astrocyte processes in close proximity to glutamate transporters in an activity-dependent manner (Chaudhry et al., 1995, Genda et al., 2011, Jackson et al., 2014). However, until now, it was unknown whether stimulating neuronal activity results in the retention of astrocyte mitochondria near synapses. Here, it was revealed that with neuronal stimulation, astrocyte mitochondria are temporarily recruited near synapses in culture and *in situ*. The timescale for recruitment was around 30 seconds, where mitochondria remained confined and immobile for 50 seconds before moving away. It would be logical to assume that mitochondria would be required to provide ATP for glutamate detoxification and also to buffer the downstream entry of Ca^{2+} occurring in response to glutamate uptake (Goldman et al., 1994). For these reasons, it may be that mitochondrial positioning in astrocytes is important for overall astrocyte function. Interestingly, the timescale of recruitment was similar to that observed in dendrites (60 seconds).

Chapter 4

The Ca^{2+}-sensing EF-hands of the Mitochondrial Rho-GTPase protein (Miro1) controls astrocyte mitochondrial trafficking and positioning.

4.1 Introduction

The mitochondrial Rho-GTPase 1, Miro1, is an important regulator of neuronal mitochondrial trafficking and contains two GTPase domains and two EF-hand Ca^{2+}-sensing domains. Miro1 binds kinesin and dynein motors to couple mitochondria to the microtubule transport network (Macaskill et al., 2009b, Wang and Schwarz, 2009). Upon Ca^{2+} binding to the EF-hand motifs of Miro1, a conformational change induces uncoupling of mitochondria from the transport network, enabling docking of mitochondria at sites requiring energy and Ca^{2+} buffering. Localised energy production and Ca^{2+} buffering is important for maintaining ion homeostasis and thus proper signalling in neurons (Attwell and Laughlin, 2001, Macaskill et al., 2009b, Vos et al., 2010).

Saotome and colleagues first describe how overexpression of the Miro1 mutant lacking the ability to bind Ca^{2+} (EF-hand domain double mutation E208K and E328K, referred to here as Miro1$^{\Delta EF}$) prevented Ca^{2+}-induced mitochondrial arrest (Saotome et al., 2008). Neuronal activity was shown to induce Miro1-EF-hand-dependent stopping of neuronal mitochondria (Macaskill et al., 2009b, Wang and Schwarz, 2009) in close proximity to synapses (Macaskill et al., 2009b). Functionally, Wang and Schwarz showed that overexpression of Miro1$^{\Delta EF}$ drastically reduces neuronal survival with application of acute NMDA (5 min, 3 μM, 10 μM and 30 μM) compared to overexpression of WT Miro1 and in experiments where Miro1 is not overexpressed. They conclude from this that disrupting Miro1-EF-hand-dependent mitochondrial trafficking in neurons diminishes neuronal resistance to excitotoxicity (Wang and Schwarz, 2009).

Although Miro has two isoforms in mammals (Miro1 and Miro2), most studies have focused on the function of Miro1. The two proteins have been suggested to have similar functions (Fransson et al., 2006), however some differences have emerged. The work of Misko and colleagues, found that knock down of Miro2, but not Miro1, in cultured neurons alters axonal mitochondrial transport (mainly anterograde transport) (Misko et al., 2010). Knock down of Miro1 only altered the somatic distribution of mitochondria (Misko et al., 2010) but this is not an expected finding. This study, therefore, suggests that Miro2 plays a more important role in regulating mitochondrial trafficking, at least in axons, but it could also indicate that Miro2 can compensate for the loss of Miro1.

The trafficking of mitochondria within astrocyte processes has been shown to be dependent on both the microtubule and actin cytoskeletons (Kremneva et al., 2013, Jackson et al., 2014) but the motor proteins and adaptors involved are yet to be identified. Astrocytes express kinesin motors at the mRNA level (KIF11 and KIF22) (Cahoy et al., 2008), however, their potential involvement in regulating astrocyte mitochondrial trafficking is unknown. While Miro1 is well established as an important regulator of mitochondrial trafficking and positioning in neurons, whether Miro proteins are present and important for the spatial regulation of mitochondria within astrocytes is not yet known. Therefore, the main aim of this chapter will be to address whether Miro, in particular the EF-hand Ca^{2+}-sensing abilities of Miro1, is conserved in astrocytes. In addition, whether Miro1 is important for regulating astrocyte function as well as the downstream impact of on neuronal function will be investigated.

4.2 Results

4.2.1 Astrocytes express Miro1 and Miro2, which localise to mitochondria along their processes.

An RNA-sequence transcriptome database indicates that astrocytes (mouse P7) express the gene for Miro1 (*Rhot1*) at higher levels than neurons (Zhang et al., 2014). However, the expression of Miro1 at the protein level has not been investigated to date. Thus, astrocytes were isolated from rat and mouse brains and probed for Miro proteins (Figure 4.2.1A). Indeed, both isoforms of Miro (Miro1 and Miro2) were present in isolated astrocyte cultures at similar levels to those seen in neurons (Macaskill et al., 2009b). Interestingly, Miro2 was present at higher levels than Miro1 in mouse cultures (E16) but no difference was seen in the expression levels in rat cultures (P1). It may be that Miro1 expression is developmentally delayed and upregulated postnatally.

Subsequently, the localisation of Miro1 was investigated in organotypic slices (Figure 4.2.1B). Labelling endogenous Miro (Miro1 and Miro2) alongside astrocyte mitochondria (AV-mtdsRed2-ir-EGFP transduced) revealed most mitochondria co-localise with Miro proteins. This novel finding reveals that Miro localises to astrocyte mitochondria *in situ*, suggesting that it may play a role in regulating their trafficking in astrocytes.

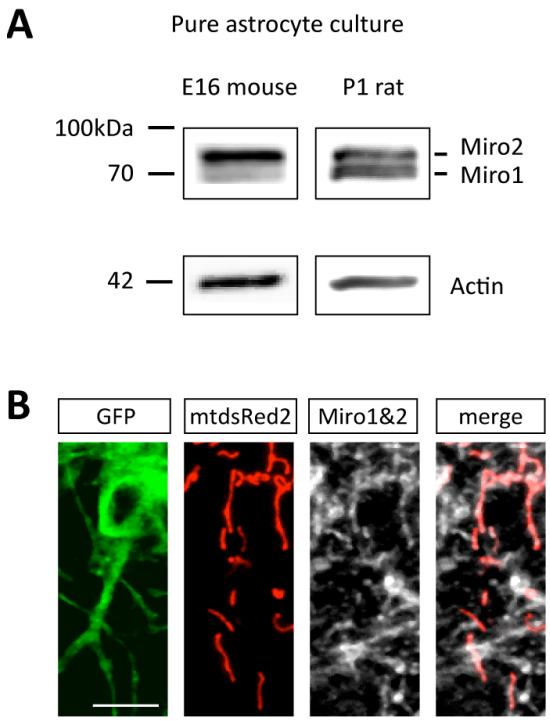

Figure 4.2.1 Astrocytes express Miro proteins (Miro1 and Miro2), which localise to mitochondria in slices. **A**. Western blot analysis of endogenous Miro expression in cultured hippocampal mouse (E16) and rat (P1) cortical astrocytes. **B.** Immuno-labelling of Miro1 and Miro2, *in situ*, which localises to mitochondria. Images show an example organotypic HPC slice infected with AVmtdsRed2-ir-EGFP and immuno-stained for Miro (atlas rabbit αMiro). Scale bar, 15 μm.

4.2.2 The EF Ca^{2+}-sensing domains of Miro1 are important for mitochondrial trafficking and morphology regulation in astrocyte processes, in culture.

To observe the role of Miro1's EF-hands in regulating mitochondrial trafficking dynamics and morphology in astrocytes, astrocyte-neuron co-cultures were transfected with either wild-type Miro1 ($Miro1^{WT}$) or EF-hand mutant Miro1 ($Miro1^{\Delta EF}$), which can no longer bind Ca^{2+} (Figure 4.2.2A). These bicistronic vectors overexpress either $Miro1^{WT}$ or $Miro1^{\Delta EF}$ along with mtdsRed2 to identify mitochondria. Cultures were co-transfected with GFAP promoter driven GFP (GFAP-GFP), to identify astrocytes (Figure 4.2.2B and C). As a further control, astrocytes were transfected with mtdsRed2 alone (not overexpressing Miro1) and GFAP driven-GFP. Potentially, the $Miro1^{\Delta EF}$ could be a dominant-negative mutant as, in previous studies, $Miro1^{\Delta EF}$ OE prevented Ca^{2+}-induced mitochondrial stopping within dendrites (Saotome et al., 2008) near synapses (Macaskill et al., 2009b). In addition, $Miro1^{\Delta EF}$ OE in neurons also diminished their resistance to excitotoxicity (Wang and Schwarz, 2009).

Interestingly, both $Miro1^{WT}$ and $Miro1^{\Delta EF}$ overexpression (OE), in culture, increased basal mitochondrial mobility (Figure 4.2.2D, $p = 0.02$ and $p = 0.01$, respectively) and speed (Figure 4.2.2E, $p = 0.001$ and $p = 0.01$, respectively). This suggests that Miro1 regulates mitochondrial trafficking under basal conditions in astrocytes and that the EF-hands of Miro1 are not necessary for mitochondria to bind their transport network.

Following glutamate treatment (100 μM + 1 μM glycine, 5 min), mitochondrial mobility and speed were reduced to a similar degree with control mtdsRed2 transfection and $Miro1^{WT}$ OE (Figure 4.2.2D, $p = 0.4$ and 4.2.2E, $p = 0.9$). Interestingly, post-glutamate treatment,

compared to Miro1$^{\Delta EF}$ OE, mitochondrial mobility (Figure 4.2.2D, p = 0.001 and p = 0.0003, respectively) and speed (Figure 4.2.2E, p = 0.0008 and p = 0.02, respectively) were significantly reduced in control conditions and with Miro1^{WT} OE i.e. Miro1$^{\Delta EF}$ OE impairs glutamate-induced halting of astrocyte mitochondria, where mobility and speed were similar to pre-treatment conditions. This reveals a previously unappreciated role for Miro1 in astrocytes, whereby its EF-hand-Ca^{2+}-sensing abilities are important for regulating basal mitochondrial trafficking and inducing mitochondrial stopping in response to glutamate treatment.

Furthermore, the role of the EF-hands of Miro1 in regulating astrocyte mitochondrial morphology was also investigated. Interestingly, with Miro1$^{\Delta EF}$ OE mitochondria were more elongated compared to Miro1^{WT} OE but not significantly different from control (mtsdRed2) conditions (figure 4.2.2F, p = 0.01). Following glutamate treatment, mitochondrial length was significantly reduced in control conditions and with Miro1^{WT} OE compared to pre-treatment conditions and compared to Miro1$^{\Delta EF}$ OE (Figure 4.2.2F, p = 0.0007 and p = 0.01). This suggests that the EF-hands of Miro1 are also important for regulating mitochondrial morphology in astrocytes. It could be that through mutating the EF-hands their interactions with pro-fission proteins, such as Drp1, are impaired (Saotome et al., 2008).

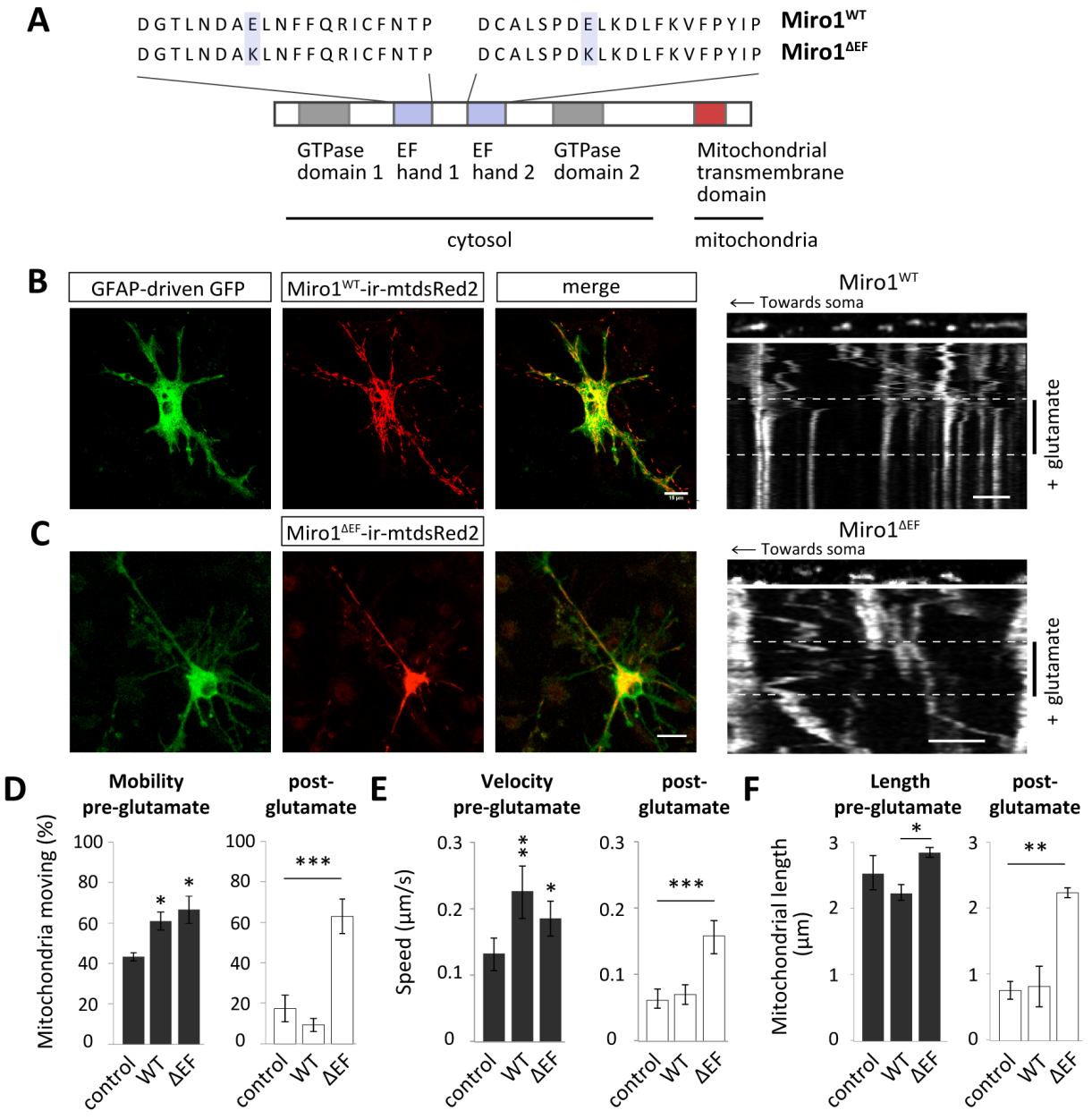

Figure 4.2.2 Miro1's EF hands regulate mitochondrial trafficking and morphology in cultured hippocampal astrocytes. **A**. Primary structure of Miro1 showing the point mutations that exist in the mutant form of Miro1$^{\Delta EE\text{-}KK}$ (Miro1$^{\Delta EF}$), which can't bind Ca^{2+}. **B**. Astrocyte transfected with Miro1^{WT}-ires-mtdsRed2 (WT) and GFAP-driven-GFP. Scale bar, 15 μm. Inset kymograph of mitochondrial trafficking with glutamate treatment (100 μM + 1 μM glycine, 5 minutes). Scale bar, 5 μm. **C**. Astrocyte transfected with Miro1$^{\Delta EF}$-ires-mtdsRed2 (ΔEF) and GFAP-GFP. Scale bar, 15μm. Inset kymograph with glutamate treatment. Scale bar, 5 μm. **D**. Mitochondria moving pre (left) and post-glutamate treatment (right). Controls were transfected with mtdsRed2 and GFAP-GFP (control and Miro1^{WT} (pre and post) n = 3 cells; Miro1$^{\Delta EF}$ (pre and post) n = 4 cells). **E**. Mitochondrial speed pre and post glutamate (control pre and Miro1^{WT} post n = 10 mitochondria, 3 cells; Miro1^{WT} pre n = 12 mitochondria, 3 cells; Miro1$^{\Delta EF}$ pre n = 11 mitochondria, 4 cells; control post n = 9 mitochondria, 3 cells; Miro1$^{\Delta EF}$ post n = 13 mitochondria, 3 cells). **F**. Mitochondrial length pre and post glutamate (Miro1^{WT} and Miro1$^{\Delta EF}$ n = 3 cells).

4.2.3 The EF-hands of Miro1 are important for regulating mitochondrial trafficking in astrocytes in response to neuronal activity *in situ*.

To further investigate the role of Miro1 in astrocytes in an intact system, organotypic slices were biolistically transfected with either $Miro1^{WT}$ or $Miro1^{\Delta EF}$, both bicistronically expressing mtdsRed2, along with co-transfection of GFAP driven-GFP (Figure 4.2.3A). This allowed the role of Miro1 in astrocytes to be examined where network connectivity is preserved.

Stimulating neuronal activity with 4-AP, resulted in a significant reduction in mitochondrial mobility (Figure 4.2.3B, $p = 0.03$), speed (Figure 4.2.3C, $p = 9x10^{-6}$) and length (Figure 4.2.3D, $p = 0.0003$) in astrocytes, with $Miro1^{WT}$ OE, which was not observed with $Miro1^{\Delta EF}$ OE (Figure 4.2.3C, $p = 0.8$, $p = 0.9$ and $p = 0.6$, respectively). These results support the results in culture and indicate that Miro1 may regulate activity-driven mitochondrial trafficking and morphology *in vivo*.

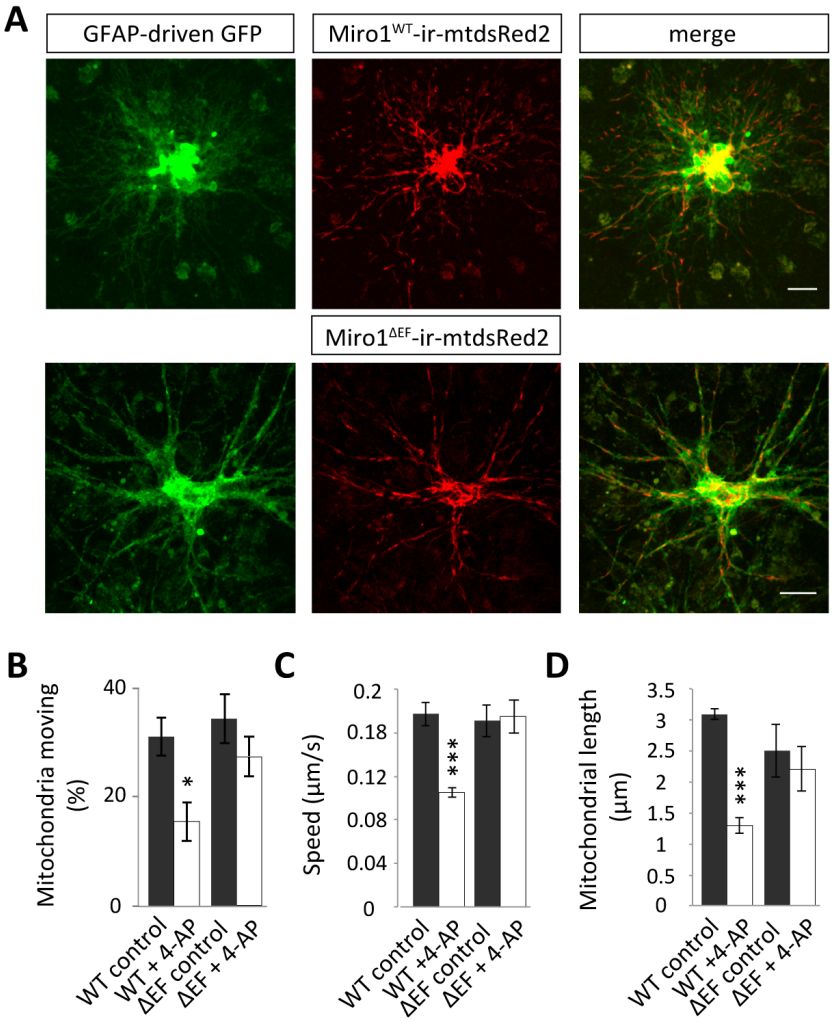

Figure 4.2.3 The EF-hands of Miro1 are essential for regulating mitochondrial trafficking in astrocytes in hippocampal slices. **A**. Example images of Miro1^{WT}-ir-mtdsRed2 (WT) and Miro1^{EF}-ir-mtdsRed2 (ΔEF) co-transfected with GFAP-driven GFP *in situ* imaged 2-3 days post shooting (slices were shot at 7 DIV). Scale bars, 15 μm. **B**. Mitochondrial mobility before (control) and after 4-AP treatment (100 μM, 5 minutes) with Miro1^{WT} and Miro1$^{\Delta EF}$ OE (Miro1^{WT} (control and 4-AP) n = 3 cells, 3 slices; Miro1$^{\Delta EF}$ (control and 4-AP) n = 3 cells, 3 slices). **C**. Speed of moving mitochondria before and after 4-AP treatment with Miro1^{WT} or Miro1$^{\Delta EF}$ OE (Miro1^{WT} control n = 11 mitochondria, 3 slices; Miro1^{WT} + 4-AP n = 10 mitochondria, 3 slices; Miro1$^{\Delta EF}$ (control and 4-AP) n = 10 mitochondria, 3 slices). **D**. Mitochondrial length before and after 4-AP treatment with Miro1^{WT} or Miro1$^{\Delta EF}$ OE (Miro1^{WT} n = 3 cells, 3 slices; Miro1$^{\Delta EF}$ n = 3 cells, 3 slices).

4.2.4 Activity-dependent positioning of astrocyte mitochondria near synapses requires the EF-hands of Miro1, *in situ*.

To investigate the role of the EF-hands of Miro1 in regulating mitochondrial positioning within astrocyte processes, in hippocampal slices, Miro1^{WT} or Miro1$^{\Delta EF}$ vectors bicistronically expressing mtdsRed2 were used to label mitochondria with biolistic transfection and synapses were immuno-labelled with VGLUT1 (Figure 4.2.4A). With Miro1^{WT} the distance between mitochondria and their nearest synapse significantly decreased following 4-AP treatment (5 minutes, 100 μM), compared to untreated controls (Figure 4.2.4B, $p = 0.02$). This decrease was not observed, however, in slices with mutant Miro1$^{\Delta EF}$ OE, where following treatment, the distribution was similar to untreated control conditions (Figure 4.2.4B, $p = 0.8$). Importantly, no significant change was seen in synapse or mitochondrial number (per μm) (Figure 4.2.4C, $p = 0.5$ and $p = 0.8$, $p = 0.1$ and $p = 0.8$, respectively). Therefore, it appears that the EF-hands of Miro1 are important for regulating activity-driven mitochondrial stopping and their concomitant retention in astrocyte processes in close proximity to synapses *in situ*. Ultimately, the spatial confinement of mitochondria within perisynaptic astrocyte processes in response to increased levels of neuronal activity is expected to not only have important consequences for astrocyte function but also neuronal synaptic transmission.

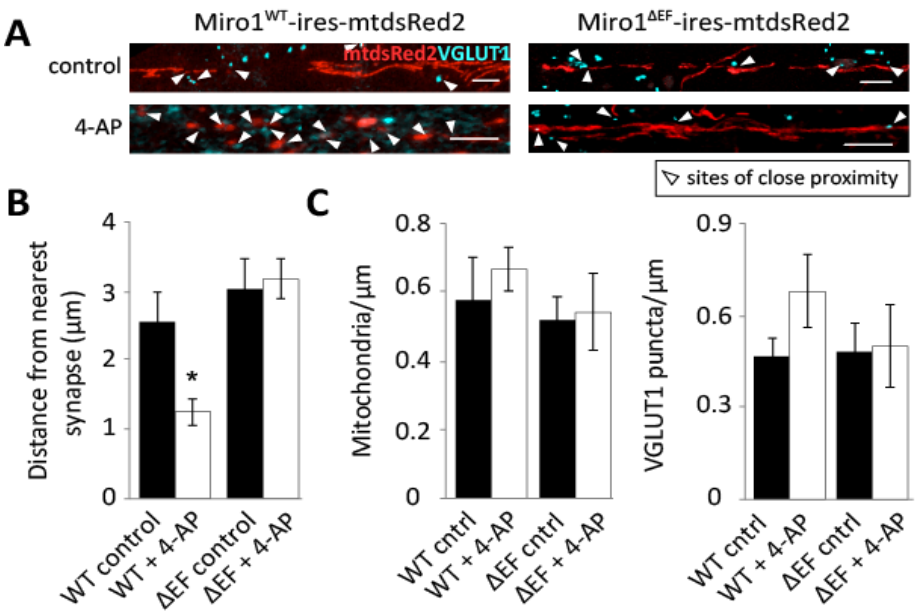

Figure 4.2.4 Astrocyte mitochondrial recruitment near synapses is dependent on the EF-hand Ca^{2+} sensing domains of Miro1, *in situ*. **A**. Representative images of mitochondrial distribution in relation to VGLUT1 labelled synapses with $Miro1^{WT}$-ir-mtdsRed2 (WT) and $Miro1^{\Delta EF}$-ir-mtdsRed2 (ΔEF) OE prior to and following 4-AP treatment (5 minutes, 100 μM). Scale bars, 5 μm. **B**. Distance between mitochondria and their nearest VGLUT1 labelled synapse (centre of mass) under basal conditions and with 4-AP treatment. **C**. Number of mitochondria and VGLUT1 puncta in analysed ROIs (per μm) with $Miro1^{WT}$ or $Miro1^{\Delta EF}$ OE. $Miro1^{WT}$ control n = 7 ROIs, 7 cells, 3 slices; $Miro1^{WT}$ + 4-AP n = 6 ROIs, 6 cells, 3 slices; $Miro1^{\Delta EF}$ control n = 7 ROIs, 7 cells, 3 slices; $Miro1^{\Delta EF}$ + 4-AP n=7 ROIs, 7 cells, 3 slices.

4.2.5 The ability of mitochondria to sense elevated intracellular Ca^{2+} is disrupted when Miro1 is mutated.

The ability of mitochondria to localise to regions of high intracellular Ca^{2+} could be important for Ca^{2+} buffering and the downstream release of neuro-active substances from astrocytes. Thus, the ability of Miro1's EF-Ca^{2+} hands to regulate this function was investigated. Slices were biolistically co-transfected with GCaMP6s to image intracellular Ca^{2+} levels and either $Miro1^{WT}$ or $Miro1^{\Delta EF}$ bicistronically expressing mtdsRed2 to label mitochondria. Subsequently, mitochondrial trafficking was analysed in regions of the same cell exhibiting relatively high or low levels of intracellular Ca^{2+}, reflected by GCaMP6s fluorescence intensity. Interestingly, the halting of mitochondria at Ca^{2+} hot spots seen in control conditions ($Miro1^{WT}$ OE) was disrupted with mutant $Miro1^{\Delta EF}$ OE (Figure 4.2.5A, $p = 0.002$). Relative levels of intracellular Ca^{2+} were quantified following measurement of mitochondrial speed (Figure 4.2.5Ai).

This result further supports a role for the EF-hand Ca^{2+}-sensing motifs of Miro1 in regulating mitochondrial trafficking in the processes of astrocytes *in situ*. The spatial regulation of astrocyte mitochondria by Miro1 could be important for their positioning near synapses during activity, where they are required to provide energy to maintain ion flux and channel activity as well as buffering Ca^{2+} influx, which can occur in a spatially restricted manner within their processes (Srinivasan et al., 2015). The spatial regulation of astrocyte mitochondria could, therefore, impact of their release of gliotransmitters.

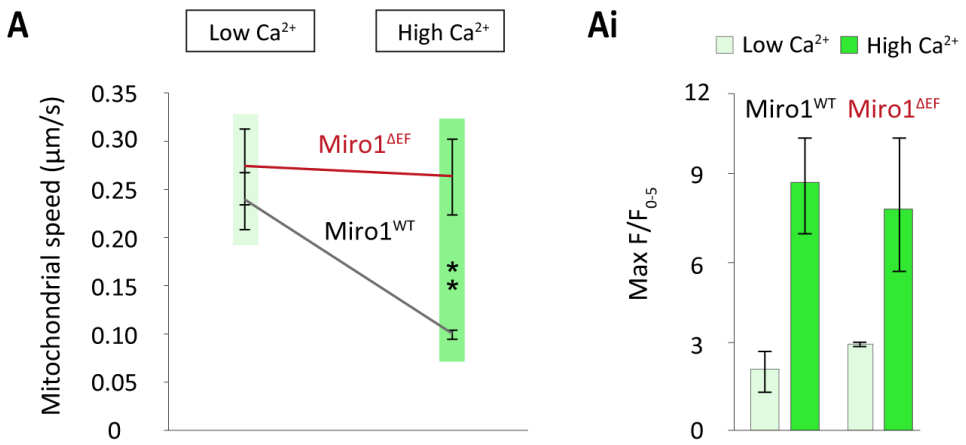

Figure 4.2.5 Mutant Miro1 (Miro1$^{\Delta EF}$) overexpression alters the ability of mitochondria to localise at regions of elevated Ca^{2+}. **A**. Mitochondrial speed in regions of low and high intracellular Ca^{2+} with overexpression of Miro1^{WT}-ires-mtdsRed2 and mutant Miro1$^{\Delta EF}$-ires-mtdsRed2 (Miro1^{WT} low n = 6 mitochondria, 3 slices; Miro1^{WT} high n = 5 mitochondria, 3 slices; Miro1$^{\Delta EF}$ low n = 5 mitochondria, 3 slices; Miro1$^{\Delta EF}$ high n = 5 mitochondria, 3 slices). **Ai**. Relative levels of intracellular Ca^{2+} (maximum GCaMP6s fluorescence normalised to the first 5 frames (10 s)) where high intracellular Ca^{2+} levels were relative to regions of the same cell where Ca^{2+} was low.

4.2.6 Mutating the EF-hands of Miro1 alters basal astrocyte Ca^{2+} signalling *in situ*.

To investigate the impact of disrupting mitochondrial trafficking and positioning in astrocytes, organotypic slices were biolistically co-transfected with GCaMP6s and either $Miro1^{WT}$ or $Miro1^{\Delta EF}$ vectors bicistronically expressing mtdsRed2 to indicate Miro1 overexpression (OE) (Figure 4.2.6A). Specific transfection of astrocytes was confirmed by significant co-localisation of the GCaMP6s signal with GFAP (as shown previously in Figure 3.2.6).

Interestingly, the frequency of basal Ca^{2+} transients was increased with $Miro1^{\Delta EF}$ OE in the processes of astrocytes compared to $Miro1^{WT}$ OE (Figure 4.2.6B and Bi $p = 4x10^{-5}$). In addition, $Miro1^{\Delta EF}$ OE significantly increased the amplitude of Ca^{2+} transients in astrocyte processes compared to $Miro1^{WT}$ OE (Figure 4.2.6B and Bi $p = 2x10^{-5}$). These results reveal that the spatial regulation of mitochondria by the EF-hands of Miro1 is important for intracellular Ca^{2+} signalling in astrocytes, which could have important consequences for their function, particularly in relation to gliotransmission.

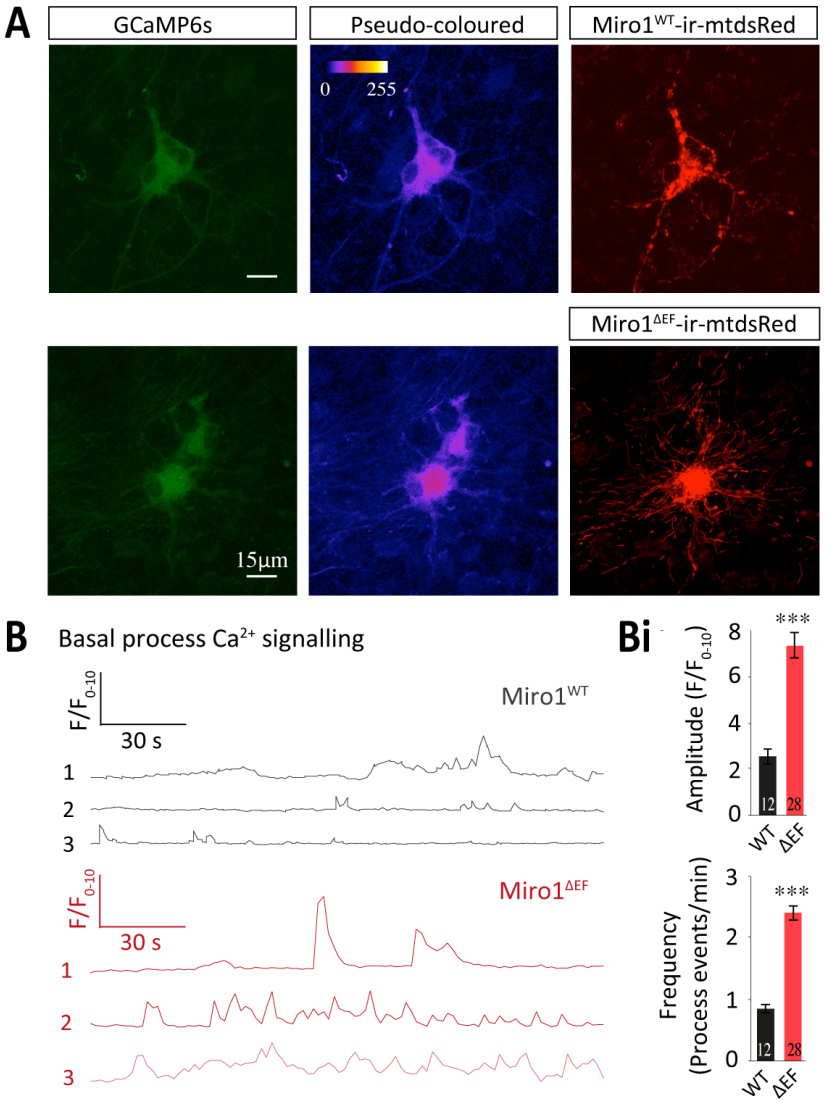

Figure 4.2.6 Mutant Miro1 (Miro1^{EF}) overexpression alters basal astrocytic Ca^{2+} signalling in hippocampal slices. **A.** Example astrocyte biolistically transfected with GCaMP6s and Miro1^{WT}-ir-mtdsRed2 (WT) or Miro1$^{\Delta EF}$-ir-mtdsRed2 (ΔEF). **B**. Example basal process Ca^{2+} signalling with Miro1^{WT} or Miro1$^{\Delta EF}$ OE, F/F_0 normalised to the first 5 frames (10 s). **Bi**. Amplitude (F/F_0, normalised to the first 5 frames (10 s)) and frequency (process events/min) of basal Ca^{2+} transients with Miro1^{WT} or Miro1$^{\Delta EF}$ OE (Miro1^{WT} n = 14 ROIs, 7 slices; Miro1$^{\Delta EF}$ n = 27 ROIs, 7 slices).

4.2.7 Mutating the EF-hands of Miro1 increases activity-driven astrocyte Ca^{2+} signalling, *in situ*.

Subsequently, the question of whether astrocytes could respond to stimulation with overexpression (OE) of the mutant form of Miro1 was addressed. Astrocytes in hippocampal slices were again biolistically co-transfected with GCaMP6s and either $Miro1^{WT}$ or $Miro1^{\Delta EF}$ vectors bicistronically expressing mtdsRed2 to indicate Miro1 overexpression (OE). With this approach, a significant increase in the dynamics of astrocyte Ca^{2+} signalling was observed following stimulation, in the processes. The response to 4-AP treatment (5 minutes, 200 μM), to stimulate neuronal activity, in astrocytes with $Miro1^{\Delta EF}$ OE was greater in amplitude compared to $Miro1^{WT}$ OE astrocytes (Figure 4.2.7A and Ai $p = 0.001$). In addition, the response frequency and duration was significantly elevated with $Miro1^{\Delta EF}$ compared to $Miro1^{WT}$ (Figure 4.2.7Ai $p = 0.002$ and $p = 1x10^{-5}$, respectively).

With ATP treatment (2 minutes, 100 μM), to stimulate a rise in intracellular Ca^{2+}, the rise in Ca^{2+} was even higher with $Miro1^{\Delta EF}$ OE compared to $Miro1^{WT}$ OE. $Miro1^{\Delta EF}$ increased the ATP response amplitude (Figure 4.2.7Ai $p = 0.02$), frequency (Figure 4.2.7Ai $p = 0.01$) and duration (Figure 4.2.7Ai $p = 0.02$).

These results reveal that the spatial regulation of mitochondria by Miro1 is important for intracellular Ca^{2+} signalling in astrocytes, which could have important consequences for the pathogenesis of disease in the CNS.

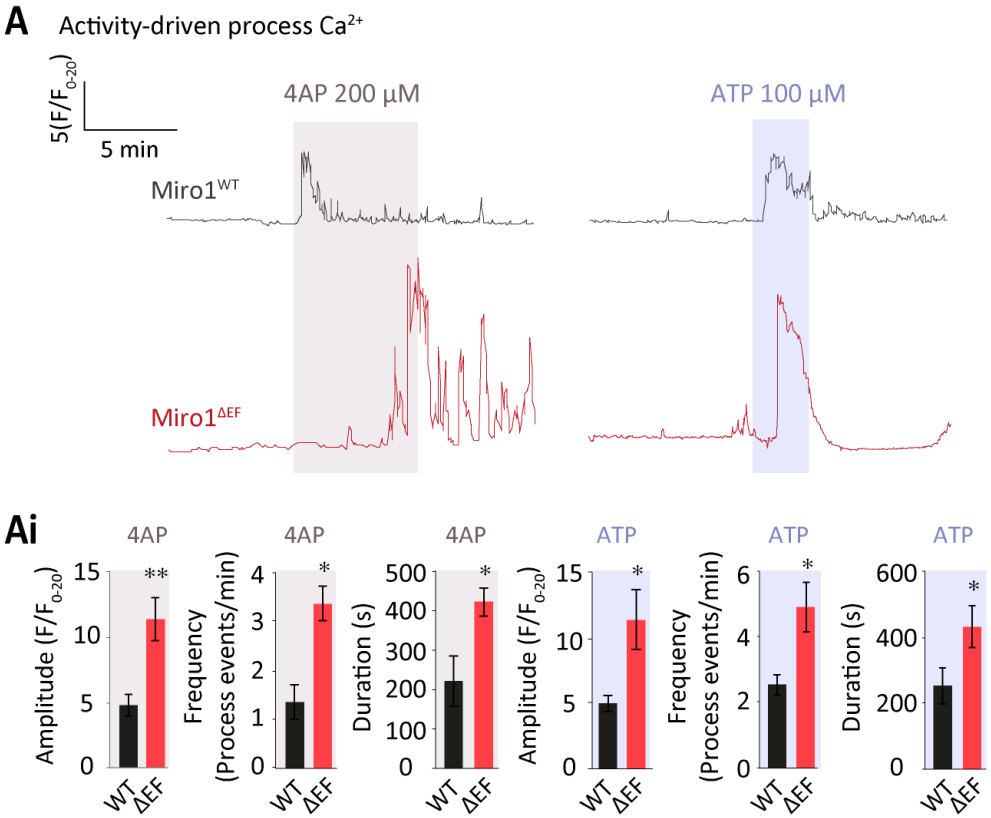

Figure 4.2.7 Mutant Miro1 (Miro1^{EF}) overexpression alters activity-driven astrocyte Ca^{2+} signalling, *in situ*. **A**. Example activity-stimulated process Ca^{2+} signalling with Miro1^{WT}-ir-mtdsRed2 (WT) or Miro1$^{\Delta EF}$-ir-mtdsRed2 (ΔEF) OE. Slices were perfused with 200 μM 4-AP for 5 minutes or 100 μM ATP for 2 minutes. **Ai**. Response amplitude (F/F_0, normalised to the first 10 frames (20 s)), frequency (process events/min) and duration with 4AP and ATP treatment (Miro1^{WT} + 4-AP n = 11 ROIs, 5 slices; Miro1$^{\Delta EF}$ + 4-AP n = 10 ROIs, 4 slices; Miro1^{WT} + ATP n = 8 ROIs, 4 slices; Miro1$^{\Delta EF}$ + ATP n = 9 ROIs, 7 slices).

4.2.8 Mutating the EF-hands of Miro1 in astrocytes alters the number of excitatory synapses, in culture.

It appears that mutating the EF-hands of Miro1 not only impact on the function of astrocytes but also that it alters the number of excitatory synapses. Cultured hippocampal astrocytes were pre-transfected with either Miro1^{WT}-ir-mtdsRed2 (WT) or Miro1$^{\Delta EF}$-ir-mtdsRed2 (ΔEF) before being co-cultured with hippocampal neurons (at 3 DIV) for 7-10 days. Excitatory pre- and post- synaptic terminals were immuno-labelled with a VGLUT1 antibody and a homer antibody, respectively.

Neurons in close proximity to astrocytes overexpressing (OE) the mutant form of Miro1 (Miro1$^{\Delta EF}$) exhibit a reduced number of VGLUT and homer puncta (per μm) compared to neurons that are not in close proximity to mutant Miro1 OE astrocytes (Figure 4.2.8B, $p = 0.02$ and $p = 0.003$, respectively). The size of VGLUT puncta were also significantly decreased but not the size of the homer puncta (Figure 4.2.8C, $p = 0.001$ and $p = 0.6$, respectively). OE of the mutant form of Miro1 (Miro1$^{\Delta EF}$) also decreased the density of synapses i.e. the proportion of homer with VGLUT contacts sites and, reciprocally, the proportion of VGLUT with homer contacts (Figure 4.2.8D, $p = 0.01$ and $p = 0.04$, respectively). Importantly, there was no significant change in the number or area of homer and VGLUT1 puncta or the proportion of VGLU1 with homer and the proportion of homer with VGLUT1 in close proximity to Miro1^{WT} OE astrocytes compared to neurons not in close proximity to Miro1^{WT} or Miro1$^{\Delta EF}$ OE astrocytes (Figure 4.2.8B-D).

This implies that improper intracellular Ca^{2+} handling in astrocytes impacts on the number of excitatory synapses. Aastrocyte Ca^{2+} elevations can induce the release of gliotransmitters, prolonged release of which, disrupts neuronal signalling and causes excitotoxic cell death (Araque et al., 1998, Di Castro et al., 2011). A decrease in synaptic density may indicate cell death or a compensatory response in order to down-regulate synaptic activity to counteract the increased presence of gliotransimitters release by nearby astrocytes. More broadly it shows that the consequence of disrupted intracellular Ca^{2+} regulating, through altered Miro1-EF-hand-dependent mitochondrial spatial regulation, does indeed have an impact on the surrounding neuronal architecture.

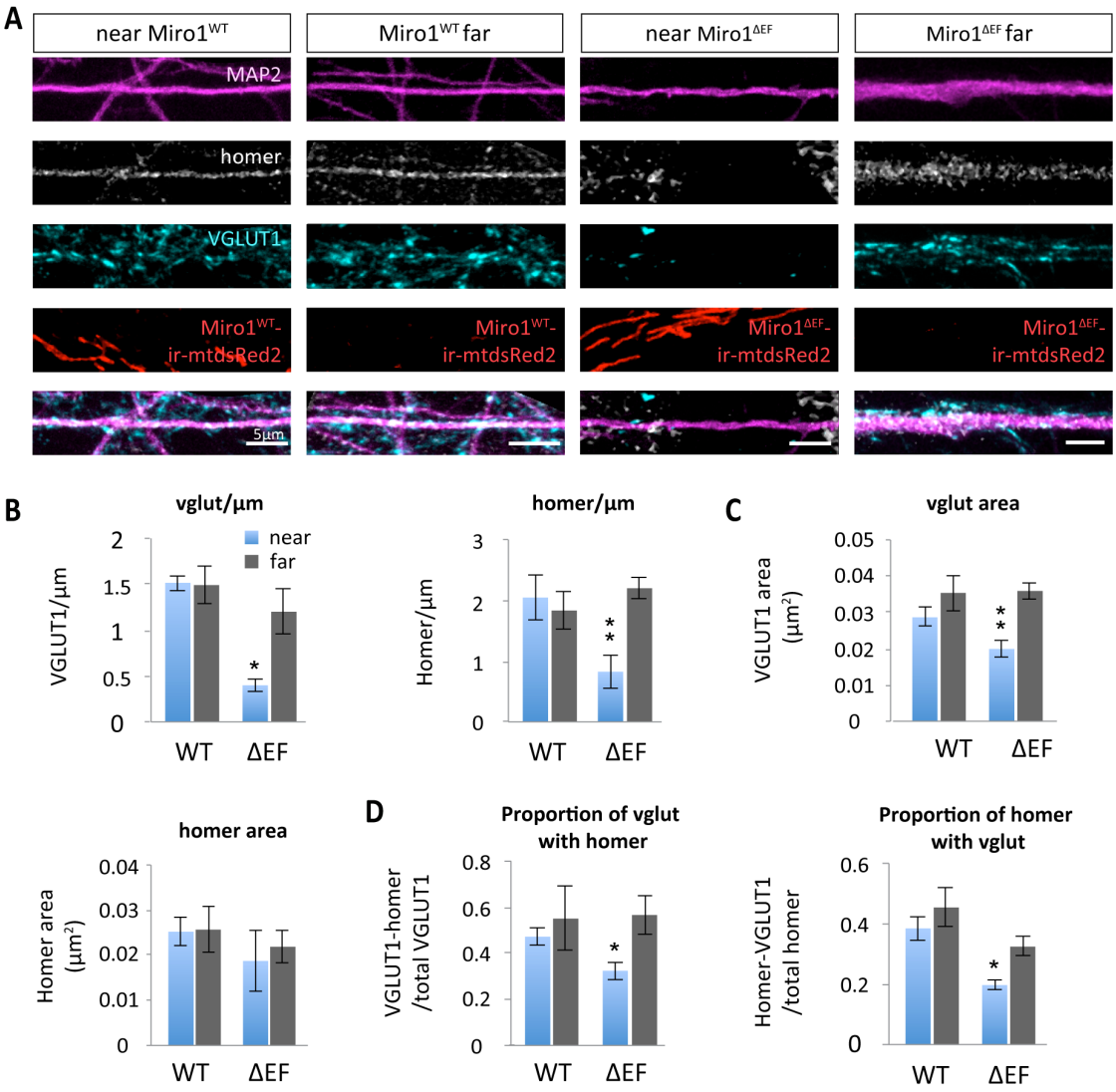

Figure 4.2.8 Mutant Miro1 (Miro1^{EF}) OE alters the number of excitatory synapses. **A.** Representative images of hippocampal neurons co-cultured with hippocampal astrocytes pre-transfected with either Miro1^{WT}-ir-mtdsRed2 (WT) or Miro1$^{\Delta EF}$-ir-mtdsRed2 (ΔEF). Neuronal dendrites were immuno-labelled with MAP2 and pre- and post-synaptic terminals were labelled with VGLUT1 and homer, respectively. These images also show synaptic labelling in close proximity to OE astrocytes (near) and not in close proximity to OE astrocytes (far). Scale bars, 5 μm. **B**. Number of VGLUT and homer puncta per μm near and far from WT/EF OE astrocytes. **C**. The size of VGLUT and homer puncta (μm^2) near and far from WT/EF OE astrocytes. **D**. The proportion of VGLUT1 with homer was quantified by calculating the number of VGLUT1 puncta that came into contact with homer puncta divided by the total number of VGLUT1 puncta (near and far from WT/EF OE astrocytes). Reciprocally, the proportion of homer with VGLUT1 was quantified by calculating the number of homer puncta that came into contact with VGLUT1 puncta divided by the total number of homer puncta (near and far from WT/EF OE astrocytes). Near Miro1^{WT} n = 10 ROIs, 10 cells; Mito1^{WT} far n = 4 ROIs, 4 cells; near Miro1$^{\Delta EF}$ n = 5 ROIs, 5 cells; Miro1$^{\Delta EF}$ far n = 6 ROIs, 6 cells).

4.2.9 Mutating the EF-hands of Miro1 in astrocytes alters the presence of GluR2-containing neuronal AMPA receptors.

Additionally, mutating the EF-hands of Miro1 not only impacts on the number of synapses but also the formation of functional excitatory GluR2-containting synapses. Cultured hippocampal astrocytes were pre-transfected with either $Miro1^{WT}$-ir-mtdsRed2 (WT) or $Miro1^{\Delta EF}$-ir-mtdsRed2 (ΔEF) before being co-cultured with hippocampal neurons (at 3 DIV) for 7-10 days. Functional synapses were immuno-labelled with a GluR2 antibody, a marker for AMPARs. These receptors, in particular GluR2-containing AMPARs, are widely accepted as critical for synaptic transmission (Liu and Zukin, 2007).

With overexpression (OE) of the mutant form of Miro1 ($Miro1^{\Delta EF}$) the number of total GluR2-positive synapses per μm was significantly decreased (Figure 4.2.9B, $p = 0.04$). The average area of GluR2-positive synapses was also significantly reduced (Figure 4.2.9C, $p = 0.009$). This implies that improper intracellular Ca^{2+} handling in astrocytes impacts on the number and size of GluR2-positive synapses. This may be because disrupted intracellular Ca^{2+} regulating through altered Miro1-EF-hand-dependent mitochondrial spatial regulation impacts on the activity of the surrounding neuronal architecture.

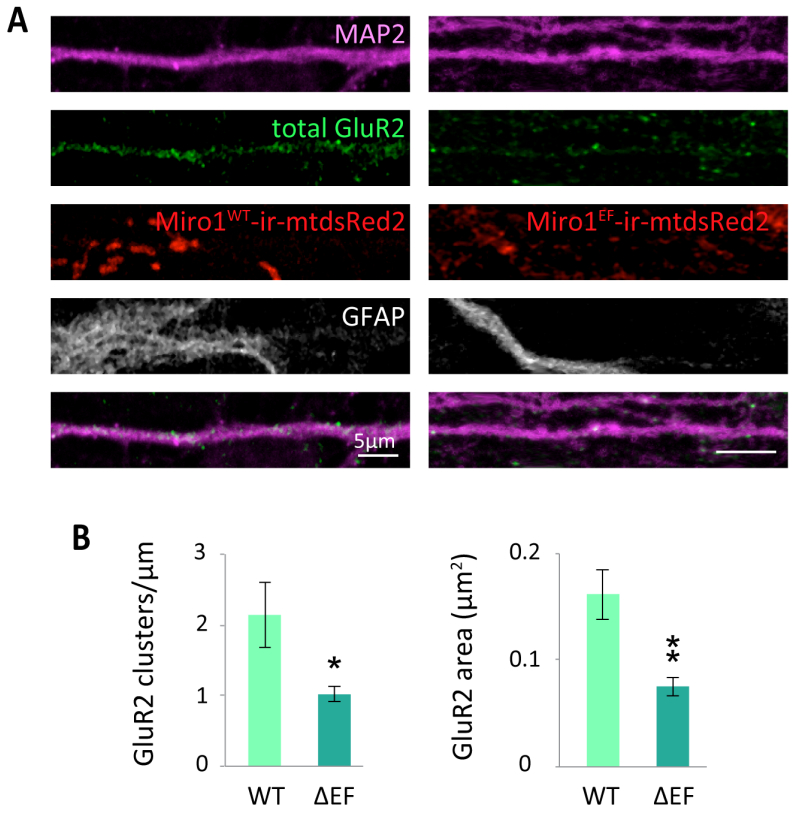

Figure 4.2.9 Mutant Miro1 (Miro1^{EF}) OE alters the formation of GluR2-containing AMPARs. **A.** Representative images of hippocampal neurons co-cultured with hippocampal astrocytes pre-transfected with either Miro1^{WT}-ir-mtdsRed2 (WT) or Miro1$^{\Delta EF}$-ir-mtdsRed2 (ΔEF). Neuronal dendrites were again immuno-labelled with MAP2 and a GluR2 antibody was used to label total process AMPARs (permeabilised staining). GFAP was also used to label nearby astrocytes OE Miro1. Scale bars, 5 μm. **B**. Number (per μm) of GluR2 puncta near Miro1^{WT} or Miro1$^{\Delta EF}$ OE astrocytes. **C**. Area (μm^2) of GluR2 puncta near Miro1^{WT} or Miro1$^{\Delta EF}$ OE astrocytes. Miro1^{WT} n = 5 ROIs, 5 cells; Miro1$^{\Delta EF}$ n = 5 ROIs, 5 cells.

4.3 Discussion

Here, a mechanism is proposed whereby mitochondrial trafficking, morphology and positioning in astrocyte processes is regulated by the Ca^{2+}-sensing abilities of Miro1. The spatial regulation of astrocyte mitochondria by the EF-Ca^{2+}-sensing hands of Miro1 is essential for astrocyte intracellular Ca^{2+} buffering, which is important downstream for the formation of excitatory synapses and post-synaptic GluR2-containing AMPARs. Mechanistically, elevations in intracellular astrocyte Ca^{2+} likely result in gliotransmitter release and a loss in the number of synapses potentially due to excitotoxic neuronal cell death.

Several novel features exist in the control of astrocyte mitochondrial trafficking and positioning involving Miro1. First, Miro1 is expressed in rodent astrocytes at the protein level and it localises to mitochondria. Second, the Ca^{2+}-binding EF-hand domains of Miro1 are not required for basal mitochondrial trafficking or for mitochondria binding to the microtubule or actin transport network, but here it is suggested that Miro1 regulates basal mitochondrial trafficking in astrocytes. It could be that increasing Miro1 ($Miro1^{WT}$ or $Miro1^{\Delta EF}$) increases the binding of mitochondria to microtubules or actin in astrocyte processes, allowing them to move more with increased speed. Third, the EF-hands of Miro1 are essential for inducing mitochondrial cessation in response to elevations in intracellular Ca^{2+}. Fourth, the EF-hands also appear to be important for regulating astrocyte mitochondrial morphology, where

mutating the EF-hands prevents mitochondrial remodelling/fission following stimulation of neuronal activity. This reveals that the EF-hands of Miro1 are important for regulating activity-driven mitochondrial stopping and morphology in astrocytes.

Another interesting observation made by this study is that the EF-hands of Miro1 appear to be important for the activity-driven retention of mitochondria at synapses. This suggests that Ca^{2+} binding the EF-hands of Miro1 is important for inducing mitochondrial stopping at predicted Ca^{2+} hot spots. Finally, overexpressing the mutant form of Miro1 ($Miro1^{\Delta EF}$) alters the ability of astrocytes to regulate their intracellular Ca^{2+} levels, *in situ*. $Miro1^{\Delta EF}$ OE increased the frequency and amplitude of basal Ca^{2+} transients and increased the response to neuronal activity and ATP. Here, astrocytes may be more vulnerable to Ca^{2+} overload when the Ca^{2+}-sensing abilities of Miro1 are disrupted. It would be interesting to test whether Miro1 OE alters mitochondrial membrane potential and consequently their ability to buffer Ca^{2+}. Disrupted intracellular Ca^{2+} regulation in astrocytes could have important consequences for their unique propagation of Ca^{2+} waves and suggests that the spatial regulation of mitochondria by Miro1 plays an important role in regulating astrocyte signalling.

Since the regulation of intracellular Ca^{2+} also has the potential to impact on gliotransmission, this thesis reveals another potential route for bi-directional communication between astrocytes and neurons. This could be linked to instances of pathology, as disrupted astrocyte Ca^{2+} dynamics due to altered mitochondrial function has devastating consequences for neuronal function (Katayama et al., 1995, Danbolt, 2001, Shin et al., 2005, Volobouéva et al., 2007, Li et al., 2008, Bradford et al., 2009, Oliveira and Goncalves, 2009). Interestingly, basal Ca^{2+} transients are elevated in astrocytes in mice expressing mutant human Aβ precursor protein (Kuchibhotla et al., 2009). Similarly, expression of proteins containing PD-related gene

mutations (for example, human protein deglycase DJ-1 mutations) in cultured astrocytes impairs mitochondrial dynamics. This compromises their neuroprotective ability and thus renders neurons more sensitive to toxic insults (Larsen et al., 2011, Schmidt et al., 2011, Lev et al., 2013).

Here, improper intracellular Ca^{2+} handling in astrocytes impacts on the formation of excitatory synapses. This may be because astrocyte Ca^{2+} elevations can induce the release of gliotransmitters, which may disrupt neuronal signalling transmission and cause exocytotic cell death (Araque et al., 1998, Di Castro et al., 2011). A reduction in synapses may indicate cell death or a compensatory response to down regulate synaptic activity in order to counteract the increased presence of gliotransimitters release by nearby astrocytes. This highlights that Miro1-dependent mitochondrial trafficking in astrocytes is functionally not only important for astrocyte signalling but also affects neuronal function. It means that understanding the tightly coupled mechanisms of feedback signalling between neurons and astrocytes are important and the results shown here implicate astrocyte mitochondrial regulation in this feedback signalling.

In summary, the EF-hands of Miro1 have been shown here to regulate trafficking and morphology of mitochondria in the processes of astrocytes, as well as retention of mitochondria in close proximity to excitatory synapses. The spatial regulation of astrocyte mitochondria by the EF-hands of Miro1 was essential for astrocyte intracellular Ca^{2+} regulation, which could have important consequences for Ca^{2+} wave propagation and gliotransmission. Here, disrupting EF-hand-dependent intracellular astrocyte Ca^{2+} regulation altered the formation of excitatory synapses. Further work is required to confirm exactly how altering Miro1-mediated astrocyte mitochondrial positioning affects glitotransmission.

Chapter 5

Miro1^{KO} astrocytes have disrupted mitochondrial trafficking dynamics and this is critical for proper synapse regulation.

5.1 Introduction

Recently, Nguyen and colleagues investigated the role of Miro1 in regulating aspects of mitochondrial localisation in motor neurons. They find that the consequence of a total loss of Miro1 is lethal (death occurs prior to birth- prenatally) (Nguyen et al., 2014). Neuron-specific loss of Miro1 causes depletion of mitochondria from corticospinal tract axons. Additionally, they find progressive neurological deficits, indicative of motor neuron disease (MND), in neuron-specific Miro1 KO mice. Defects were observed in retrograde axonal mitochondrial transport, although mitochondrial respiratory function is preserved. Moreover, they deduce that Miro1 is not essential for Ca^{2+}-mediated inhibition of mitochondrial mobility or

mitochondrial Ca^{2+} buffering. It could be that Miro2 compensates for a loss of Miro1 to regulate mitochondrial mobility and mitochondrial Ca^{2+} buffering. This, however, has not been conclusively demonstrated to date. It could be that normal astrocyte Miro1 function can somehow compensate for a neuronal loss of Miro1. Nguyen and colleagues do conclude that neuronal mitochondrial mobility defects and impaired mitochondrial distribution are sufficient to cause neurological disease (Nguyen et al., 2014). In conclusion, this study indicates that Miro1 is important for regulating mitochondrial density and proper neuronal function and suggests a need to investigate the role of Miro1 in astrocytes.

The consequence of a total loss of astrocyte Miro1, however, has not been determined. Due to the importance of the EF-hand domains of Miro1 in regulating intracellular astrocyte Ca^{2+} and ultimately synapse formation (shown in chapter 4), this indicates that astrocyte mitochondrial positioning is important for astrocyte signalling, which has important consequences for the surrounding neuronal environment. Thus, a total loss of Miro1 in astrocytes may have even more important consequences for astrocyte function and neuronal synapse formation. Where Miro-independent trafficking regulation has been proposed in neurons (Cai et al., 2005, Nguyen et al., 2014), this may not be the case in astrocytes and thus a total loss of Miro1 in astrocytes was investigated. Astrocytes do express genes for other proteins that could potentially recruit kinesin-1 motors to mitochondria. These include syntabulin (SYBU) and Trak (Trak1 and Trak2) genes (Cahoy et al., 2008). However, whether these proteins are expressed and if they are capable of mediating astrocyte mitochondrial transport in the absence of Miro is not known. As mentioned previously, astrocytes were shown to express Miro2, which may be able to compensate for the total loss of astrocyte Miro1.

It may be that through the loss of all of Miro1's regulatory domains that mitochondrial morphology is affected in astrocytes as well as potential trafficking defects. This is because the GTPase domains of Miro1 have been proposed to regulate mitochondrial morphology (Fransson et al., 2006) as well as trafficking (MacAskill et al., 2009a). For example, the recruitment of Trak2 to neuronal mitochondria is dependent on the activity of the first GTPase domain of Miro1, where GDP-bound Miro1 recruits Trak2, allowing mitochondrial coupling to the microtubule network (MacAskill et al., 2009a). In addition, removing the EF-hand domains of Miro1 completely, as apposed to overexpressing the EF-hand mutant, that only has a single point mutation in each EF-hand domain, might disrupt Miro1's potential interactions with mitofusins (Misko et al., 2010) (astrocytes express the genes for Mfn1 and Mfn2 (Cahoy et al., 2008)). Additionally, Miro1 interactions with the adaptor proteins Trak and KIF are thought to occur via the EF-hands (Macaskill et al., 2009b). Thus, completely removing astrocyte Miro1 might affect these interactions more so than mutating the EF-hand domains.

Investigating the total loss of Miro1 in astrocytes was also investigated to overcome the caveats of overexpressing the EF-hand mutant, where endogenous Miro1 is present. By utilising the Miro1^{KO} mouse it was possible to obtain isolated astrocytes that lack the ability to synthesise Miro1. Thus any impact of the isolated astrocytes on aspect of astrocyte mitochondrial dynamics or neuronal defects would be due, specifically, to astrocyte loss of Miro1. Thus, an improved system was established for examining the role of Miro1, not only in astrocytes, but also to examine the consequences of disrupted astrocyte Miro1 on neuronal synapse formation.

5.2 Results

5.2.1 A total loss of Miro1 is perinatally lethal.

In order to remove Miro1 from astrocytes a transgenic line was used that globally lacks Miro1 (i.e. the *Rhot1* gene, which encodes for Miro1) from all cells. From this line astrocytes could then be isolated to investigate the effects of removing Miro1 from astrocytes in culture.

The *Rhot1* transgenic line was obtained from the Wellcome Trust Sanger Institute (Skarnes et al., 2011). The transgenic line was generated following the Knockout-First strategy to disrupt *Rhot1* transcription. The targeted knockout-first allele (tm1a) has a *lacZ*/neo cassette inserted between exons 1 and 2, resulting in a null allele through splicing to the *lacZ-trapping* element (Figure 5.2.1A). Genotyping was carried out using DNA gel electrophoresis, confirming that the lacZ cassette was only present in the Rhot1$^{-/-}$ embryos (Figure 5.2.1B). Miro1 KO offspring were born alive at the expected Mendelian ratios and were similar in size and shape to their WT littermates (Figure 5.2.1C). However, they died 15-30 minutes following birth (perinatally) (Figure 5.2.1D). Western blot analysis of the protein levels in Miro1 WT and KO astrocyte cultures confirmed that indeed Miro1 was absent in the KO astrocytes (Figure 5.2.1E). Miro2 was present in the Miro1 KO cultures at comparable levels to the WT (Figure 5.2.1E).

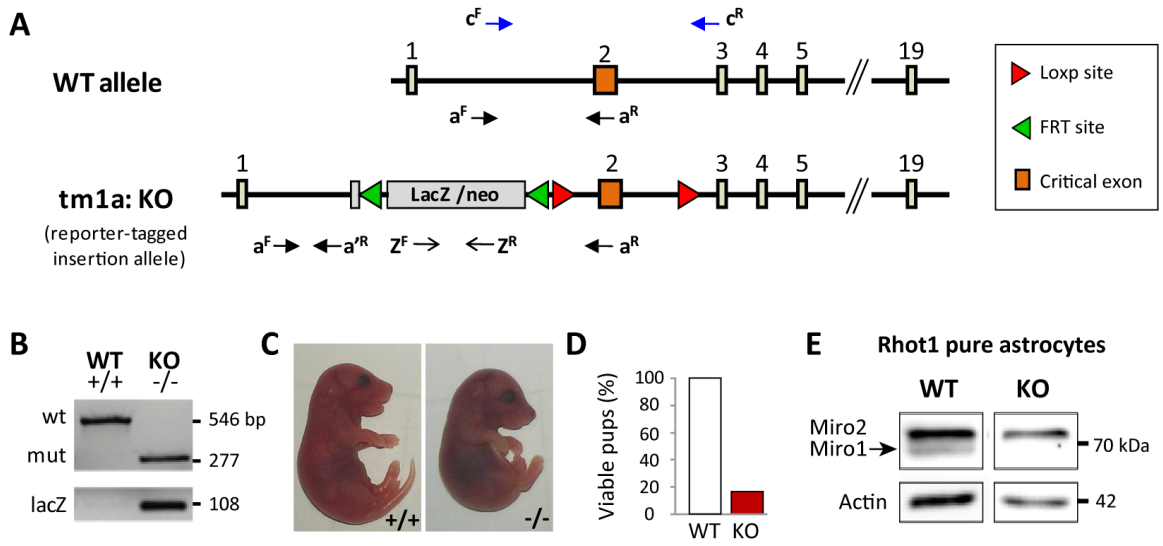

Figure 5.2.1 The Rhot1 transgenic mouse line. **A**. Diagram of the wildtype (WT, +/+) and Rhot1 knock-out (KO, -/-) alleles. The *lacZ*/neo cassette is inserted after the first exon and is flanked (3' and 5') by FRT sites. Exon 2 has a 3' and 5' *loxP* sites. **B**. Example DNA gel used for genotyping the transgenic mouse cultures. The higher band at 546 base pairs (bp) represents expression of the full-length protein (primers a^F and a^R shown in panel A), while the lower band represents expression of the disrupted mutant allele (a^F and a'^R primers). *LacZ* is expressed in Rhot1$^{-/-}$ embryos, but not in WT embryos (z^F and z^R primers). **C**. WT (Rhot1$^{+/+}$) and KO (Rhot1$^{-/-}$) embryos taken at E16 (pictures were taken by Dr Guillermo Lopez-Domenech). **D**. Percentage of pups born alive (quantified by Dr Lopez-Domenech). E. Western blot expression analysis of Miro1 protein levels in WT and KO pure hippocampal-cortical astrocyte cultures showing a complete loss of Miro1 in KO astrocytes compared to WT littermates.

5.2.2 Co-culture system - culturing Miro1^{KO} astrocytes with WT neurons.

Utilising the Rhot1 KO transgenic line, as described above, it was possible to obtain pure astrocyte cultures lacking Miro1, prior to perinatal death (E18). Isolated astrocytes lacking Miro1 were subsequently added to WT neurons of the same species, stage of development and density (mouse E18, 800-1 million cells/coverslip). With this approach, any defects in astrocyte mitochondrial dynamics can be attributed to astrocyte specific loss of Miro1. It may be that through the loss of all of Miro1's regulatory domains that mitochondrial morphology is affected in astrocytes as well as potential trafficking defects. This is because the GTPase domains of Miro1 have been proposed to regulate mitochondrial trafficking (MacAskill et al., 2009a) and morphology (Fransson et al., 2006). In addition, removing the EF-hand domains of Miro1 completely might disrupt Miro1's potential interactions with mitofusins (Misko et al., 2010) and the adaptor proteins Trak and KIF. Thus, completely removing astrocyte Miro1 might affect these interactions more so than mutating the EF-hand domains.

Interestingly, neuronal specific Miro1 loss shows preserved mitochondrial respiratory function (Nguyen et al., 2014). This could indicate that normal astrocyte Miro1 function can somehow compensate for a neuronal loss of Miro1 and thus it is particularly important to establish the role of Miro1 in astrocytes.

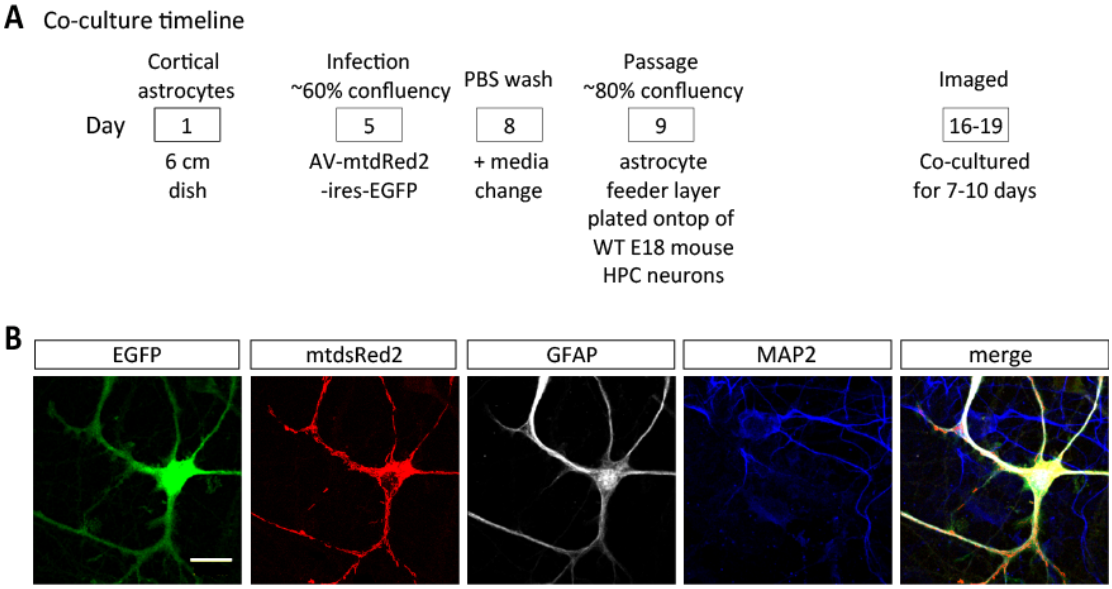

Figure 5.2.2 Rhot1 KO astrocyte co-culture system with WT neurons. **A**. Diagram of the co-culture system, which involved culturing isolated cortical astrocytes from the Rhot1 KO transgenic line (E18) for around 5-10 days. When the cultures were ~ 60 % confluent they were infected with AV-mtdsRed2-ir-EGFP to enable visualisation of the KO astrocytes after plating them onto WT E18 mouse neurons. **B**. An example astrocyte AV-tansduced to label the cell with EGFP and mitochondria with mtdsRed2 before being added to mouse neurons. Neuronal dendrites were labelled with MAP2. Scale bar, 15 μm.

5.2.3 Miro1 KO astrocytes display profoundly disrupted mitochondrial dynamics in co-culture with WT neurons.

Using the co-culture technique described above, it was possible to monitor mitochondrial trafficking dynamics in astrocytes that were co-cultured with WT mouse neurons. With this approach the astrocyte mitochondria exhibited dramatically altered dynamics compared to $Miro1^{WT}$ astrocytes co-cultured in the same way.

Where $Miro1^{WT}$ astrocyte mitochondria were mobile, almost all $Miro1^{KO}$ astrocyte mitochondria were immobile (Figure 5.2.3A). Around 40 % of mitochondria were moving in $Miro1^{WT}$ astrocytes, while only around 10 % of mitochondria were moving in $Miro1^{KO}$ astrocytes (Figure 5.2.3B, $p = 0.04$). The speed of mobile mitochondria was significantly reduced in $Miro1^{KO}$ astrocytes (0.05 μm/s ± 0.009) compared to $Miro1^{WT}$ astrocytes (0.16 ± 0.02 μm/s) (Figure 5.2.3C, $p = 0.0007$). Mitochondria were also significantly more round and less elongated in $Miro1^{KO}$ astrocytes (0.6 μm ± 0.06) compared to $Miro1^{WT}$ astrocytes (1.4 μm ± 0.2) (Figure 5.2.3D, $p = 0.02$).

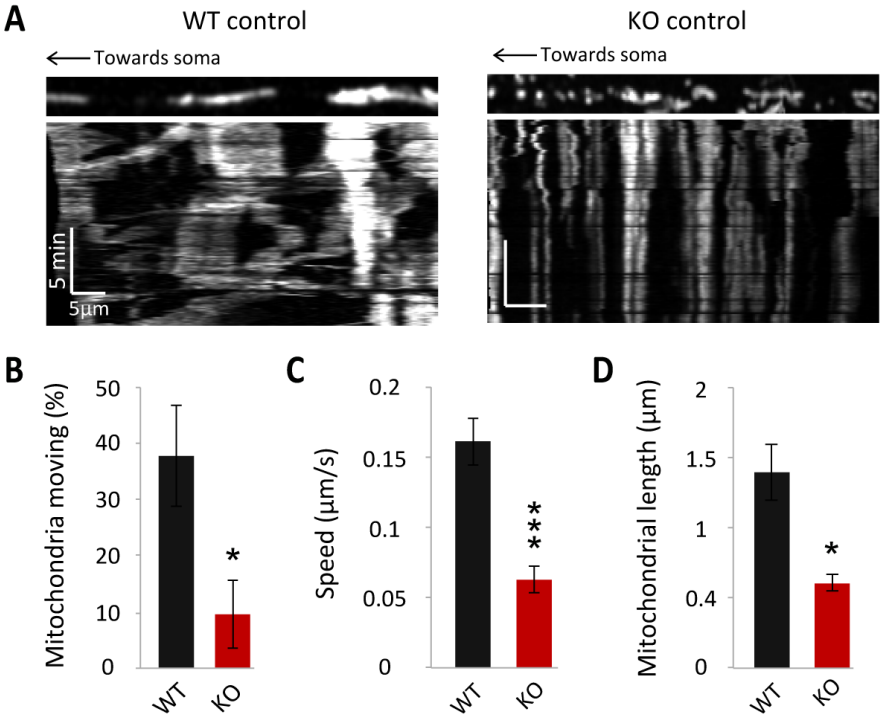

Figure 5.2.3 Miro1^{KO} astrocytes in co-culture with WT neurons exhibit altered mitochondrial dynamics. **A.** Example kymographs of mitochondrial trafficking in transgenic astrocytes transduced with AV-mtdsRed2-ir-EGFP. Scale bars, 5 μm. **B**. Mitochondria moving in Miro1^{WT} and Miro1^{KO} astrocytes. Miro1^{WT} n=4 cells; Miro1^{KO} n=4 cells. **C**. Speed of moving mitochondria in Miro1^{WT} and Miro1^{KO} astrocytes. Miro1^{WT} n = 20 mitochondria, 4 cells; Miro1^{KO} n = 10 mitochondria, 3 cells. **D**. Mitochondrial length in Miro1^{WT} and Miro1^{KO} astrocytes. Miro1^{WT} n = 3 cells; Miro1^{KO} n = 3 cells.

5.2.4 A total lack of astrocyte Miro1 disrupts the ability of astrocyte mitochondria to position themselves near synapses

Previously, the EF-hands of Miro1 were shown here to be important for regulating activity-driven mitochondrial stopping and their concomitant retention in astrocyte processes in close proximity to synapses. Therefore, it was investigated whether a total loss of astrocyte Miro1 supports this data.

Cultured cortical mouse $Miro1^{WT}$ or $Miro1^{KO}$ astrocytes were pre-infected with AV-mtdsRed2-ir-EGFP before co-culturing with WT hippocampal mouse neurons (isolated from the Rhot1 transgenic line) (Figure 5.2.4A). With this approach, the distance between $Miro1^{WT}$ astrocyte mitochondria and their nearest synapse significantly decreased following glutamate treatment (5 minutes, 100 μM + 1 μM glycine), compared to untreated controls (Figure 5.2.4B, $p = 0.04$). This decrease was not observed in $Miro1^{KO}$ astrocytes, where following treatment, the distribution was similar to untreated control conditions (Figure 5.2.4B, $p = 0.9$). In addition, no significant change was seen in synapse or mitochondrial number (per μm) (Figure 5.2.4C, $p > 0.2$). Ultimately, the spatial confinement of mitochondria within peri-synaptic astrocyte processes in response to increased levels glutamate could not only have important consequences for astrocyte function but also neuronal function.

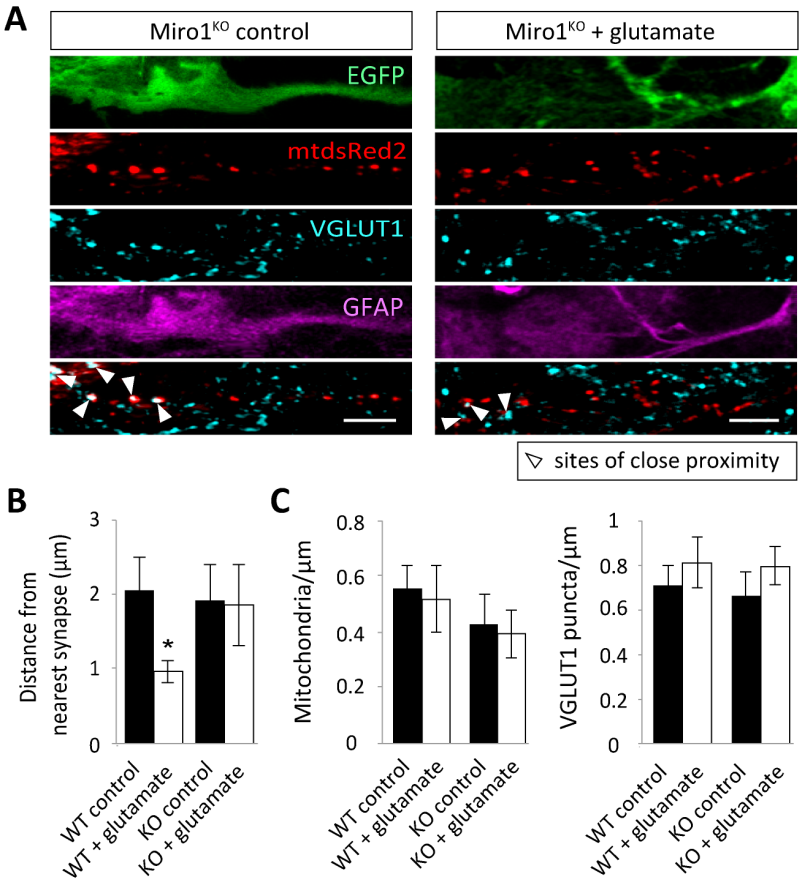

Figure 5.2.4 Miro1^{KO} astrocytes in co-culture with WT neurons exhibit altered mitochondrial positioning near synapses with glutamate treatment. **A.** Example images of Miro1^{KO} astrocytes transduced with AV-mtdsRed2-ir-EGFP and synapses immuno-labelled with VGLUT1 under basal conditions and with glutamate treatment (100 μM + 1 μM glycine, 5 min). Arrows show points of close proximity between astrocyte mitochondria and VGLUT1 labelled pre-synaptic terminals. Scale bars, 5 μm. **B**. The distance between Miro1^{WT} and Miro1^{KO} astrocyte mitochondria (co-cultured with WT neurons) in relation to their nearest synapse (centre of mass) before and after glutamate treatment. **C**. Mitochondria and VGLUT1 labelled synapses normalised to GFAP processes length (per μm). Miro1^{WT} control n = 6 ROIs, 6 cells, Miro1^{WT} + glutamate n = 7 ROIs, 7 cells; Miro1^{KO} control n = 7 ROIs, 7 cells, Miro1^{KO} + glutamate n = 6 ROIs, 6 cells.

5.2.5 Morphology is altered in Miro1^{KO} astrocytes

Axonal mitochondrial pre-synaptic capture is required for proper axonal development, where it appears that immobile mitochondria have the unique ability to stimulate axonal branching, through promoting axon branch formation and/or branch stabilization and this ability is not shared by mobile mitochondria (Courchet et al., 2013). As mitochondrial positioning was shown to be particularly important for other aspects of astrocyte function, such as Ca^{2+} signalling, there was a need to investigate whether disrupted mitochondrial positioning would have consequences for astrocyte process extension. Interestingly, astrocytes isolated from aging brains (26-29 months) exhibited slower growth rates, along with elevated ATP-induced Ca^{2+} responses and mitochondrial disruptions (Lin et al., 2007).

Firstly, Miro1^{WT} and Miro1^{KO} astrocytes were isolated and co-cultured with WT neurons. Prior to co-culturing, the transgenic astrocytes were transduced with AV-mtdsRed2-ir-EGFP, where EGFP was used to label astrocyte processes (Figure 5.2.5A). An automated Sholl analysis was then performed on sparsely labelled individual astrocytes (Gensel et al., 2010). With this approach, Miro1^{KO} astrocytes displayed reduced process complexity compared to Miro1^{WT} astrocytes (Figure 5.2.5B, p = 0.001, 0.002, 0.0009, 0.002 and 0.001, respectively). This provides evidence that Miro1-dependent astrocyte mitochondrial positioning is important for the arborisation of astrocyte processes, whereby localised energy production is likely required to induce process outgrowth/stabilisation. This could have important consequences for the modulatory role of astrocytes processes at the tri-partite synapse.

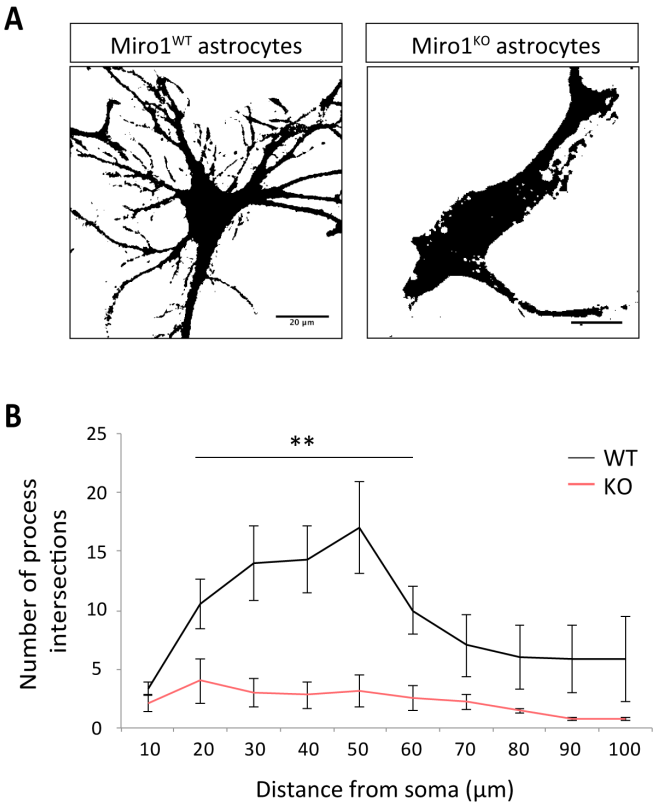

Figure 5.2.5 Miro1^{KO} astrocytes in co-culture with WT neurons exhibit altered cell morphology. **A.** Example Miro1^{WT} and Miro1^{KO} astrocytes AV-transduced to label cells with EGFP (images are manually thresholded). Scale bars 20 μm. **B**. Automated blind Sholl analysis of astrocyte process intersections at 10 μm increments radiating out from the central soma. Miro1^{WT} astrocytes n = 6 cells. Miro1^{KO} astrocytes n = 9 cells.

5.2.6 Neurons co-cultured with Miro1^{KO} astrocytes display altered synapses density.

Previously, the EF-hands of Miro1 were shown to impact on the number of excitatory synapses and so it was investigated if a total loss of astrocyte Miro1 had similar, or possibly, more profound effects on synapse formation.

Using WT hippocampal mouse neurons (5-6 DIV) co-cultured with cortical mouse Miro1^{WT} or Miro1^{KO} (for 5 days) alongside immuno-labelled pre- and post-synaptic terminals (using VGLUT1 and homer antibodies, respectively) it was possible to analyse the influence of Miro1^{KO} astrocytes on aspects of excitatory synapse formation (Figure 5.2.6A). With Miro1^{KO} astrocytes, WT neurons exhibited a reduction in the number of VGLUT and homer puncta (per μm) compared to neurons co-cultured with Miro1^{WT} astrocytes (Figure 5.2.6B, $p = 0.0004$ and $p = 0.01$, respectively). The average area (μm^2) of VGLUT puncta were also significantly decreased but not the size of the homer puncta (Figure 5.2.6C, $p = 0.01$ and $p = 0.4$, respectively). Additionally, Miro1^{KO} astrocytes also decreased the density of synapses i.e. the proportion of homer with VGLUT contacts and reciprocally, the proportion of VGLUT with homer contacts (Figure 5.2.6D, $p = 0.0003$ and $p = 0.02$, respectively).

This supports previous data showing that the EF-hands of Miro1 are important for regulating the number of excitatory synapses in cultured neurons but in a non-overexpression system. It is proposed that a total loss of astrocyte Miro1 induces a more profound loss of synapses than OE mutant Miro1. Although it is important to note that there may be some endogenous WT astrocytes present in this system, it did not appear to impact on the effects observed by co-culturing these neuro-glia cultures with Miro1^{KO} astrocytes.

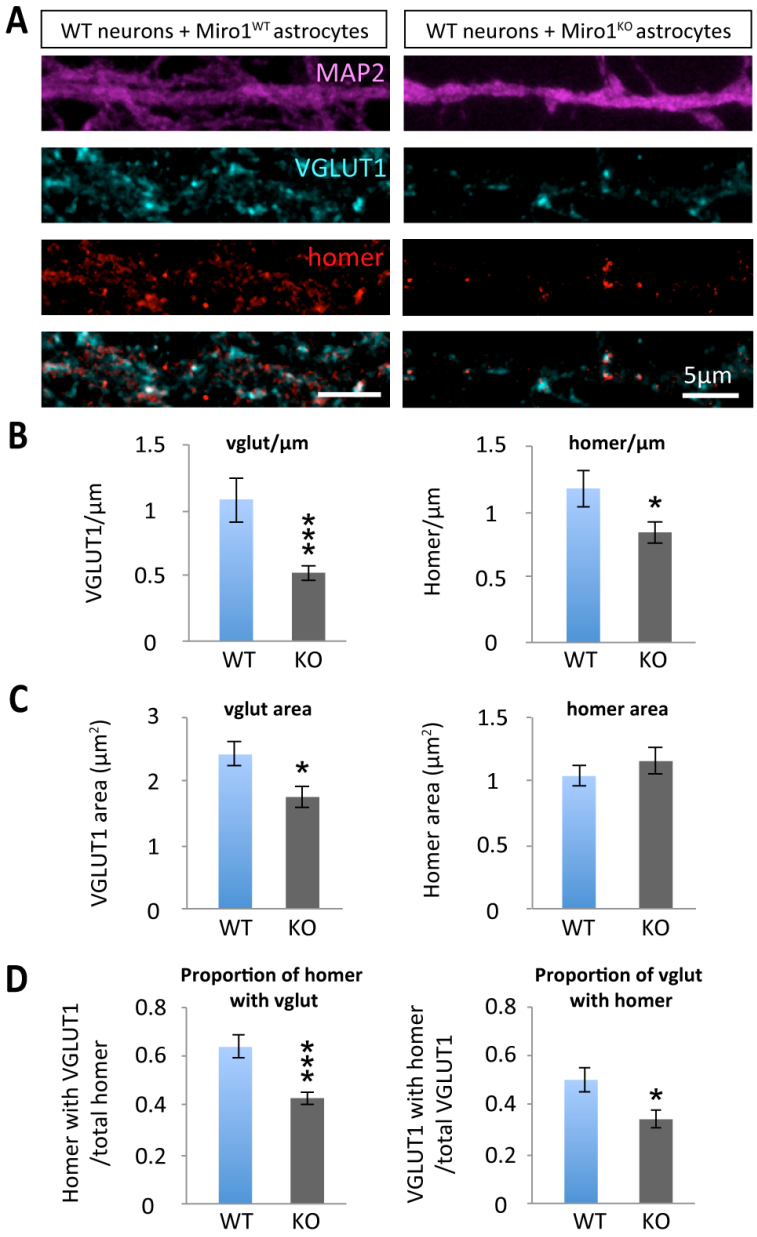

Figure 5.2.6 WT neurons in the presence of Miro1^{KO} astrocytes exhibit altered synapse formation. **A.** Representative images of WT neurons (DIV 10-12) in the presence of Miro1^{WT} or Miro1^{KO} astrocytes (DIV 5). Pre-and post-synaptic terminals were immuno-labelled with VGLUT1 and homer, respectively. Neuronal dendrites were immuno-labelled with MAP2. Scale bars, 5 μm. **B**. VGLUT1 and homer puncta normalised to MAP2 process length (per μm) with Miro1^{WT} or Miro1^{KO} astrocytes. **C**. VGLUT1 and homer area (μm^2) with Miro1^{WT} or Miro1^{KO} astrocytes. **D**. Synapse density with Miro1^{WT} or Miro1^{KO} astrocytes. This was calculated by quantifying the proportion of homer puncta in contact with VGLUT1 puncta (normalised to the total number of homer puncta) and the proportion of VGLUT1 puncta in contact with homer puncta (normalised to the total number of VGLUT1 puncta). Miro1^{WT} n = 18 ROIs, 14 cells; Miro1^{KO} n = 17 ROIs, 16 cells.

5.2.7 Miro1^{KO} astrocytes alter the presence of post-synaptic GluR2-containing AMPARs.

Furthermore, co-culturing WT neurons with Miro1^{KO} astrocytes altered the presence of excitatory GluR2-containting AMPARs. Miro1^{KO} astrocytes were co-cultured with WT mouse neurons (at 5-6 DIV) for 9-10 days. GluR2-containting AMPARs were then immuno-labelled with a GluR2 antibody (Figure 5.2.7A).

In the presence of Miro1^{KO} astrocytes, WT neurons displayed a reduction in the number (per μm) and size (average area, μm^2) of GluR2-positive synapses (Figure 5.2.7B, $p = 0.003$ and $p = 0.03$, respectively). This implies that a total loss of Miro1 also impacts on the formation of functional synapses. It would be important to investigate the spiking activity of these neurons as this data suggests that a total loss of astrocyte Miro1 might impact on synaptic transmission in this culture system.

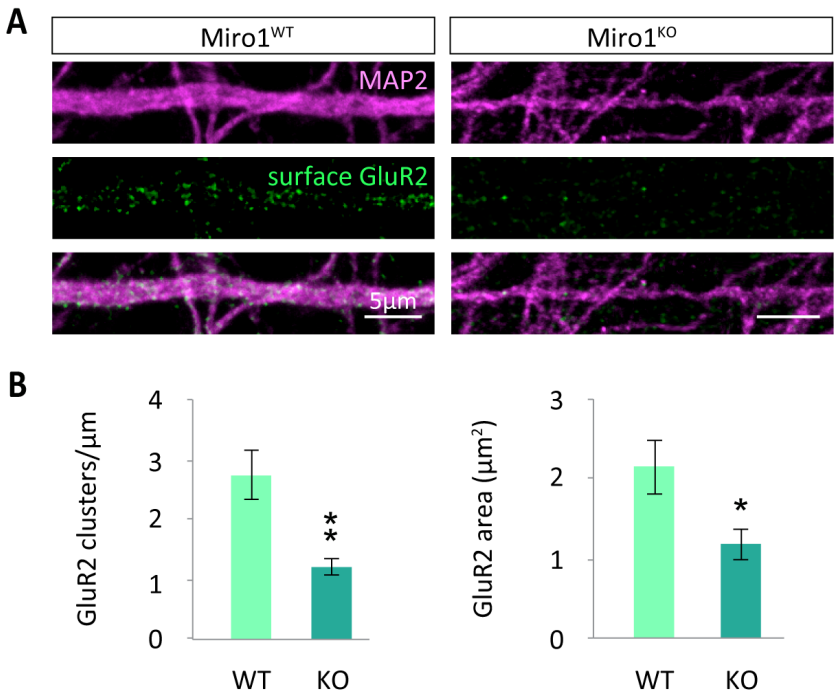

Figure 5.2.7 WT neurons in the presence of Miro1^{KO} astrocytes exhibit reduced GuR2-containing AMPARs. **A.** Representative images of WT neurons (DIV 13-16) in the presence of Miro1^{WT} or Miro1^{KO} astrocytes (DIV 9-10). GuR2-containing AMPARs were immuno-labelled with a mouse GluR2 antibody. Neuronal dendrites were immuno-labelled with MAP2. Scale bars, 5 μm. **B**. Number (per μm) and area (μm^2) of GluR2 puncta with Miro1^{WT} or Miro1^{KO} astrocytes. Miro1^{WT} n = 7 ROIs, 7 cells; Miro1^{KO} n = 7 ROIs, 7 cells.

5.3 Discussion

The results in this section support the data showing that the EF-hands of Miro1 are crucial for regulating aspects of astrocyte mitochondrial trafficking and positioning, which has important consequences for astrocyte signalling. More specifically, these results indicate that the total loss of astrocyte Miro1 induces more profound effects than mutating the EF-hands of Miro1 in an overexpression system. The main advantage of the KO system is that there is no Miro1 present in astrocytes and thus it overcomes the caveats of overexpressing the EF-hand mutant, where endogenous Miro1 is present.

Astrocytes isolated from the Miro1^{KO} transgenic line displayed severely disrupted mitochondrial morphology and trafficking dynamics, where the majority of the mitochondria were round and immobile compared to Miro1^{WT} astrocytes in the presence of WT neurons. This may be due to the loss of all of Miro1's regulatory domains and where Miro-independent trafficking regulation has been proposed in neurons (Cai et al., 2005, Nguyen et al., 2014), this may not be the case in astrocytes. It may be that the GTPase domains of Miro1 play an important role in mediating mitochondrial morphology in astrocytes. Given that the EF-hand mutant only has two point mutations, it may be that the EF-hand domains are still capable of maintaining elongated mitochondrial morphology potentially via interactions with mitofusins (Misko et al., 2010) (astrocytes express the genes for Mfn1 and Mfn2 (Cahoy et al., 2008), where the Miro1^{KO} astrocytes loose this ability. In addition, Miro1^{KO} astrocytes may loose the

ability to interact with adaptors and motors proteins that mediate astrocyte mitochondrial trafficking. Miro1 has been proposed to interact with the adaptor proteins Trak and KIF via the EF-hands (Macaskill et al., 2009b). Thus, completely removing astrocyte Miro1 might affect these interactions more so than mutating the EF-hand domains. Further investigation is required to decipher exactly which domains of Miro1 regulate mitochondrial morphology and trafficking in astrocytes.

As well as having severely disrupted mitochondrial trafficking dynamics, it appears that the total loss of astrocyte Miro1 prevents the docking of astrocyte mitochondria in close proximity to synapses. This supports the previous data showing that this ability is lost when the EF-hand mutant from of Miro1 is overexpressed in astrocytes. Functionally, altering astrocyte mitochondrial trafficking and positioning appears to have important consequences for the outgrowth of astrocyte processes, which would undoubtedly impact on the ability of astrocytes to modulate signalling at the tri-partite synapse. Specifically, $Miro1^{KO}$ astrocytes appear to have severely reduced process complexity compared to $Miro1^{WT}$ astrocytes. Thus, it can be concluded that Miro1-dependent regulation of astrocyte mitochondrial positioning is important for the arborisation/stabilisation of astrocyte processes.

In addition, removing Miro1 from astrocytes impairs the formation of excitatory synapses. Importantly, the number of homer-VGLUT1 contact was greatly reduced when WT neurons were co-cultured with $Miro1^{KO}$ astrocytes. This supports the data in the previous chapter showing that the EF-hand mutant form of Miro1 overexpressed in astrocytes reduces the formation of excitatory synapses and the presence of GluR2-containing post-synaptic AMPARs. Removing astrocyte Miro1 also reduced the number and area of GluR2-containing post-synaptic AMPARs, critical for functional synaptic transmission. Interestingly, there was

a greater reduction in synapse density with the total loss of Miro1 than with overexpression of the EF-hand mutant form of Miro1. This links with the idea that peri-synaptic astrocyte processes alter the formation and functionality of synapses and here this was shown to be dependent on the spatial regulation of astrocyte mitochondria by Miro1. This potentially implicates astrocyte Miro1 in the pathogenesis of neurological diseases/disorders.

Interestingly, WT neurons grown with astrocytes from patients with Down's syndrome have abnormal spine development, reduced synaptic density and activity (Garcia et al., 2010). Astrocytes from Fmr1 deficient mice (Fmr1 loss induces Fragile X Syndrome) also contribute to abnormal dendrite and synapse development (Jacobs et al., 2010). Methyl-CpG-binding protein 2 (MeCP2) deficient astrocytes (Rett Syndrome) have also been shown to impair neuronal outgrowth and dendrite development (Ballas et al., 2009). Additionally, DJ-1 KO astrocytes (a Parkinson's Disease-associated mutation) render neurons more sensitive to toxic insults (Lev et al., 2013). Taken together, these results suggest that it would be interesting to investigate whether other aspects of neuronal functionality and development are altered when Miro1 is removed specifically from astrocytes, such as spine development and dendritic arborisation. Especially since totally removing Miro1 is lethal and neuron-specific loss of Miro1 causes a MND-like phenotype (Nguyen et al., 2014).

Chapter 6

Final discussion

6.1 Summary

The trafficking of mitochondria within astrocyte processes has been shown to be dependent on both the microtubule and actin cytoskeletons (Kremneva et al., 2013, Jackson et al., 2014) but the motor proteins and adaptors involved were, until now, unknown. This thesis provides a clearer understanding of the mechanisms that underlie the control of mitochondrial trafficking in astrocyte processes, involving the EF-hand Ca^{2+}-sensing motifs of the mitochondrial Rho-GTPase protein, Miro1. This thesis reveals novel evidence that disrupting the spatial regulation of astrocyte mitochondrial, dependent on Miro1, has consequences not only for intracellular astrocyte Ca^{2+} signalling and astrocyte process outgrowth, but also for excitatory synapse formation, including the presence of post-synaptic GluR2-contaning AMPARs. This, crucially, implicates astrocyte Miro1 in modulating the formation of synapses, where disrupted astrocyte Miro1 may induce elevated gliotransmission affecting signalling of the surrounding neurons.

6.2 Basal mitochondrial trafficking in astrocytes

Initially, mitochondria were shown to be present in the processes of astrocytes where the thinner processes contained smaller, more round mitochondria. When compared to neuronal mitochondria *in situ*, the number of mobile mitochondria was decreased in astrocytes processes, as well as the speed at which they were capable of moving, supporting previous investigations (Jackson et al., 2014). However, astrocyte mitochondria were still capable of covering the same distances as neuronal mitochondria. These differences in trafficking dynamics could be due to different trafficking machinery utilised by neurons and astrocytes. Mitochondrial mobility in astrocyte processes was directly related to intracellular Ca^{2+}, where they were mobile in regions of low intracellular Ca^{2+} and relatively immobile in regions of high intracellular Ca^{2+}. These results, taken together, reveal that mitochondrial trafficking in astrocyte processes is dependent on the levels of intracellular Ca^{2+}.

6.3 Activity-dependent mitochondrial trafficking regulation in astrocytes

Enhancing neuronal activity alters astrocytic mitochondrial morphology and trafficking dynamics in culture and *in situ*. Mitochondria became shorter with a concomitant reduction in movement in astrocyte processes, when synaptic activity was stimulated with 4-AP and when glutamatergic signalling was stimulated with glutamate. This reduction in mobility was transient, where recovery was seen 30 minutes and 15 minutes following treatment with 4-AP and glutamate, respectively. Conversely, blocking neuronal activity with TTX increased mitochondrial trafficking in astrocyte processes. Stimulating neuronal activity with electrical

field stimulation, in culture, also rapidly reduced astrocyte mitochondrial trafficking. This reduction was also transient, where astrocyte mitochondrial mobility and **speed** recovered to basal levels (pre-stimulation) within 5 minutes. Thus, it can be concluded that mitochondrial trafficking in astrocytes is tightly coupled to neuronal activity. The response to activity is shown here to dependent on activation of glutamate receptors and involves elevations in intracellular Ca^{2+}, possibly occurring via mGluRs and/or astrocyte NMDARs (Figure 6.1).

In addition to arresting mitochondria and inducing remodelling/fission in astrocyte processes, stimulating neuronal activity resulted in astrocyte mitochondrial becoming confined near synapses. Astrocyte mitochondria position themselves near VGLUT1 labelled pre-synaptic terminals, following glutamate treatment in culture and 4-AP *in situ*. This retention was also transient, where mitochondria remained confined and immobile near Sy-GCAMP5 labelled pre-synaptic terminals for ~ 100 seconds, before moving away ~ 160 seconds following field stimulation. The timescale for astrocyte mitochondrial confinement near pre-synaptic terminals (~ 60s) was comparable to neuronal dendrite post-synaptic mitochondrial retention (~ 60s). However, neuronal mitochondrial retention persisted for longer than in astrocytes (120 s vs 100 s). This may have important consequences for the modulatory role of astrocytes at the synapse. Taken together, these results reveal that neuronal activity regulates mitochondrial trafficking in astrocytes and when synaptic transmission is elevated, astrocyte mitochondria become transiently confined in close proximity to synapses to provide localised energetic and metabolic support. The spatial regulation of astrocyte mitochondria could have important consequences for Ca^{2+} wave propagation and gliotransmission. This means that astrocytes regulate mitochondrial positioning along their processes to meet the demands, not only of astrocyte signalling but that of the surrounding neurons.

6.4 Miro1 EF-hand-dependent regulation of astrocyte mitochondrial trafficking dynamics

The first attempts to examine the role of Miro1 in astrocytes were made in this thesis. Miro1 was shown, for the first time, to be expressed in rodent astrocytes, where it is present on the mitochondria. Subsequently, as mitochondrial mobility in astrocyte processes was inversely correlated to intracellular Ca^{2+}, it was investigated if this ability was dependent on the EF-hand Ca^{2+}-sensing domains of Miro1. Overexpression (OE) of the EF-hand Miro1 mutant (Miro1$^{\Delta EF}$) disrupted the ability of astrocyte mitochondria to immobilise within regions of high intracellular Ca^{2+}, indicating that these domains are important for regulating Ca^{2+}-dependent stopping under basal conditions. The EF-hands of Miro1 are not, however, required for basal mitochondrial trafficking. The EF-hand Ca^{2+}-sensing motifs of Miro1 where, however, shown to be necessary for activity-dependent stopping of astrocyte mitochondria, both in culture and *in situ*. OE of the Miro1 mutant (Miro1$^{\Delta EF}$) abolished the ability of astrocyte mitochondria to respond to neuronal activity (preventing their activity-dependent stopping and remodelling). Both mobility and **speed** of astrocyte mitochondria were similar to basal conditions (prior to treatment) with Miro1$^{\Delta EF}$ OE. Mutating the EF-hands is, therefore, proposed to disrupt Miro1's interactions with pro-fission proteins, such as Drp1. In conclusion, the EF-hands of Miro1 are important for regulating activity-driven mitochondrial stopping and remodelling in astrocyte processes (Figure 6.1).

The EF-hands of Miro1 also appear to be important for the activity-driven retention of mitochondria in close proximity to synapses. This further suggests that Ca^{2+} binding the EF-

hands of Miro1 are important for inducing mitochondrial stopping at predicted Ca^{2+} hot spots, such as synapses. Finally, Miro1$^{\Delta EF}$ OE, *in situ*, alters the ability of astrocytes to regulate their intracellular Ca^{2+} levels. Miro1$^{\Delta EF}$ OE increased the frequency and amplitude of basal Ca^{2+} transients and increased the intracellular Ca^{2+} response to 4-AP and ATP. Here, astrocytes may be more vulnerable to Ca^{2+} overload when the Ca^{2+}-sensing abilities of Miro1 are disrupted. Disrupted intracellular Ca^{2+} regulation in astrocytes could have important consequences for their unique propagation of Ca^{2+} waves and suggests that the spatial regulation of mitochondria by Miro1 plays an important role in regulating astrocyte signalling. Since the regulation of intracellular Ca^{2+} also has the potential to impact on gliotransmission, this reveals another potential route for bi-directional communication between astrocytes and neurons. This could be linked to instances of pathology, as disrupted astrocyte Ca^{2+} dynamics due to altered mitochondrial function has devastating consequences for neuronal function (Katayama et al., 1995, Danbolt, 2001, Shin et al., 2005, Volobouéva et al., 2007, Li et al., 2008, Bradford et al., 2009, Oliveira and Goncalves, 2009).

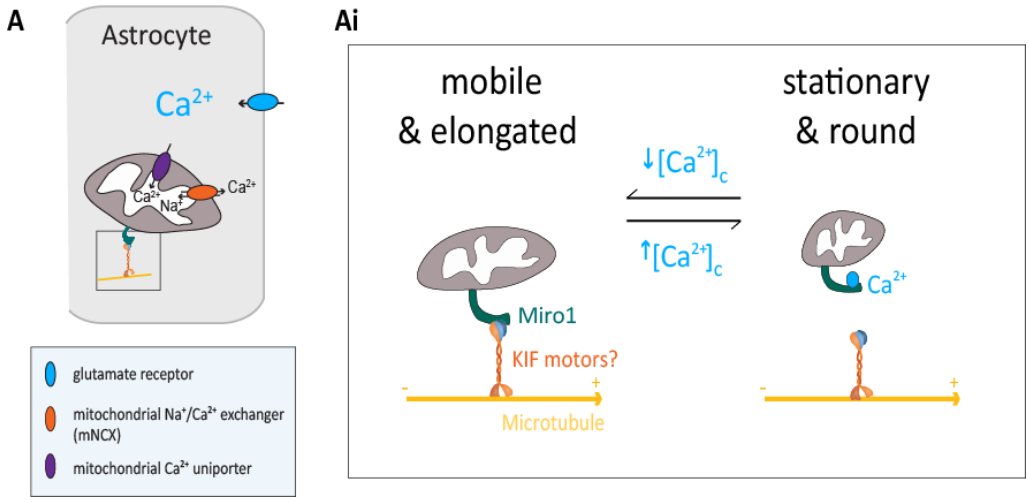

Figure 6.1 Proposed Miro1 EF-hand-dependent mitochondrial trafficking regulation in astrocyte processes. **A**. Schematic representation of an astrocyte containing a mitochondrion that buffers the uptake of Ca^{2+} expected to ensue from increased neuronal activity. This is proposed to involve ionotropic glutamate mediated astrocyte Ca^{2+} entry. **Ai**. During low levels of activity astrocyte Ca^{2+} is low and mitochondria are mobile and elongated. Upon Ca^{2+} elevations, which occur as a result of increased neuronal activity astrocyte mitochondria become round and their trafficking ceases. Subsequently, they dock near synapses. Downstream, this regulation has important consequences for the surrounding neuronal architecture.

Interestingly, basal Ca^{2+} transients are elevated in astrocytes in mice expressing mutant human Aβ precursor protein (Kuchibhotla et al., 2009). This was observed to induce mitochondrial depolarisation through activation of the DNA repairing enzyme poly ADP-ribose polymerase-1 (PARP-1) and opening mitochondrial permeability transition pore (mPTP) (Angelova and Abramov 2014). With beta-amyloid peptide treatment astrocyte specific mitochondrial disruptions precedes any neuronal phenotype associated with AD. In the study conducted by Angelova and Abramov 2014, amyloid-β peptide (Aβ) induced elevated Ca^{2+} signalling in astrocytes but not in neurons. This was due to the high levels of membrane cholesterol expression in astrocytes. Aβ significantly reduced the levels of glutathione (GSH) in neurons and astrocytes, an effect that was dependent on Ca^{2+} entry from external sources. Altering membrane cholesterol regulation modified the astrocyte response to Aβ (elevated Ca^{2+} signalling, ROS production and mitochondrial depolarisation), which lead to improved neuroprotection (Angelova and Abramov, 2014, Narayan et al., 2014). This indicates that astrocyte intracellular Ca^{2+} regulates mitochondrial function and that both are disrupted in disease.

Astrocyte mitochondrial positioning could be important for regulating the release of neuro-active substances from astrocytes. This could include synaptogenic molecules or substances that promote synapse elimination. The mechanisms controlling release of these astrocyte-derived factors are relatively unclear. Although there are caveats to using an overexpression system, where endogenous astrocyte Miro1 is present it does highlight the functional importance of mitochondrial positioning in astrocyte processes.

Importantly, in addition to regulating astrocyte signalling, the EF-hands of Miro1 also appear to have important functional consequences for the surrounding neuronal architecture. OE of the mutant form of Miro1 alters the formation of excitatory synapses as well as the number and size of GluR2-containing post-synaptic AMPARs. Mutating the Ca^{2+} sensing domains of Miro1 may mean that there is an increased likelihood of gliotransmitter release, since the rise in intracellular Ca^{2+} directly correlates to the release probability of transmitters such as glutamate from astrocytes (Parpura and Zorec, 2010). Subsequently, prolonged gliotransmitter release may disrupt neuronal signalling and cause excitotoxic cell death. A decrease in synaptic density may indicate cell death or a compensatory response in order to down-regulate synaptic activity to counteract the increased presence of gliotransimitters released by nearby astrocytes. More broadly it shows that the consequence of disrupted intracellular astrocyte Ca^{2+} signalling, through altered Miro1-EF-hand-dependent mitochondrial positioning, does indeed have an impact on the surrounding neuronal environment.

6.5 Consequences of the total loss of astrocyte Miro1

A total loss of astrocyte Miro1, in culture, supports the data showing that the EF-hands of Miro1 are important for regulating aspects of astrocyte mitochondrial trafficking and positioning, which has important consequences for astrocyte signalling. More specifically, $Miro1^{KO}$ in astrocytes induces more profound effects than mutating the EF-hands of Miro1 in an overexpression system.

$Miro1^{KO}$ astrocytes displayed severely disrupted mitochondrial morphology and trafficking dynamics, where the majority of the mitochondria were round and immobile compared to

Miro1^{WT} astrocytes (in the presence of WT neurons). This may be due to the loss of all of Miro1's regulatory domains and where other mitochondrial adaptors/regulators have been proposed in neurons (Cai et al., 2005, Nguyen et al., 2014), this may not be the case in astrocytes. Given that the EF-hand mutant only has two point mutations, it may be that the EF-hand domains are still capable of maintaining elongated mitochondrial morphology potentially via interactions with mitofusins (Misko et al., 2010), where the Miro1^{KO} astrocytes loose this ability. This warrants experimentations to decipher exactly which domains of Miro1 regulate mitochondrial morphology and trafficking.

As well as having severely disrupted basal mitochondrial trafficking dynamics, it appears that the total loss of astrocyte Miro1 prevents activity-dependent docking of astrocyte mitochondria in close proximity to synapses. This supports the previous data showing that this ability is lost when the EF-hand mutant from of Miro1 is overexpressed in astrocytes. Similarly, removing Miro1 from astrocytes impairs the formation of excitatory synapses. Importantly, the number of homer-VGLUT1 contact was greatly reduced. Additionally, removing astrocyte Miro1 also reduced the number and area of GluR2-containing AMPARs, critical for functional synapse formation. Interestingly, there was a greater reduction in synapse density with the total loss of Miro1 than with OE of the EF-hand mutant form of Miro1. Even though there are still native WT astrocytes in the WT neuronal cultures used in co-culture with Miro1^{KO} astrocytes, the effects were still observed. However, it would be interesting to titre down the number of Miro1^{KO} introduced to the WT cultures to see if fewer astrocytes may induce these effects on synapse formation.

Disrupted astrocyte mitochondrial positioning might affect the formation of excitatory synapses through increased release of astrocyte factors that promote synapse elimination, a decrease in astrocyte-released synaptogenic molecules or through direct activation of astrocytic phagocytic pathways. A candidate astrocyte factor SPARC negatively regulates synaptogenesis, which is important for preventing over-excitation in the CNS (Jones and Bouvier, 2014). Astrocyte-released SPARC reduces the levels of post-synaptic AMPARs. Neurons grown with SPARC KO astrocytes had significantly more surface containing GluR1 and GluR2 synapses than neurons co-cultured with SPARC WT astrocytes. Jones and colleagues also found enhanced synaptic signalling and impaired LTP in hippocampal slices from SPARC KO mice (Jones et al., 2011). They show that SPARC regulates surface AMPARs through β3-integrin receptors, which have been shown to stabilise GluR2 subunits at synapses (Clingolani et al., 2008). SPARC-like-1 or Hevin increases synapses in RGCs *in vitro* and *in vivo* and is required for their maturation (Kucukdereli et al., 2011). Thrombospondins (TSPs) decrease synaptic AMPARs, so decreasing neuronal excitability (Sloan and Barres, 2014). Lack of TSPs leads to defects in injury-induced structural plasticity of the developing barrel cortex (Eroglu et al., 2009) and hampers synaptic recovery after stroke, showing an important role for astrocyte-derived TSPs in regulating the formation of new synapses. In addition, reducing the levels of Gpc4 and Gpc6 reduced clustering of surface GluR1-containing AMPARs and reduced synaptic activity (Allen et al., 2012). It may be that through disrupted astrocyte mitochondrial dynamics the release of synaptogengic molecules such as SPARC-like-1 (Hevin), TSPs or Gpc4/6 are reduced.

Astrocytes increase postsynaptic activity by inducing AMPA receptor localization to the postsynaptic density, and enhance presynaptic function by increasing release probabilities

(Chung et al., 2015). Interestingly, reactive astrocytes have been shown to release GABA in a mouse model of Alzheimer's disease (AD), reducing the spiking activity of granule cells in the dentate gyrus (Jo et al., 2014). A reduction in excitatory synapse formation might be explained by an increase in inhibitory signalling either through homeostatic plasticity or through the release of inhibitory transmitters from disrupted astrocytes. In terms of pathology, disrupted glutamatergic signalling contributes to the pathogenesis of schizophrenia (Moghaddam and Javitt, 2012). Importantly, Motori and colleagues highlight that a failure to maintain the functional architecture of mitochondria affects astrocyte survival (Motori et al. 2013). In addition, specific disruption of astrocyte mitochondrial function has dramatic consequences for aspects of neuronal function and in some cases survival. Treatment with flurocitrate (FC) induced specific disruptions in astrocyte mitochondrial function and resulted in focal, followed by global epileptiform activity (epilepsy) with some animals exhibiting convulsive seizures (Volobouéva et al., 2007). This resulted in neuronal damage and eventual death. In addition to this, abnormal synapse development, function and elimination were observed along with an imbalance in the E/I balance. mHtt (a mutation associated with HD) compromised the ability of astrocytes to buffer glutamate at the synapse, decreasing the threshold for excitotoxic neurodegeneration (Oliveria and Goncalves, 2009). In Fragile X Syndrome, astrocytes contribute to abnormal dendrite and synapse development in Fmr1 (loss of which induces Fragile X) deficient mice (Jacobs et al., 2010).

6.6 Future directions

Future studies will seek to determine the precise role of astrocytes in altering synapse formation, which may help to develop new therapies for synaptopathies, for example. A

question that should be addressed is under what circumstances are astrocyte-derived factors released? Alternatively, blocking gliotransmission in the early stages of pathology may improve disease outcome. Additionally, human iPSC-derived astrocytes from affected patients could help to confirm observations made in rodent models and lead to potential therapeutic strategies.

Further work is required to confirm the exact interactions that mediate mitochondrial binding to the astrocytic transport network, which could be actin or microtubule dependent (Jackson et al., 2014). Whether direct astrocyte Ca^{2+} entry occurs through activation of the reverse mode of the Na^{+}/Ca^{2+} exchanger (NCX) also remains to be investigated. The results showing that the EF-hands of Miro1 play an important role in regulating mitochondrial trafficking dynamics in slices reveals that there may be an equally important role for Miro1 *in vivo*. It would be interesting to test whether Miro1 OE alters mitochondrial membrane potential and consequently their ability to buffer Ca^{2+}.

Miro1 OE has been shown to improve disease outcome. Specifically, it has been shown to rescue epithelial damage by enhancing mitochondrial transfer from mesenchymal stem cells to epithelial cells (Ahmad et al., 2014). However, it remains to be investigated if Miro1 OE can improve the outcome of neurodegenerative diseases, such as AD, where mitochondrial dysfunction has been implicated specifically in astrocytes. More specifically, a potential therapeutic intervention exists in the form of astrocyte specific antioxidants along with increasing astrocyte mitochondrial biogenesis.

While ablating astrocyte Miro1 was shown in this thesis to disrupt the number of excitatory synapses, it would be useful to investigate whether astrocyte Ca^{2+} signalling was also disrupted in $Miro1^{KO}$ astrocytes in the same way as OE the EF-hand mutant in astrocytes. Further, it would be interesting to analyse the dynamics of spontaneous synaptic events of WT neurons in the presence of $Miro1^{KO}$ astrocytes. Spiking activity of WT neurons could be analysed using electrophysiological techniques or by transfection with a GECI such as GCaMP6f in the presence of $Miro1^{KO}$ astrocytes. Additionally, a total loss of astrocyte Miro1 might affect other aspects of neuronal development such as dendrite arborisation and/or spine maturation.

Analysis of neuronal transmission in specific astrocyte $Miro1^{KO}$ slices using GFAP-cre/lox induced KO requires investigation. This astrocyte specific $Miro1^{KO}$ system could also be used for *in vivo* analysis of astrocyte mitochondrial trafficking and positioning and the consequences for the neuronal development and function. Another approach could be to use an adenovirus or biolistic Rnai knockdown of Miro1 in astrocytes in slices, allowing analysis of a total loss of astrocyte Miro1 in an intact system.

In this thesis Miro2 was also expressed by astrocytes and in the case of mouse hippocampal astrocytes to a higher degree than Miro1. Therefore bearing this in mind, it would be interesting to investigate the consequences of a total loss of Miro2 on astrocyte signalling. More importantly the loss of both astrocyte Miro1 and Miro2 requires investigation, as this may have more profound consequences for astrocyte and neuronal signalling.

Miro has also recently been shown to be involved in the cascade that regulates neuronal mitophagy (Wang et al., 2011, Birsa et al., 2014, Tsai et al., 2014) and consequently, the exact regulation of mitophagy in astrocytes is an important mechanism that remains to be addressed (Stephen et al., 2014). It may be that mitophagy is regulated on a different timescale to neuronal mitophagy and if this is the case it could explain why astrocyte dysfunction precedes signs of pathology in neurons (Abramov et al., 2004). Miro itself has also been implicated in disease (Iijima-Ando et al., 2012, Liu et al., 2012). Therefore, along with the data shown in this thesis, this alludes to the possibility that astrocyte mitochondrial regulation by Miro is important, not only for astrocyte function, but also for neuronal signalling, especially in the context of pathology.

6.7 Concluding remarks

In conclusion, this thesis answers a few crucial questions regarding astrocyte energetic and metabolic support of neurons. Miro1 was shown to be important for regulating mitochondrial positioning in astrocyte processes. This spatial regulation of astrocyte mitochondrial is shown here to be important for maintaining astrocyte process outgrowth and Ca^{2+} signalling, potentially impacting on the release of gliotransmitters, which affects the number of excitatory synapses and the presence of GluR2-containing post-synaptic AMPARs.

Bibliography

Abbott NJ, Ronnback L, Hansson E (2006) Astrocyte-endothelial interactions at the blood-brain barrier. Nature reviews Neuroscience 7:41-53.

Abramov AY, Canevari L, Duchen MR (2004) Beta-amyloid peptides induce mitochondrial dysfunction and oxidative stress in astrocytes and death of neurons through activation of NADPH oxidase. The Journal of neuroscience : the official journal of the Society for Neuroscience 24:565-575.

Adams JC, Lawler J (2004) The thrombospondins. Int J Biochem Cell Biol 36:961-968.

Agulhon C, Fiacco TA, McCarthy KD (2010) Hippocampal short- and long-term plasticity are not modulated by astrocyte Ca2+ signaling. Science 327:1250-1254.

Ahmad T, Mukherjee S, Pattnaik B, Kumar M, Singh S, Kumar M, Rehman R, Tiwari BK, Jha KA, Barhanpurkar AP, Wani MR, Roy SS, Mabalirajan U, Ghosh B, Agrawal A (2014) Miro1 regulates intercellular mitochondrial transport & enhances mesenchymal stem cell rescue efficacy. The EMBO journal 33:994-1010.

Akerboom J, Chen TW, Wardill TJ, Tian L, Marvin JS, Mutlu S, Calderon NC, Esposti F, Borghuis BG, Sun XR, Gordus A, Orger MB, Portugues R, Engert F, Macklin JJ, Filosa A, Aggarwal A, Kerr RA, Takagi R, Kracun S, Shigetomi E, Khakh BS, Baier H, Lagnado L, Wang SS, Bargmann CI, Kimmel BE, Jayaraman V, Svoboda K, Kim DS, Schreiter ER, Looger LL (2012) Optimization of a GCaMP calcium indicator for neural activity imaging. The Journal of neuroscience : the official journal of the Society for Neuroscience 32:13819-13840.

Al Awabdh S, Miserey-Lenkei S, Bouceba T, Masson J, Kano F, Marinach-Patrice C, Hamon M, Emerit MB, Darmon M (2012) A new vesicular scaffolding complex mediates the G-protein-coupled 5-HT1A receptor targeting to neuronal dendrites. The Journal of neuroscience : the official journal of the Society for Neuroscience 32:14227-14241.

Alberts B (2008) Molecular Biology of the Cell: Reference edition: Garland Science.

Alberts B, Johnson A, Lewis J, Walter P, Raff M, Roberts KUhbgcubio (2002) Molecular Biology of the Cell 4th Edition: International Student Edition: Routledge.

Allen NJ, Bennett ML, Foo LC, Wang GX, Chakraborty C, Smith SJ, Barres BA (2012) Astrocyte glypicans 4 and 6 promote formation of excitatory synapses via GluA1 AMPA receptors. Nature 486:410-414.

Angelova PR, Abramov AY (2014) Interaction of neurons and astrocytes underlies the mechanism of Abeta-induced neurotoxicity. Biochemical Society transactions 42:1286-1290.

Araque A, Carmignoto G, Haydon PG (2001) Dynamic Signaling Between Astrocytes and Neurons. Annu Rev Physiol 795-813.

Araque A, Sanzgiri RP, Parpura V, Haydon PG (1999) Astrocyte-induced modulation of synaptic transmission. Canadian journal of physiology and pharmacology 77:699-706.

Araque et al. (1998) Glutamate-dependent astrocyte modulation of synaptic transmission between cultured hippocampal neurons. The European journal of neuroscience 10:2129-2142.

Attwell D, Buchan AM, Charpak S, Lauritzen M, Macvicar BA, Newman EA (2010) Glial and neuronal control of brain blood flow. Nature 468:232-243.

Attwell D, Laughlin SB (2001) An energy budget for signaling in the grey matter of the brain. Journal of cerebral blood flow and metabolism : official journal of the International Society of Cerebral Blood Flow and Metabolism 21:1133-1145.

Azevedo FA, Carvalho LR, Grinberg LT, Farfel JM, Ferretti RE, Leite RE, Jacob Filho W, Lent R, Herculano-Houzel S (2009) Equal numbers of neuronal and nonneuronal cells make the human brain an isometrically scaled-up primate brain. J Comp Neurol 513:532-541.

Ballas N, Lioy DT, Grunseich C, Mandel G (2009) Non-cell autonomous influence of MeCP2-deficient glia on neuronal dendritic morphology. Nature neuroscience 12:311-317.

Banker G, Goslin K (1998) Culturing nerve cells: MIT press.

Bartlett et al. (1998) Selective and Rapid Uptake of Adeno-Associated Virus Type 2 in Brain. HUMAN GENE THERAPY 9:1181-1186.

Bauer DE, Jackson JG, Genda EN, Montoya MM, Yudkoff M, Robinson MB (2012) The glutamate transporter, GLAST, participates in a macromolecular complex that supports glutamate metabolism. Neurochemistry international 61:566-574.

Beattie EC, Stellwagen D, Morishita W, Bresnahan JC, Ha BK, Von Zastrow M, Beattie MS, Malenka RC (2002) Control of synaptic strength by glial TNFalpha. Science 295:2282-2285.

Benard G, Rossignol R (2008) Ultrastructure of the mitochondrion and its bearing on function and bioenergetics. Antioxid Redox Signal 10:1313-1342.

Benediktsson AM, Schachtele SJ, Green SH, Dailey ME (2005) Ballistic labeling and dynamic imaging of astrocytes in organotypic hippocampal slice cultures. Journal of neuroscience methods 141:41-53.

Bennett MV, Contreras JE, Bukauskas FF, Saez JC (2003) New roles for astrocytes: gap junction hemichannels have something to communicate. Trends in neurosciences 26:610-617.

Bergles DE, Jahr CE (1997) Synaptic activation of glutamate transporters in hippocampal astrocytes. Neuron 19:1297-1308.

Bezzi P, Gundersen V, Galbete JL, Seifert G, Steinhauser C, Pilati E, Volterra A (2004) Astrocytes contain a vesicular compartment that is competent for regulated exocytosis of glutamate. Nat Neurosci 7:613-620.

Bhakar AL, Dolen G, Bear MF (2012) The pathophysiology of fragile X (and what it teaches us about synapses). Annu Rev Neurosci 35:417-443.

Birsa N, Norkett R, Higgs N, Lopez-Domenech G, Kittler JT (2013) Mitochondrial trafficking in neurons and the role of the Miro family of GTPase proteins. Biochemical Society transactions 41:1525-1531.

Birsa N, Norkett R, Wauer T, Mevissen TE, Wu HC, Foltynie T, Bhatia K, Hirst WD, Komander D, Plun-Favreau H, Kittler JT (2014) Lysine 27 ubiquitination of the mitochondrial transport protein Miro is dependent on serine 65 of the Parkin ubiquitin ligase. The Journal of biological chemistry 289:14569-14582.

Bliss TVP, Collingridge GL (1993) A synaptic model of memory: long-term potentiation in the hippocampus. Nature 361:31-39.

Boitier E, Rea R, Duchen MR (1999) Mitochondria exert a negative feedback on the propagation of intracellular Ca2+ waves in rat cortical astrocytes. The Journal of cell biology 145:795-808.

Bolte S, Cordelieres FP (2006) A guided tour into subcellular colocalization analysis in light microscopy. Journal of Microscopy 224:213-232.

Bradford J, Shin JY, Roberts M, Wang CE, Li XJ, Li S (2009) Expression of mutant huntingtin in mouse brain astrocytes causes age-dependent neurological symptoms. Proceedings of the National Academy of Sciences of the United States of America 106:22480-22485.

Cahoy JD, Emery B, Kaushal A, Foo LC, Zamanian JL, Christopherson KS, Xing Y, Lubischer JL, Krieg PA, Krupenko SA, Thompson WJ, Barres BA (2008) A transcriptome database for astrocytes, neurons, and oligodendrocytes: a new resource for understanding brain development and function. The Journal of neuroscience : the official journal of the Society for Neuroscience 28:264-278.

Cai Q, Gerwin C, Sheng ZH (2005) Syntabulin-mediated anterograde transport of mitochondria along neuronal processes. The Journal of cell biology 170:959-969.

Cai Z, Schools GP, Kimelberg HK (2000) Metabotropic glutamate receptors in acutely isolated hippocampal astrocytes: developmental changes of mGluR5 mRNA and functional expression. Glia 29:70-80.

Carmignoto G (2000) Reciprocal communication systems between astrocytes and neurones. Prog Neurobiol 62:561-581.

Carmona MA, Murai KK, Wang L, Roberts AJ, Pasquale EB (2009) Glial ephrin-A3 regulates hippocampal dendritic spine morphology and glutamate transport. Proceedings of the National Academy of Sciences of the United States of America 106:12524-12529.

Cassina P, Cassina A, Pehar M, Castellanos R, Gandelman M, de Leon A, Robinson KM, Mason RP, Beckman JS, Barbeito L, Radi R (2008) Mitochondrial dysfunction in SOD1G93A-bearing astrocytes promotes motor neuron degeneration: prevention by mitochondrial-targeted antioxidants. The Journal of neuroscience : the official journal of the Society for Neuroscience 28:4115-4122.

Chang DT, Honick AS, Reynolds IJ (2006) Mitochondrial trafficking to synapses in cultured primary cortical neurons. The Journal of neuroscience : the official journal of the Society for Neuroscience 26:7035-7045.

Chatton JY, Pellerin L, Magistretti PJ (2003) GABA uptake into astrocytes is not associated with significant metabolic cost: implications for brain imaging of inhibitory transmission. Proceedings of the National Academy of Sciences of the United States of America 100:12456-12461.

Chaudhry FA, Lehre KP, van Lookeren Campagne M, Ottersen OP, Danbolt NC, Storm-Mathisen J (1995) Glutamate Transporters in Glial Plasma Membranes: Highly Differentiated Localizations Revealed by Quantitative Ultrastructural Immunocytochemistry. Neuron 15:711-720.

Chen H, Chomyn A, Chan DC (2005) Disruption of fusion results in mitochondrial heterogeneity and dysfunction. The Journal of biological chemistry 280:26185-26192.

Chen J, Tan Z, Zeng L, Zhang X, He Y, Gao W, Wu X, Li Y, Bu B, Wang W, Duan S (2013a) Heterosynaptic long-term depression mediated by ATP released from astrocytes. Glia 61:178-191.

Chen TW, Wardill TJ, Sun Y, Pulver SR, Renninger SL, Baohan A, Schreiter ER, Kerr RA, Orger MB, Jayaraman V, Looger LL, Svoboda K, Kim DS (2013b) Ultrasensitive fluorescent proteins for imaging neuronal activity. Nature 499:295-300.

Christopherson KS, Ullian EM, Stokes CC, Mullowney CE, Hell JW, Agah A, Lawler J, Mosher DF, Bornstein P, Barres BA (2005) Thrombospondins are astrocyte-secreted proteins that promote CNS synaptogenesis. Cell 120:421-433.

Chung WS, Allen NJ, Eroglu C (2015) Astrocytes Control Synapse Formation, Function, and Elimination. Cold Spring Harbor perspectives in biology.

Cingolani LA, Thalhammer A, Yu LM, Catalano M, Ramos T, Colicos MA, Goda Y (2008) Activity-dependent regulation of synaptic AMPA receptor composition and abundance by beta3 integrins. Neuron 58:749-762.

Conti F, DeBiasi S, Minelli A, Melone M (1996) Expression of NR1 and NR2A/B subunits of the NMDA receptor in cortical astrocytes. Glia 17:254-258.

Courchet J, Lewis TL, Jr., Lee S, Courchet V, Liou DY, Aizawa S, Polleux F (2013) Terminal axon branching is regulated by the LKB1-NUAK1 kinase pathway via presynaptic mitochondrial capture. Cell 153:1510-1525.

Csordas G, Varnai P, Golenar T, Roy S, Purkins G, Schneider TG, Balla T, Hajnoczky G (2010) Imaging interorganelle contacts and local calcium dynamics at the ER-mitochondrial interface. Mol Cell 39:121-132.

D'Ascenzo M, Fellin T, Terunuma M, Revilla-Sanchez R, Meaney DF, Auberson YP, Moss SJ, Haydon PG (2007) mGluR5 stimulates gliotransmission in the nucleus accumbens. Proceedings of the National Academy of Sciences of the United States of America 104:1995-2000.

Danbolt NC (2001) Glutamate uptake. Progress in Neurobiology 65:1-105.

Dani JW, Chernjavsky A, Smith SJ (1992) Neuronal activity triggers calcium waves in hippocampal astrocyte networks. Neuron 8:429-440.

Davis CH, Kim KY, Bushong EA, Mills EA, Boassa D, Shih T, Kinebuchi M, Phan S, Zhou Y, Bihlmeyer NA, Nguyen JV, Jin Y, Ellisman MH, Marsh-Armstrong N (2014) Transcellular degradation of axonal mitochondria. Proceedings of the National Academy of Sciences of the United States of America 111:9633-9638.

De Simoni A, Yu LM (2006) Preparation of organotypic hippocampal slice cultures: interface method. Nature protocols 1:1439-1445.

Derouiche A, Haseleu J, Korf HW (2015) Fine Astrocyte Processes Contain Very Small Mitochondria: Glial Oxidative Capability May Fuel Transmitter Metabolism. Neurochemical research.

Di Castro MA, Chuquet J, Liaudet N, Bhaukaurally K, Santello M, Bouvier D, Tiret P, Volterra A (2011) Local Ca2+ detection and modulation of synaptic release by astrocytes. Nature neuroscience 14:1276-1284.

Dienel GA (2013) Astrocytic energetics during excitatory neurotransmission: What are contributions of glutamate oxidation and glycolysis? Neurochemistry international 63:244-258.

Dienel GA, Cruz NF (2004) Nutrition during brain activation: does cell-to-cell lactate shuttling contribute significantly to sweet and sour food for thought? Neurochemistry international 45:321-351.

Ding F, O'Donnell J, Thrane AS, Zeppenfeld D, Kang H, Xie L, Wang F, Nedergaard M (2013) alpha1-Adrenergic receptors mediate coordinated Ca2+ signaling of cortical astrocytes in awake, behaving mice. Cell calcium 54:387-394.

Drago I, Pizzo P, Pozzan T (2011) After half a century mitochondrial calcium in- and efflux machineries reveal themselves. The EMBO journal 30:4119-4125.

Dreosti E, Odermatt B, Dorostkar MM, Lagnado L (2009) A genetically encoded reporter of synaptic activity in vivo. Nature methods 6:883-889.

Duale H, Kasparov S, Paton JF, Teschemacher AG (2005) Differences in transductional tropism of adenoviral and lentiviral vectors in the rat brainstem. Experimental physiology 90:71-78.

Duan S, Anderson CM, Keung EC, Chen Y, Chen Y, Swanson RA (2003) P2X7 receptor-mediated release of excitatory amino acids from astrocytes. The Journal of neuroscience : the official journal of the Society for Neuroscience 23:1320-1328.

Duffy S, MacVicar BA (1995) Adrenergic calcium signaling in astrocyte networks within the hippocampal slice. The Journal of neuroscience : the official journal of the Society for Neuroscience 15:5535-5550.

Eccles (1964) The Physiology of Synapses. Springer.

Edelstein A, Amodaj N, Hoover K, Vale R, Stuurman N (2010) Computer control of microscopes using microManager. Current protocols in molecular biology / edited by Frederick M Ausubel [et al] Chapter 14:Unit14 20.

Elmenhorst D, Meyer PT, Winz OH, Matusch A, Ermert J, Coenen HH, Basheer R, Haas HL, Zilles K, Bauer A (2007) Sleep deprivation increases A1 adenosine receptor binding in the human brain: a positron emission tomography study. The Journal of neuroscience : the official journal of the Society for Neuroscience 27:2410-2415.

Eroglu C, Barres BA (2010) Regulation of synaptic connectivity by glia. Nature 468:223-231.

Evers MR, Salmen B, Bukalo O, Rollenhagen A, Bosl MR, Morellini F, Bartsch U, Dityatev A, Schachner M (2002) Impairment of L-type Ca2+ channel-dependent forms of hippocampal synaptic plasticity in mice deficient in the extracellular matrix glycoprotein tenascin-C. The Journal of neuroscience : the official journal of the Society for Neuroscience 22:7177-7194.

Exner N, Lutz AK, Haass C, Winklhofer KF (2012) Mitochondrial dysfunction in Parkinson's disease: molecular mechanisms and pathophysiological consequences. The EMBO journal 31:3038-3062.

Fabricius C, Berthold CH, Rydmark M (1993) Axoplasmic organelles at nodes of Ranvier. II. Occurrence and distribution in large myelinated spinal cord axons of the adult cat. J Neurocytol 22:941-954.

Facci L, Barbierato M, Marinelli C, Argentini C, Skaper SD, Giusti P (2014) Toll-like receptors 2, -3 and -4 prime microglia but not astrocytes across central nervous system regions for ATP-dependent interleukin-1beta release. Scientific reports 4:6824.

Fellin T (2009) Communication between neurons and astrocytes: relevance to the modulation of synaptic and network activity. Journal of neurochemistry 108:533-544.

Fellin T, D'Ascenzo M, Haydon PG (2007) Astrocytes control neuronal excitability in the nucleus accumbens. ScientificWorldJournal 7:89-97.

Fiacco TA, McCarthy KD (2006) Astrocyte calcium elevations: properties, propagation, and effects on brain signaling. Glia 54:676-690.

Fields RD (2008) Oligodendrocytes changing the rules: action potentials in glia and oligodendrocytes controlling action potentials. The Neuroscientist : a review journal bringing neurobiology, neurology and psychiatry 14:540-543.

Filosa JA, Bonev AD, Nelson MT (2004) Calcium dynamics in cortical astrocytes and arterioles during neurovascular coupling. Circ Res 95:e73-81.

Finger SUhbgcubiOWUwC (2004) Minds Behind the Brain: A History of the Pioneers and Their Discoveries: Oxford University Press, USA.

Frank S, Gaume B, Bergmann-Leitner ES, Leitner WW, Robert EG, Catez F, Smith CL, Youle RJ (2001) The role of dynamin-related protein 1, a mediator of mitochondrial fission, in apoptosis. Dev Cell 1:515-525.

Fransson S, Ruusala A, Aspenstrom P (2006) The atypical Rho GTPases Miro-1 and Miro-2 have essential roles in mitochondrial trafficking. Biochem Biophys Res Commun 344:500-510.

Frederick RL, Shaw JM (2007) Moving mitochondria: establishing distribution of an essential organelle. Traffic 8:1668-1675.

Gahring LC, Persiyanov K, Dunn D, Weiss R, Meyer EL, Rogers SW (2004) Mouse strain-specific nicotinic acetylcholine receptor expression by inhibitory

interneurons and astrocytes in the dorsal hippocampus. J Comp Neurol 468:334-346.

Gahwiler BH (1981) Organotypic monolayer cultures of nervous tissue. Journal of neuroscience methods 4:329-342.

Gahwiler BH, Capogna M, Debanne D, McKinney RA, Thompson SM (1997) Organotypic slice cultures: a technique has come of age. Trends in neurosciences 20:471-477.

Gao YJ, Ji RR (2010) Chemokines, neuronal-glial interactions, and central processing of neuropathic pain. Pharmacology & therapeutics 126:56-68.

Garcia O, Torres M, Helguera P, Coskun P, Busciglio J (2010) A role for thrombospondin-1 deficits in astrocyte-mediated spine and synaptic pathology in Down's syndrome. PloS one 5:e14200.

Genda EN, Jackson JG, Sheldon AL, Locke SF, Greco TM, O'Donnell JC, Spruce LA, Xiao R, Guo W, Putt M, Seeholzer S, Ischiropoulos H, Robinson MB (2011) Co-compartmentalization of the astroglial glutamate transporter, GLT-1, with glycolytic enzymes and mitochondria. The Journal of neuroscience : the official journal of the Society for Neuroscience 31:18275-18288.

Gensel JC, Schonberg DL, Alexander JK, McTigue DM, Popovich PG (2010) Semi-automated Sholl analysis for quantifying changes in growth and differentiation of neurons and glia. Journal of neuroscience methods 190:71-79.

Giorgi C, De Stefani D, Bononi A, Rizzuto R, Pinton P (2009) Structural and functional link between the mitochondrial network and the endoplasmic reticulum. Int J Biochem Cell Biol 41:1817-1827.

Goldman WF, Yarowsky PJ, Juhaszova M, Krueger BK, Blaustein MP (1994) Sodium/Calcium Exchange in Rat Cortical Astrocytes The Journal of Neuroscience 14:5834-5843.

Golovina VA (2005) Visualization of localized store-operated calcium entry in mouse astrocytes. Close proximity to the endoplasmic reticulum. The Journal of physiology 564:737-749.

Gourine AV, Kasymov V, Marina N, Tang F, Figueiredo MF, Lane S, Teschemacher AG, Spyer KM, Deisseroth K, Kasparov S (2010) Astrocytes control breathing through pH-dependent release of ATP. Science 329:571-575.

Grosche J, Matyash V, Moller T, Verkhratsky A, Reichenbach A, Kettenmann H (1999) Microdomains for neuron-glia interaction: parallel fiber signaling to Bergmann glial cells. Nature neuroscience 2:139-143.

Guo X, Macleod GT, Wellington A, Hu F, Panchumarthi S, Schoenfield M, Marin L, Charlton MP, Atwood HL, Zinsmaier KE (2005) The GTPase dMiro is required for axonal transport of mitochondria to Drosophila synapses. Neuron 47:379-393.

Guthrie PB, Knappenberger J, Segal M, Bennett MV, Charles AC, Kater SB (1999) ATP released from astrocytes mediates glial calcium waves. The Journal of neuroscience : the official journal of the Society for Neuroscience 19:520-528.

Halassa MM, Florian C, Fellin T, Munoz JR, Lee SY, Abel T, Haydon PG, Frank MG (2009) Astrocytic modulation of sleep homeostasis and cognitive consequences of sleep loss. Neuron 61:213-219.

Hanisch UK, Kettenmann H (2007) Microglia: active sensor and versatile effector cells in the normal and pathologic brain. Nature neuroscience 10:1387-1394.

Haustein MD, Kracun S, Lu XH, Shih T, Jackson-Weaver O, Tong X, Xu J, Yang XW, O'Dell TJ, Marvin JS, Ellisman MH, Bushong EA, Looger LL, Khakh BS (2014) Conditions and constraints for astrocyte calcium signaling in the hippocampal mossy fiber pathway. Neuron 82:413-429.

Hayashi-Nishino M, Fujita N, Noda T, Yamaguchi A, Yoshimori T, Yamamoto A (2009) A subdomain of the endoplasmic reticulum forms a cradle for autophagosome formation. Nature cell biology 11:1433-1437.

Haydon PG, Carmignoto G (2006) Astrocyte control of synaptic transmission and neurovascular coupling. Physiological reviews 86:1009-1031.

He L, Linden DJ, Sapirstein A (2012) Astrocyte inositol triphosphate receptor type 2 and cytosolic phospholipase A2 alpha regulate arteriole responses in mouse neocortical brain slices. PloS one 7:e42194.

Heneka MT, Sastre M, Dumitrescu-Ozimek L, Dewachter I, Walter J, Klockgether T, Van Leuven F (2005) Focal glial activation coincides with increased BACE1 activation and precedes amyloid plaque deposition in APP[V717I] transgenic mice. J Neuroinflammation 2:22.

Heneka MT, Wiesinger H, Dumitrescu-Ozimek L, Riederer P, Feinstein DL, Klockgether T (2001) Neuronal and glial coexpression of argininosuccinate

synthetase and inducible nitric oxide synthase in Alzheimer disease. J Neuropathol Exp Neurol 60:906-916.

Henze K, Martin W (2003) Essence of mitochondria. Nature news and views 426.

Hernandez-Morales M, Garcia-Colunga J (2009) Effects of nicotine on K+ currents and nicotinic receptors in astrocytes of the hippocampal CA1 region. Neuropharmacology 56:975-983.

Hertz L, Peng L, Dienel GA (2007) Energy metabolism in astrocytes: high rate of oxidative metabolism and spatiotemporal dependence on glycolysis/glycogenolysis. Journal of cerebral blood flow and metabolism : official journal of the International Society of Cerebral Blood Flow and Metabolism 27:219-249.

Hollenbeck PJ, Saxton WM (2005) The axonal transport of mitochondria. Journal of cell science 118:5411-5419.

Hormuzdi SG, Filippov MA, Mitropoulou G, Monyer H, Bruzzone R (2004) Electrical synapses: a dynamic signaling system that shapes the activity of neuronal networks. Biochimica et biophysica acta 1662:113-137.

Hua X, Malarkey EB, Sunjara V, Rosenwald SE, Li WH, Parpura V (2004) C(a2+)-dependent glutamate release involves two classes of endoplasmic reticulum Ca(2+) stores in astrocytes. Journal of neuroscience research 76:86-97.

Huang ZL, Urade Y, Hayaishi O (2011) The role of adenosine in the regulation of sleep. Curr Top Med Chem 11:1047-1057.

Iijima-Ando K, Sekiya M, Maruko-Otake A, Ohtake Y, Suzuki E, Lu B, Iijima KM (2012) Loss of axonal mitochondria promotes tau-mediated neurodegeneration and Alzheimer's disease-related tau phosphorylation via PAR-1. PLoS genetics 8:e1002918.

Inoue H, Nojima H, Okayama H (1990) High efficiency transformation of Escherichia coli with plasmids. Gene 96:23-28.

Ishibashi T, Dakin KA, Stevens B, Lee PR, Kozlov SV, Stewart CL, Fields RD (2006) Astrocytes promote myelination in response to electrical impulses. Neuron 49:823-832.

Ito U, Hakamata Y, Kawakami E, Oyanagi K (2009) Degeneration of astrocytic processes and their mitochondria in cerebral cortical regions peripheral to the

cortical infarction: heterogeneity of their disintegration is closely associated with disseminated selective neuronal necrosis and maturation of injury. Stroke 40:2173-2181.

Jackson JG, O'Donnell JC, Takano H, Coulter DA, Robinson MB (2014) Neuronal activity and glutamate uptake decrease mitochondrial mobility in astrocytes and position mitochondria near glutamate transporters. The Journal of neuroscience : the official journal of the Society for Neuroscience 34:1613-1624.

Jacobs S, Doering LC (2010) Astrocytes prevent abnormal neuronal development in the fragile x mouse. The Journal of neuroscience : the official journal of the Society for Neuroscience 30:4508-4514.

Jacobs S, Nathwani M, Doering LC (2010) Fragile X astrocytes induce developmental delays in dendrite maturation and synaptic protein expression. BMC Neurosci 11:132.

Jo S, Yarishkin O, Hwang YJ, Chun YE, Park M, Woo DH, Bae JY, Kim T, Lee J, Chun H, Park HJ, Lee da Y, Hong J, Kim HY, Oh SJ, Park SJ, Lee H, Yoon BE, Kim Y, Jeong Y, Shim I, Bae YC, Cho J, Kowall NW, Ryu H, Hwang E, Kim D, Lee CJ (2014) GABA from reactive astrocytes impairs memory in mouse models of Alzheimer's disease. Nature medicine 20:886-896.

Jones EV, Bernardinelli Y, Tse YC, Chierzi S, Wong TP, Murai KK (2011) Astrocytes control glutamate receptor levels at developing synapses through SPARC-beta-integrin interactions. The Journal of neuroscience : the official journal of the Society for Neuroscience 31:4154-4165.

Jones EV, Bouvier DS (2014) Astrocyte-secreted matricellular proteins in CNS remodelling during development and disease. Neural plasticity 2014:321209.

Jouaville LS, Ichas F, Holmuhamedov EL, Camacho P, Lechleiter JD (1995) Synchronization of calcium waves by mitochondrial substrates in Xenopus laevis oocytes. Nature 377:438-441.

Kandel ER, Schwartz JH, Jessell TM (2000) Principles of neural science: McGraw-Hill New York.

Katayama Y, Maeda T, Koshinaga M, Kawamata T, Tsubokawa T (1995) Role of excitatory amino acid-mediated ionic fluxes in traumatic brain injury. Brain pathology 5:427-435.

Kenney JW, Gould TJ (2008) Modulation of hippocampus-dependent learning and synaptic plasticity by nicotine. Mol Neurobiol 38:101-121.

Kew J, Davies C (2010) Ion Channles from Structure to Function: Oxford University Press.

Kimelberg HK, Nedergaard M (2010) Functions of astrocytes and their potential as therapeutic targets. Neurotherapeutics : the journal of the American Society for Experimental NeuroTherapeutics 7:338-353.

Kintner DB, Luo J, Gerdts J, Ballard AJ, Shull GE, Sun D (2007) Role of Na+-K+-Cl- cotransport and Na+/Ca2+ exchange in mitochondrial dysfunction in astrocytes following in vitro ischemia. American journal of physiology Cell physiology 292:C1113-1122.

Kofuji P, Newman EA (2004) Potassium buffering in the central nervous system. Neuroscience 129:1045-1056.

Kolomeets NS, Uranova N (2010) Ultrastructural abnormalities of astrocytes in the hippocampus in schizophrenia and duration of illness: a postortem morphometric study. World J Biol Psychiatry 11:282-292.

Koyama R, Muramatsu R, Sasaki T, Kimura R, Ueyama C, Tamura M, Tamura N, Ichikawa J, Takahashi N, Usami A, Yamada MK, Matsuki N, Ikegaya Y (2007) A Low-Cost Method for Brain Slice Cultures. Journal of Pharmacological Sciences 104:191-194.

Krebs C, Fernandes HB, Sheldon C, Raymond LA, Baimbridge KG (2003) Functional NMDA Receptor Subtype 2B Is Expressed in Astrocytes after Ischemia In Vivo and Anoxia In Vitro. The Journal of Neuroscience 23:3364-3372.

Kremneva E, Kislin M, Kang X, Khiroug L (2013) Motility of astrocytic mitochondria is arrested by Ca2+-dependent interaction between mitochondria and actin filaments. Cell calcium 53:85-93.

Kriegstein A, Alvarez-Buylla A (2009) The glial nature of embryonic and adult neural stem cells. Annu Rev Neurosci 32:149-184.

Kristal BS, Dubinsky JM (1997) Mitochondrial Permeability Transition in the Central Nervous System: Induction by Calcium Cycling-Dependent and -Independent Pathways. Journal of neurochemistry 69:524-538.

Kuchibhotla KV, Lattarulo CR, Hyman BT, Bacskai BJ (2009) Synchronous hyperactivity and intercellular calcium waves in astrocytes in Alzheimer mice. Science 323:1211-1215.

Kucukdereli H, Allen NJ, Lee AT, Feng A, Ozlu MI, Conatser LM, Chakraborty C, Workman G, Weaver M, Sage EH, Barres BA, Eroglu C (2011) Control of excitatory CNS synaptogenesis by astrocyte-secreted proteins Hevin and SPARC. Proceedings of the National Academy of Sciences of the United States of America 108:E440-449.

Lalo U, Pankratov Y, Kirchhoff F, North RA, Verkhratsky A (2006) NMDA receptors mediate neuron-to-glia signaling in mouse cortical astrocytes. The Journal of neuroscience : the official journal of the Society for Neuroscience 26:2673-2683.

Landy A (1989) Dynamic, structural, and regulatory aspects of lambda site-specific recombination. Annu Rev Biochem 58:913-949.

Larsen NJ, Ambrosi G, Mullett SJ, Berman SB, Hinkle DA (2011) DJ-1 knock-down impairs astrocyte mitochondrial function. Neuroscience 196:251-264.

Latour I, Gee CE, Robitaille R, Lacaille JC (2001) Differential mechanisms of Ca2+ responses in glial cells evoked by exogenous and endogenous glutamate in rat hippocampus. Hippocampus 11:132-145.

Lavialle M, Aumann G, Anlauf E, Prols F, Arpin M, Derouiche A (2011) Structural plasticity of perisynaptic astrocyte processes involves ezrin and metabotropic glutamate receptors. PNAS 108:12915-12919.

Ledesma MD, Galvan C, Hellias B, Dotti C, Jensen PH (2002) Astrocytic but not neuronal increased expression and redistribution of parkin during unfolded protein stress. Journal of neurochemistry 83:1431-1440.

Lev N, Barhum Y, Ben-Zur T, Melamed E, Steiner I, Offen D (2013) Knocking out DJ-1 attenuates astrocytes neuroprotection against 6-hydroxydopamine toxicity. Journal of molecular neuroscience : MN 50:542-550.

Li H, Alavian KN, Lazrove E, Mehta N, Jones A, Zhang P, Licznerski P, Graham M, Uo T, Guo J, Rahner C, Duman RS, Morrison RS, Jonas EA (2013) A Bcl-xL-Drp1 complex regulates synaptic vesicle membrane dynamics during endocytosis. Nature cell biology 15:773-785.

Li L, Lundkvist A, Andersson D, Wilhelmsson U, Nagai N, Pardo AC, Nodin C, Stahlberg A, Aprico K, Larsson K, Yabe T, Moons L, Fotheringham A, Davies

I, Carmeliet P, Schwartz JP, Pekna M, Kubista M, Blomstrand F, Maragakis N, Nilsson M, Pekny M (2008) Protective role of reactive astrocytes in brain ischemia. Journal of cerebral blood flow and metabolism : official journal of the International Society of Cerebral Blood Flow and Metabolism 28:468-481.

Li Z, Okamoto K, Hayashi Y, Sheng M (2004) The importance of dendritic mitochondria in the morphogenesis and plasticity of spines and synapses. Cell 119:873-887.

Ligon LA, Steward O (2000) Role of microtubules and actin filaments in the movement of mitochondria in the axons and dendrites of cultured hippocampal neurons. J Comp Neurol 427:351-361.

Lin CH, Tallaksen-Greene S, Chien WM, Cearley JA, Jackson WS, Crouse AB, Ren S, Li XJ, Albin RL, Detloff PJ (2001) Neurological abnormalities in a knock-in mouse model of Huntington's disease. Human molecular genetics 10:137-144.

Lin DT, Wu J, Holstein D, Upadhyay G, Rourk W, Muller E, Lechleiter JD (2007) Ca2+ signaling, mitochondria and sensitivity to oxidative stress in aging astrocytes. Neurobiol Aging 28:99-111.

Liu S, Sawada T, Lee S, Yu W, Silverio G, Alapatt P, Millan I, Shen A, Saxton W, Kanao T, Takahashi R, Hattori N, Imai Y, Lu B (2012) Parkinson's disease-associated kinase PINK1 regulates Miro protein level and axonal transport of mitochondria. PLoS genetics 8:e1002537.

Liu SJ, Zukin RS (2007) Ca2+-permeable AMPA receptors in synaptic plasticity and neuronal death. Trends in neurosciences 30:126-134.

Lo KJ, Luk HN, Chin TY, Chueh SH (2002) Store depletion-induced calcium influx in rat cerebellar astrocytes. British journal of pharmacology 135:1383-1392.

Lopez-Hidalgo M, Salgado-Puga K, Alvarado-Martinez R, Medina AC, Prado-Alcala RA, Garcia-Colunga J (2012) Nicotine uses neuron-glia communication to enhance hippocampal synaptic transmission and long-term memory. PloS one 7:e49998.

Lordkipanidze T, Dunaevsky A (2005) Purkinje cell dendrites grow in alignment with Bergmann glia. Glia 51:229-234.

Lovatt D, Sonnewald U, Waagepetersen HS, Schousboe A, He W, Lin JH, Han X, Takano T, Wang S, Sim FJ, Goldman SA, Nedergaard M (2007) The transcriptome and metabolic gene signature of protoplasmic astrocytes in the

adult murine cortex. The Journal of neuroscience : the official journal of the Society for Neuroscience 27:12255-12266.

MacAskill AF, Brickley K, Stephenson FA, Kittler JT (2009a) GTPase dependent recruitment of Grif-1 by Miro1 regulates mitochondrial trafficking in hippocampal neurons. Molecular and cellular neurosciences 40:301-312.

MacAskill AF, Kittler JT (2010) Control of mitochondrial transport and localization in neurons. Trends in cell biology 20:102-112.

Macaskill AF, Rinholm JE, Twelvetrees AE, Arancibia-Carcamo IL, Muir J, Fransson A, Aspenstrom P, Attwell D, Kittler JT (2009b) Miro1 is a calcium sensor for glutamate receptor-dependent localization of mitochondria at synapses. Neuron 61:541-555.

MacDonald JF, Xiong ZG, Jackson MF (2006) Paradox of Ca2+ signaling, cell death and stroke. Trends in neurosciences 29:75-81.

Magistretti PJ, Pellerin L (1999) Cellular mechanisms of brain energy metabolism and their relevance to functional brain imaging. Philos Trans R Soc Lond B Biol Sci 354:1155-1163.

Magrane J, Sahawneh MA, Przedborski S, Estevez AG, Manfredi G (2012) Mitochondrial dynamics and bioenergetic dysfunction is associated with synaptic alterations in mutant SOD1 motor neurons. The Journal of neuroscience : the official journal of the Society for Neuroscience 32:229-242.

Malarkey EB, Ni Y, Parpura V (2008) Ca2+ entry through TRPC1 channels contributes to intracellular Ca2+ dynamics and consequent glutamate release from rat astrocytes. Glia 56:821-835.

Mangiarini L, Sathasivam K, Seller M, Cozens B, Harper A, Hetherington C, Lawton M, Trottier Y, Lehrach H, Davies SW, Bates GP (1996) Exon 1 of the HD gene with an expanded CAG repeat is sufficient to cause a progressive neurological phenotype in transgenic mice. Cell 87:493-506.

Matsuo N, Reijmers L, Mayford M (2008) Spine-type-specific recruitment of newly synthesized AMPA receptors with learning. Science 319:1104-1107.

Mauch DH, Nagler K, Schumacher S, Goritz C, Muller EC, Otto A, Pfrieger FW (2001) CNS synaptogenesis promoted by glia-derived cholesterol. Science 294:1354-1357.

McBride HM, Neuspiel M, Wasiak S (2006) Mitochondria: more than just a powerhouse. Current biology : CB 16:R551-560.

McNamara JO, Huang YZ, Leonard AS (2006) Molecular signaling mechanisms underlying epileptogenesis. Sci STKE 2006:re12.

Miller KE, Sheetz MP (2006) Direct evidence for coherent low velocity axonal transport of mitochondria. The Journal of cell biology 173:373-381.

Mink JW, Blumenschine RJ, Adams DB (1981) Ratio of central nervous system to body metabolism in vertebrates: its constancy and functional basis. The American journal of physiology 241:R203-212.

Misko A, Jiang S, Wegorzewska I, Milbrandt J, Baloh RH (2010) Mitofusin 2 is necessary for transport of axonal mitochondria and interacts with the Miro/Milton complex. The Journal of neuroscience : the official journal of the Society for Neuroscience 30:4232-4240.

Moghaddam B, Javitt D (2012) From revolution to evolution: the glutamate hypothesis of schizophrenia and its implication for treatment. Neuropsychopharmacology 37:4-15.

Molofsky AV, Kelley KW, Tsai HH, Redmond SA, Chang SM, Madireddy L, Chan JR, Baranzini SE, Ullian EM, Rowitch DH (2014) Astrocyte-encoded positional cues maintain sensorimotor circuit integrity. Nature 509:189-194.

Morris RL, Hollenbeck PJ (1993) The regulation of bidirectional mitochondrial transport is coordinated with axonal outgrowth. Journal of cell science 104 (Pt 3):917-927.

Morris RL, Hollenbeck PJ (1995) Axonal transport of mitochondria along microtubules and F-actin in living vertebrate neurons. The Journal of cell biology 131:1315-1326.

Motori E, Puyal J, Toni N, Ghanem A, Angeloni C, Malaguti M, Cantelli-Forti G, Berninger B, Conzelmann KK, Gotz M, Winklhofer KF, Hrelia S, Bergami M (2013) Inflammation-induced alteration of astrocyte mitochondrial dynamics requires autophagy for mitochondrial network maintenance. Cell metabolism 18:844-859.

Muir J, Arancibia-Carcamo IL, MacAskill AF, Smith KR, Griffin LD, Kittler JT (2010) NMDA receptors regulate GABAA receptor lateral mobility and clustering at inhibitory synapses through serine 327 on the gamma2 subunit. Proceedings

of the National Academy of Sciences of the United States of America 107:16679-16684.

Mulligan SJ, MacVicar BA (2004) Calcium transients in astrocyte endfeet cause cerebrovascular constrictions. Nature 431:195-199.

Nagler K, Mauch DH, Pfrieger FW (2001) Glia-derived signals induce synapse formation in neurones of the rat central nervous system. The Journal of physiology 533:665-679.

Nam HS, Benezra R (2009) High levels of Id1 expression define B1 type adult neural stem cells. Cell stem cell 5:515-526.

Narayan P, Holmstrom KM, Kim DH, Whitcomb DJ, Wilson MR, St George-Hyslop P, Wood NW, Dobson CM, Cho K, Abramov AY, Klenerman D (2014) Rare individual amyloid-beta oligomers act on astrocytes to initiate neuronal damage. Biochemistry 53:2442-2453.

Navarrete M, Araque A (2011) Basal synaptic transmission: astrocytes rule! Cell 146:675-677.

Navarrete M, Perea G, Maglio L, Pastor J, Garcia de Sola R, Araque A (2013) Astrocyte calcium signal and gliotransmission in human brain tissue. Cerebral cortex 23:1240-1246.

Neary JT, Kang Y, Willoughby KA, Ellis EF (2003) <2348.full.pdf>. The Journal of Neuroscience 23:2348-2356.

Newman EA (2003) New roles for astrocytes: Regulation of synaptic transmission. Trends in neurosciences 26:536-542.

Nguyen TT, Oh SS, Weaver D, Lewandowska A, Maxfield D, Schuler MH, Smith NK, Macfarlane J, Saunders G, Palmer CA, Debattisti V, Koshiba T, Pulst S, Feldman EL, Hajnoczky G, Shaw JM (2014) Loss of Miro1-directed mitochondrial movement results in a novel murine model for neuron disease. Proceedings of the National Academy of Sciences of the United States of America 111:E3631-3640.

Noctor SC, Flint AC, Weissman TA, Dammerman RS, Kriegstein AR (2001) Neurons derived from radial glial cells establish radial units in neocortex. Nature 409.

Oberheim NA, Takano T, Han X, He W, Lin JH, Wang F, Xu Q, Wyatt JD, Pilcher W, Ojemann JG, Ransom BR, Goldman SA, Nedergaard M (2009) Uniquely

hominid features of adult human astrocytes. The Journal of neuroscience : the official journal of the Society for Neuroscience 29:3276-3287.

Oliveira G, Diogo L, Grazina M, Garcia P, Ataide A, Marques C, Miguel T, Borges L, Vicente AM, Oliveira CR (2005) Mitochondrial dysfunction in autism spectrum disorders: a population-based study. Dev Med Child Neurol 47:185-189.

Oliveira JM (2010) Mitochondrial bioenergetics and dynamics in Huntington's disease: tripartite synapses and selective striatal degeneration. Journal of bioenergetics and biomembranes 42:227-234.

Oliveira JM, Goncalves J (2009) In situ mitochondrial Ca2+ buffering differences of intact neurons and astrocytes from cortex and striatum. The Journal of biological chemistry 284:5010-5020.

Otsu Y, Couchman K, Lyons DG, Collot M, Agarwal A, Mallet JM, Pfrieger FW, Bergles DE, Charpak S (2015) Calcium dynamics in astrocyte processes during neurovascular coupling. Nature neuroscience 18:210-218.

Pacey LK, Doering LC (2007) Developmental expression of FMRP in the astrocyte lineage: implications for fragile X syndrome. Glia 55:1601-1609.

Palty R, Silverman WF, Hershfinkel M, Caporale T, Sensi SL, Parnis J, Nolte C, Fishman D, Shoshan-Barmatz V, Herrmann S, Khananshvili D, Sekler I (2010) NCLX is an essential component of mitochondrial Na+/Ca2+ exchange. Proceedings of the National Academy of Sciences of the United States of America 107:436-441.

Palygin O, Lalo U, Verkhratsky A, Pankratov Y (2010) Ionotropic NMDA and P2X1/5 receptors mediate synaptically induced Ca2+ signalling in cortical astrocytes. Cell calcium 48:225-231.

Panatier A, Vallee J, Haber M, Murai KK, Lacaille JC, Robitaille R (2011) Astrocytes are endogenous regulators of basal transmission at central synapses. Cell 146:785-798.

Parnis J, Montana V, Delgado-Martinez I, Matyash V, Parpura V, Kettenmann H, Sekler I, Nolte C (2013) Mitochondrial exchanger NCLX plays a major role in the intracellular Ca2+ signaling, gliotransmission, and proliferation of astrocytes. The Journal of neuroscience : the official journal of the Society for Neuroscience 33:7206-7219.

Parpura V, Zorec R (2010) Gliotransmission: Exocytotic release from astrocytes. Brain research reviews 63:83-92.

Parri R, Crunelli V (2003) An astrocyte bridge from synapse to blood flow. Nature neuroscience 6:5-6.

Pascual O, Casper KB, Kubera C, Zhang J, Revilla-Sanchez R, Sul JY, Takano H, Moss SJ, McCarthy K, Haydon PG (2005) Astrocytic purinergic signaling coordinates synaptic networks. Science 310:113-116.

Pasti L, Volterra A, Pozzan T, Carmignoto G (1997) Intracellular calcium oscillations in astrocytes: a highly plastic, bidirectional form of communication between neurons and astrocytes in situ. The Journal of neuroscience : the official journal of the Society for Neuroscience 17:7817-7830.

Paukert M, Agarwal A, Cha J, Doze VA, Kang JU, Bergles DE (2014) Norepinephrine controls astroglial responsiveness to local circuit activity. Neuron 82:1263-1270.

Perea G, Araque A (2005) Properties of synaptically evoked astrocyte calcium signal reveal synaptic information processing by astrocytes. The Journal of neuroscience : the official journal of the Society for Neuroscience 25:2192-2203.

Perez-Alvarez A, Navarrete M, Covelo A, Martin ED, Araque A (2014) Structural and functional plasticity of astrocyte processes and dendritic spine interactions. The Journal of neuroscience : the official journal of the Society for Neuroscience 34:12738-12744.

Pfrieger FW, Barres BA (1997) Synaptic efficacy enhanced by glial cells in vitro. Science 277:1684-1687.

Pham AH, McCaffery JM, Chan DC (2012) Mouse lines with photo-activatable mitochondria to study mitochondrial dynamics. Genesis 50:833-843.

Pitts K.R YY, Krueger E.W, and McNiven M.A (1999) The Dynamin-like Protein DLP1 Is Essential for Normal Distribution and Morphology of the Endoplasmic Reticulum and Mitochondria in Mammalian Cells. Molecular biology of the cell 10:4403-4417.

Porter JT, McCarthy KD (1995) GFAP-positive hippocampal astrocytes in situ respond to glutamatergic neuroligands with increases in [Ca2+]i. Glia 13:101-112.

Porter JT, McCarthy KD (1996) Hippocampal Astrocytes In Situ Respond to Glutamate Released from Synaptic Terminals. The Journal of Neuroscience 16:5073-5081.

Prudent J, Zunino R, Sugiura A, Mattie S, Shore GC, McBride HM (2015) MAPL SUMOylation of Drp1 Stabilizes an ER/Mitochondrial Platform Required for Cell Death. Mol Cell 59:941-955.

Rangani RJ, Upadhya MA, Nakhate KT, Kokare DM, Subhedar NK (2012) Nicotine evoked improvement in learning and memory is mediated through NPY Y1 receptors in rat model of Alzheimer's disease. Peptides 33:317-328.

Reyes RC, Brennan AM, Shen Y, Baldwin Y, Swanson RA (2012) Activation of neuronal NMDA receptors induces superoxide-mediated oxidative stress in neighboring neurons and astrocytes. The Journal of neuroscience : the official journal of the Society for Neuroscience 32:12973-12978.

Reyes RC, Parpura V (2008) Mitochondria modulate Ca2+-dependent glutamate release from rat cortical astrocytes. The Journal of neuroscience : the official journal of the Society for Neuroscience 28:9682-9691.

Rintoul GL, Filiano AJ, Brocard JB, Kress GJ, Reynolds IJ (2003) Glutamate Decreases Mitochondrial Size and Movement in

Primary Forebrain Neurons. The Journal of Neuroscience 23:7881-7888.

Rintoul GL, Reynolds IJ (2010) Mitochondrial trafficking and morphology in neuronal injury. Biochimica et biophysica acta 1802:143-150.

Risher WC, Patel S, Kim IH, Uezu A, Bhagat S, Wilton DK, Pilaz LJ, Singh Alvarado J, Calhan OY, Silver DL, Stevens B, Calakos N, Soderling SH, Eroglu C (2014) Astrocytes refine cortical connectivity at dendritic spines. eLife 3.

Rojas H, Ramos M, Benaim G, Caputo C, DiPolo R (2008) The activity of the Na+/Ca2+ exchanger largely modulates the Ca2+i signal induced by hypo-osmotic stress in rat cerebellar astrocytes. The effect of osmolarity on exchange activity. J Physiol Sci 58:277-279.

Rose CR, Ransom BR (1996) Intracellular sodium homeostasis in rat hippocampal astrocytes. The Journal of physiology 491 (Pt 2):291-305.

Rose EM, Koo JC, Antflick JE, Ahmed SM, Angers S, Hampson DR (2009) Glutamate transporter coupling to Na,K-ATPase. The Journal of neuroscience : the official journal of the Society for Neuroscience 29:8143-8155.

Rusakov DA, Bard L, Stewart MG, Henneberger C (2014) Diversity of astroglial functions alludes to subcellular specialisation. Trends in neurosciences 37:228-242.

Santello M, Bezzi P, Volterra A (2011) TNFalpha controls glutamatergic gliotransmission in the hippocampal dentate gyrus. Neuron 69:988-1001.

Saotome M, Safiulina D, Szabadkai G, Das S, Fransson A, Aspenstrom P, Rizzuto R, Hajnoczky G (2008) Bidirectional Ca2+-dependent control of mitochondrial dynamics by the Miro GTPase. Proceedings of the National Academy of Sciences of the United States of America 105:20728-20733.

Scannevin RH, Huganir RL (2000) Postsynaptic Organisation and Regulation of Excitatory Synapses. Nature reviews Neuroscience 1:133-141.

Scharwey M, Tatsuta T, Langer T (2013) Mitochondrial lipid transport at a glance. Journal of cell science 126:5317-5323.

Schildge S, Bohrer C, Beck K, Schachtrup C (2013) Isolation and culture of mouse cortical astrocytes. Journal of visualized experiments : JoVE.

Schipke CG, Ohlemeyer C, Matyash M, Nolte C, Kettenmann H, Kirchhoff F (2001) Astrocytes of the mouse neocortex express functional N-methyl-D-aspartate receptors. FASEB journal : official publication of the Federation of American Societies for Experimental Biology 15:1270-1272.

Schmidt S, Linnartz B, Mendritzki S, Sczepan T, Lubbert M, Stichel CC, Lubbert H (2011) Genetic mouse models for Parkinson's disease display severe pathology in glial cell mitochondria. Human molecular genetics 20:1197-1211.

Schummers J, Yu H, Sur M (2008) Tuned responses of astrocytes and their influence on hemodynamic signals in the visual cortex. Science 320:1638-1643.

Schwarz TL (2013) Mitochondrial trafficking in neurons. Cold Spring Harbor perspectives in biology 5.

Serrano A, Haddjeri N, Lacaille JC, Robitaille R (2006) GABAergic network activation of glial cells underlies hippocampal heterosynaptic depression. The Journal of neuroscience : the official journal of the Society for Neuroscience 26:5370-5382.

Serres S, Raffard G, Franconi JM, Merle M (2008) Close coupling between astrocytic and neuronal metabolisms to fulfill anaplerotic and energy needs in the rat brain. Journal of cerebral blood flow and metabolism : official journal of the International Society of Cerebral Blood Flow and Metabolism 28:712-724.

Sharma G, Vijayaraghavan S (2001) Nicotinic cholinergic signaling in hippocampal astrocytes involves calcium-induced calcium release from intracellular stores. Proceedings of the National Academy of Sciences of the United States of America 98:4148-4153.

Shelton MK, McCarthy KD (1999) Mature hippocampal astrocytes exhibit functional metabotropic and ionotropic glutamate receptors in situ. Glia 26:1-11.

Shigetomi E, Bushong EA, Haustein MD, Tong X, Jackson-Weaver O, Kracun S, Xu J, Sofroniew MV, Ellisman MH, Khakh BS (2013) Imaging calcium microdomains within entire astrocyte territories and endfeet with GCaMPs expressed using adeno-associated viruses. The Journal of general physiology 141:633-647.

Shin JY, Fang ZH, Yu ZX, Wang CE, Li SH, Li XJ (2005) Expression of mutant huntingtin in glial cells contributes to neuronal excitotoxicity. The Journal of cell biology 171:1001-1012.

Simard M, Nedergaard M (2004) The neurobiology of glia in the context of water and ion homeostasis. Neuroscience 129:877-896.

Simpson PB, Russell JT (1998) Role of mitochondrial Ca2q regulation in neuronal and glial cell signalling. Brain Research Rev 26:72-81.

Singaravelu K, Lohr C, Deitmer JW (2006) Regulation of store-operated calcium entry by calcium-independent phospholipase A2 in rat cerebellar astrocytes. The Journal of neuroscience : the official journal of the Society for Neuroscience 26:9579-9592.

Skarnes WC, Rosen B, West AP, Koutsourakis M, Bushell W, Iyer V, Mujica AO, Thomas M, Harrow J, Cox T, Jackson D, Severin J, Biggs P, Fu J, Nefedov M, de Jong PJ, Stewart AF, Bradley A (2011) A conditional knockout resource for the genome-wide study of mouse gene function. Nature 474:337-342.

Sloan SA, Barres BA (2014) Mechanisms of astrocyte development and their contributions to neurodevelopmental disorders. Current opinion in neurobiology 27:75-81.

Sofroniew MV (2005) Reactive astrocytes in neural repair and protection. The Neuroscientist : a review journal bringing neurobiology, neurology and psychiatry 11:400-407.

Sofroniew MV (2009) Molecular dissection of reactive astrogliosis and glial scar formation. Trends in neurosciences 32:638-647.

Sofroniew MV, Vinters HV (2010) Astrocytes: biology and pathology. Acta neuropathologica 119:7-35.

Solano RM, Casarejos MJ, Menendez-Cuervo J, Rodriguez-Navarro JA, Garcia de Yebenes J, Mena MA (2008) Glial dysfunction in parkin null mice: effects of aging. The Journal of neuroscience : the official journal of the Society for Neuroscience 28:598-611.

Srinivasan R, Huang BS, Venugopal S, Johnston AD, Chai H, Zeng H, Golshani P, Khakh BS (2015) Ca(2+) signaling in astrocytes from Ip3r2(-/-) mice in brain slices and during startle responses in vivo. Nature neuroscience 18:708-717.

Stephen TL, Gupta-Agarwal S, Kittler JT (2014) Mitochondrial dynamics in astrocytes. Biochemical Society transactions 42:1302-1310.

Stoppini L, Buchs PA, Muller D (1991) A simple method for organotypic cultures of nervous tissue. Journal of neuroscience methods 37:173-182.

Tan AR, Cai AY, Deheshi S, Rintoul GL (2011) Elevated intracellular calcium causes distinct mitochondrial remodelling and calcineurin-dependent fission in astrocytes. Cell calcium 49:108-114.

Theodosis DT, Poulain DA, Oliet SH (2008) Activity-dependent structural and functional plasticity of astrocyte-neuron interactions. Physiological reviews 88:983-1008.

Thiele C, Hannah MJ, Fahrenholz F, Huttner WB (2000) Cholesterol binds to synaptophysin and is required for biogenesis of synaptic vesicles. Nature cell biology 2:42-49.

Tran MD, Neary JT (2006) Purinergic signaling induces thrombospondin-1 expression in astrocytes. Proceedings of the National Academy of Sciences of the United States of America 103:9321-9326.

Tsai PI, Course MM, Lovas JR, Hsieh CH, Babic M, Zinsmaier KE, Wang X (2014) PINK1-mediated phosphorylation of Miro inhibits synaptic growth and protects dopaminergic neurons in Drosophila. Scientific reports 4:6962.

Twelvetrees AE, Yuen EY, Arancibia-Carcamo IL, MacAskill AF, Rostaing P, Lumb MJ, Humbert S, Triller A, Saudou F, Yan Z, Kittler JT (2010) Delivery of GABAARs to synapses is mediated by HAP1-KIF5 and disrupted by mutant huntingtin. Neuron 65:53-65.

Ullian EM, Sapperstein SK, Christopherson KS, Barres BA (2001) Control of synapse number by glia. Science 291:657-661.

Varoqueaux F, Aramuni G, Rawson RL, Mohrmann R, Missler M, Gottmann K, Zhang W, Sudhof TC, Brose N (2006) Neuroligins determine synapse maturation and function. Neuron 51:741-754.

Verkhratsky A, Kirchhoff F (2007) NMDA Receptors in glia. The Neuroscientist : a review journal bringing neurobiology, neurology and psychiatry 13:28-37.

Verkhratsky A, Rodriguez JJ, Parpura V (2012) Calcium signalling in astroglia. Molecular and cellular endocrinology 353:45-56.

Virchow R (1858) Die Cellularpathologie in ihrer Begründung auf physiologische und pathologische Gewebelehre. Verlag von August Hirschwald.

Volobouéva LA, Suh SW, Swanson RA, Giffard RG (2007) Inhibition of mitochondrial function in astrocytes: implications for neuroprotection. Journal of neurochemistry 102:1383-1394.

Volonte C, Amadio S, Cavaliere F, D'Ambrosi N, Vacca F, Bernardi G (2003) Extracellular ATP and neurodegeneration. Curr Drug Targets CNS Neurol Disord 2:403-412.

Volterra A, Liaudet N, Savtchouk I (2014) Astrocyte Ca(2)(+) signalling: an unexpected complexity. Nature reviews Neuroscience 15:327-335.

von Lenhossék M (1893) Der Feinere Bau des Nervensystems im Lichte neuerer Forschung. Fischer's Medicin Buchhandlung H Kornfeld 176-247.

Vos M, Lauwers E, Verstreken P (2010) Synaptic mitochondria in synaptic transmission and organization of vesicle pools in health and disease. Frontiers in synaptic neuroscience 2:139.

Wang F, Xu Q, Wang W, Takano T, Nedergaard M (2012) Bergmann glia modulate cerebellar Purkinje cell bistability via Ca2+-dependent K+ uptake. PNAS 109:7911–7916.

Wang X, Lou N, Xu Q, Tian GF, Peng WG, Han X, Kang J, Takano T, Nedergaard M (2006) Astrocytic Ca2+ signaling evoked by sensory stimulation in vivo. Nature neuroscience 9:816-823.

Wang X, Schwarz TL (2009) The mechanism of Ca2+ -dependent regulation of kinesin-mediated mitochondrial motility. Cell 136:163-174.

Wang X, Winter D, Ashrafi G, Schlehe J, Wong YL, Selkoe D, Rice S, Steen J, LaVoie MJ, Schwarz TL (2011) PINK1 and Parkin target Miro for phosphorylation and degradation to arrest mitochondrial motility. Cell 147:893-906.

Wiese S, Karus M, Faissner A (2012) Astrocytes as a source for extracellular matrix molecules and cytokines. Front Pharmacol 3:120.

Wong PC, Pardo CA, Borchelt DR, Lee MK, Copeland NG, Jenkins NA, Sisodia SS, Cleveland DW, Price DL (1995) An Adverse Property of a Familial ALS-Linked SOD1 Mutation Causes Motor Neuron Disease Characterized by Vacuolar Degeneration of Mitochondria. Neuron 14:1105-1116.

Woods G, Zito K (2008) Preparation of gene gun bullets and biolistic transfection of neurons in slice culture. Journal of visualized experiments : JoVE 1-4.

Wyss MT, Weber B, Treyer V, Heer S, Pellerin L, Magistretti PJ, Buck A (2009) Stimulation-induced increases of astrocytic oxidative metabolism in rats and humans investigated with 1-11C-acetate. Journal of cerebral blood flow and metabolism : official journal of the International Society of Cerebral Blood Flow and Metabolism 29:44-56.

Zhang Q, Pangrsic T, Kreft M, Krzan M, Li N, Sul JY, Halassa M, Van Bockstaele E, Zorec R, Haydon PG (2004) Fusion-related release of glutamate from astrocytes. The Journal of biological chemistry 279:12724-12733.

Zhang QH, Bo; Sun, Shenggang; Tong, Etang (2003) Induction of Increased Intracellular Calcium in Astrocytes by Glutamate through Activating NMDA and AMPA Receptors. Journal of Huazhong University of Science and Technology 23:254-257.

Zhang Y, Chen K, Sloan SA, Bennett ML, Scholze AR, O'Keeffe S, Phatnani HP, Guarnieri P, Caneda C, Ruderisch N, Deng S, Liddelow SA, Zhang C, Daneman R, Maniatis T, Barres BA, Wu JQ (2014) An RNA-sequencing transcriptome and splicing database of glia, neurons, and vascular cells of the cerebral cortex. The Journal of neuroscience : the official journal of the Society for Neuroscience 34:11929-11947.

Zhuang Z, Yang B, Theus MH, Sick JT, Bethea JR, Sick TJ, Liebl DJ (2010) EphrinBs regulate D-serine synthesis and release in astrocytes. The Journal

of neuroscience : the official journal of the Society for Neuroscience 30:16015-16024.